A time spread diversity technique with integrated coding and interference cancellation

Stefanus A. Swanepoel

Submitted in partial fulfilment of the requirements
for the degree

Master of Engineering

in the

Faculty of Engineering, Building Environment
and Information Technology,

University of Pretoria

2002

ABSTRACT

A time spread diversity technique with integrated
coding and interference cancellation
by
S.A. Swanepoel
Advisor: Professor L.P. Linde
Department of Electrical, Electronic and Computer Engineering
Master of Engineering (Electronic)

Keywords:
Time Spread, Diversity, Interleave, Rayleigh flat-fading, Mobile Communication, Channel Estimation, Pilot Symbol, Interference Cancellation, Soft Decision Viterbi Decoding, Turbo Coding

Conventional signal diversity techniques increase system complexity and/or result in an increase in the required signal bandwidth. A novel *Time Spread* (TS) diversity technique has been proposed in [1] aimed at improving the performance of digital communication systems in flat-fading channels without increasing their complexity or bandwidth usage. With TS, time diversity is obtained by transmitting a modulated spreading sequence, spanning over a temporal period longer than the channel coherence time T_c, for each information symbol. Unfortunately, this TS technique exhibits a *Bit Error Rate* (BER) performance floor at higher SNR values that renders the original technique less attractive.

This dissertation is primarily concerned with the nullification of this BER performance floor. Secondly, the ability of the TS technique to transform a flat-fading channel into an *Additive White Gaussian Noise* (AWGN) channel is investigated and exploited to enhance the performance of coding techniques designed for AWGN channels, when used in flat-fading channels.

A new method is described by which TS sequences can be temporally expanded, thereby increasing their obtainable time diversity gains. This method also reduces the computational complexity of a TS system, while retaining the signal diversity properties of a longer non-expanded sequence.

The BER floor in TS systems is caused by the distortion of the *Aperiodic Auto-Correlation* (AAC) properties of overlapping spreading sequences in fading channels, resulting in *Inter Code(Sequence) Interference* (ICI) between spreading sequences. A *Pilot Symbol Aided Modulation* (PSAM) technique is adapted for the TS system to provide accurate channel estimates required by the *Inter Code(Sequence) Interference Cancellation* (ICIC) module. A hybrid ICIC technique, which corrects the fading TS symbol amplitudes during periods of above average instantaneous SNR levels, is shown to be the most effective. This ICIC technique enables the TS technique to provide gains similar to that of conventional third order diversity techniques at average E_b/N_0 ratios above 10 dB.

Finally, the transparency and ability of the TS technique to transform fading channels into Gaussian channels are exploited to allow the integration of conventional convolutional codes with the TS system. The coded TS system achieves substantial gains when operating in a Rayleigh flat-fading channel when a soft decision Viterbi decoder is used in the TS receiver. A strategy by which *Turbo Code* (TC) techniques can be integrated with the TS technique is discussed as a concluding notion to illustrate the flexibility of the TS technique.

Future research areas are identified based on the findings of this dissertation. These include the investigation of more effective adaptive ICIC schemes and the possibility of using *Code Division Multiple Access* (CDMA) communication techniques over a narrow band channel by employing TS- and *Multi-User* (MU)-detection methods, combined with existing ICIC techniques. The cryptographic value of the TS technique also provides ground for future research.

SAMEVATTING

'n tyd sprei diversiteits tegniek met geïntegreerde
kodering en steurseinkansellering
deur
S.A. Swanepoel
Studieleier: Professor L.P. Linde
Departement Elektriese, Elektroniese en Rekenaar Ingenieurswese
Meester in Ingenieurswese (Elektronies)

Sleutelwoorde: Tyd Sprei, Diversiteit, Invleg, Rayleigh plat deining, Mobiele Kommunikasie, Kanaalestimasie, Loods Simbool, Steurseinkansellering, Sagte Beslissing Viterbi-Dekodering, Turbo-Kodering

Konvensionele diversiteitstegnieke verhoog stelsel kompleksiteit en/of die benodigde transmissiebandwydte van digitale kommunikasiestelsels. 'n Nuwe *Tyd-Sprei* (TS) diversiteitstegniek is in [1] voorgestel wat die werksverrigting van 'n digitale kommunikasiestelsel in plat deinende kanale verbeter sonder die gepaardgaande verhoging in kompleksiteit en benodigde seinbandwydte van konvensionele stelsels. Tyddiversiteit word verkry deur 'n volledig gemoduleerde spreisekwensie, wat strek oor 'n periode langer as die koherensie-tyd T_c van die kanaal, te versend vir elke nuwe informasiesimbool wat gegenereer word. Die tegniek gaan egter gebuk onder 'n onverminderbare *Bis-Fout-Tempo* (BER) verrigtingslimiet vir hoër SNR-waardes.

Hierdie verhandeling is hoofsaaklik gemoeid met die eliminasie van bg. probleem. Tweedens word die vermoë van die TS-tegniek om 'n deinende kanaal na 'n Gaussiese kanaal te transformeer, gebruik om koderingstegnieke wat vir die *Sommeerbare Wit Gausiese Ruis* (AWGN) kanaal ontwerp is, in deinende kanale te gebruik.

Die onvermoë van kort spreisekwensies om voldoende tyddiversiteit te verskaf is geïdentifiseer as 'n leemte in die bestaande TS-stelsel en 'n effektiewe metode word voorgestel waardeur kort spreisekwensies d.m.v. nul-interpolasie, temporaal uitgebrei kan word om sodoende beter tyddiversiteit te verskaf.

Laasgenoemde BER verrigtingslimiet word veroorsaak deur die vervorming van die *Aperiodiese Outo-Korrelasie* (AAC)-eienskappe van die oorvleuelende spreisekwensies in deinende kanale, wat aanleiding gee tot *Inter-Kode(Sekwensie)-Interferensie* (ICI). 'n *Loods-Simbool Ondersteunde Modulasie* (PSAM)-tegniek is aangepas om akkurate kanaalestimasies aan die *Inter-Kode(Sekwensie)-Steuringskanselleering* (ICIC) module te verskaf. Daar word aangetoon dat 'n hibriede ICIC-tegniek, wat die amplitudes van deinende TS-simbole korrigeer, tydens periodes wanneer die oombliks SNR-vlakke vir die ontvangde sein bogemiddeld is, die mees effektiewe tegniek is. Hierdie ICIC-tegniek stel die TS-tegniek in staat om winste ekwivalent aan die van konvensionele derde orde diversiteit-stegnieke te bewerkstellig vir E_b/N_0-vlakke bo 10 dB.

Die deursigtigheid en vermoë van die TS-tegniek om 'n deinende kanaal na 'n Gaussiese kanaal te transformeer, word benut om die integrasie van konvensionele konvolusiekodes met die TS-stelsel moontlik te maak. Aansienlike winste word verkry deur die kombinasie van die gekodeerde TS-tegniek en 'n sagtebeslissing Viterbi-dekodeerder in Rayleigh plat deinende kanale. 'n Strategie waarvolgens *Turbo Kodering* (TC)-tegnieke met TS geïntegreer kan word, word bespreek ter illustrasie van die buigsaamheid van die TS-tegniek m.b.t. integrasie met ander stelsels en koderingstegnieke.

Toekomstige navorsingsvelde word geïdentifiseer gebaseer op bevindinge in hierdie verhandeling. Dit sluit ondersoeke na meer effektiewe, aanpasbare rekursiewe ICIC-skemas in, asook die moontlikheid om 'n nouband *Kode Deel Veelvuldige Toegang* (CDMA) stelsel daar te stel. Die kriptografiese waarde van die TS-tegniek is 'n verdere onderwerp wat baie ruimte laat vir toekomstige navorsing.

This dissertation is dedicated to God from Whom
we receive our talents, and to my parents,
who supported and encouraged me in using them.

ACKNOWLEDGEMENTS

I would like to express my gratitude to my promoter, Professor Louis Linde. Without his contributions this project would not have been possible. His endless enthusiasm is contagious and inspiring at times when little progress is made. Initiatives and insights from Professor Linde brought his students into contact with aspects of the communications field reaching much wider than the narrow scope of a dissertation.

I am grateful to the Laboratory for Advanced Engineering, the University of Pretoria, the National Research Foundation, and Nokia South Africa, all whom provided funding during the completion of my masters degree.

Special thanks to my friends and colleagues, Leon Staphorst, Ben Waldeck and Jacques van Wyk with whom I shared many profitable discussions regarding aspects of this research.

Years of support, patients and prayers from my parents and family have not gone unnoticed and are greatly appreciated.

Much more is put into and gained from completing a masters dissertation than what is seen in this book and I am grateful to everyone who played a part in this process.

Thanking all these people and organizations we know that everything is received through the grace of God and we thank Him for that.

TABLE OF CONTENTS

LIST OF FIGURES

LIST OF TABLES

LIST OF ABBREVIATIONS

AAC	Aperiodic Auto-Correlation
AC	Auto-Correlation
AC-ICIC	Amplitude Correction-Inter Code(Sequence) Interference Cancellation
AWGN	Additive White Gaussian Noise
BER	Bit Error Rate
BPSK	Binary Phase Shift Keying
CAZAC	Constant Amplitude Zero Auto-Correlation
CC	Cross Correlation
CDF	Cumulative Distribution Function
CDMA	Code Division Multiple Access
CRDC	Center for Radio and Digital Communication
CSI	Channel State Information
DC	Direct Current
DS-CDMA	Direct Sequence-Code Division Multiple Access
DSP	Digital Signal Processing
FEC	Forward Error Correction
FIR	Finite Impulse Response
FOM	Figure Of Merrit
FZC	Frank Zadoff Chu
GCL	Generalized Chirp Like
IC	Interference Cancellation
ICI	Inter Code Interference
ICIC	Inter Code(Sequence) Interference Cancellation
IF	Intermediate Frequency
ISI	Inter Symbol Interference
LAE	Laboratory for Advanced Engineering
LCR	Level Crossing Rate
LO	Local Oscillator
LOS	Line Of Sight

LPF	Low Pass Filter
MFD	Maximum Free Distance
ML	Maximum Likelihood
MLSE	Maximum Likelihood Sequence Estimator
MU	Multi-User
MUI	Multi-User Interference
NFSF	Normalized Fade Sensitivity Factor
PAM	Pulse Amplitude Modulation
PDF	Probability Density Function
PN	Pseudo Noise
PRBS	Piece-wise Random Binary Sequence
PSAM	Pilot Symbol Aided Modulation
PSD	Power Spectral Density
PSK	Phase Shift Keying
QAM	Quadrature Amplitude Modulation
RADAR	Radio Detection And Ranging
RF	Radio Frequency
RMS	Root Mean Square
SNR	Signal to Noise Ratio
TC	Turbo Code
TCM	Trellis Coded Modulation
TS	Time Spread
TTIB	Transparent Tone In Band

LIST OF SYMBOLS

$\overline{E}_b/N_0$	Average bit energy to noise spectral density ratio
f_D	Doppler spread
f_d	Doppler shift
$\overline{\tau}$	Fading channel mean eccess delay
σ_τ	*Root Mean Square* (RMS) delay spread
λ	Transmitted signal wave length
v	Relative speed between transmitter and receiver antennas
B_C	Channel coherence bandwidth
f_c	Transmitted signal carrier frequency
f_m	Maximum Doppler frequence shift
T_C	Channel coherence time
T_S	Resiprocal signal bandwidth
B_S	Transmitted signal bandwidth
B_D	Doppler spread bandwidth
K	Rician *Line Of Sight* (LOS) to fading signal strength ratio
σ^2	Multipath envelope variance
ρ	Fading depth threshold
ψ	Phase distortion induced by a fading communication channel
N	Number of elements in a non-expanded *Time Spread* (TS) sequence
α	Nyquist filter spectral roll-off factor
R_S	Transmitted symbol rate
I	In-phase
Q	Quadrature-phase
M	Number of symbols in a pilot symbol frame/Number of bits per M-Ary symbol
${\sigma_g}^2$	*Additive White Gaussian Noise* (AWGN) variance
f_0	Channel induced frequency offset
$\tilde{R}_c$	Unity power channel *Auto-Correlation* (AC) function
J_0	0^{th} Bessel function
q	Pilot to data symbol power ratio

N_P	Number of symbols in a pilot symbol synchronization sequence
N_S	Number of elements in a pilot symbol sequence
δ_{ik}	Kronecker delta
σ_e^2	Channel estimation error variance
σ_v^2	Estimated symbol gain variance
γ_b	*Signal to Noise Ratio* (SNR) per bit
d_{Avg}	Absolute average symbol level of a random TS symbol stream
$\angle$	Returns the phase angle of the argument
R_c	Error correction code rate
L	Convolutional code constraint length, unless otherwise specified

CHAPTER ONE

INTRODUCTION

Modern society is becoming ever more dependent on the efficient transfer of information. Transferred information may include voice, multimedia or data and needs to be available wherever required. All these demands come at a time when the available radio spectrum is diminishing rapidly, while the number of people requiring services is increasing.

Due to the current drive to apply wireless technology to a broader range of applications, the modern communications engineer is faced with the challenge of finding solutions to problems such as spectrum overcrowding, fading mobile channels, indoor propagation considerations, and data security, to name but a few. This study is concerned with alleviating some of the negative effects imposed on digital communication systems by fading mobile radio channels. More specifically, a technique used to lessen the effects of deep fades occurring in a Rayleigh flat-fading channel is described and enhanced in this study.

A *Time Spread* (TS) technique [6, 1, 7], proposed to reduce the adverse effects of Rayleigh flat-fading, serves as the basis of this project. The contribution made by this project in improving the understanding and performance of this basic TS technique will be discussed in later sections of this chapter. Note that only a few references on or relating to the TS technique are available in the open literature, since the techniques used in this project have not been studied widely. A similar technique relying on time diversity, used to reduce the effects of Rayleigh flat-fading, has been proposed in [8]. It is of note that the results presented in [8], which are based on theoretical derivations, could not be reproduced for practical simulated systems. This observation will be discussed in more detail when some of the limitations of TS are discussed in Chapter 4. This dissertation evaluates the TS technique from a different perspective than [6] and the emphasis falls on the diversity properties of the TS technique.

1.1 TIME SPREADING FOR MOBILE COMMUNICATIONS

The TS technique [1], described in this dissertation, relies on spreading the energy of each channel symbol over a period of time much larger than the original symbol period. Each channel symbol's energy is spread using an orthogonal spreading sequence with perfect *Aperiodic Auto-Correlation* (AAC) properties. Channel symbols are spread before being transmitted over a fading mobile communication channel.

TS can be seen as the introduction of a form of transmitter diversity aimed at limiting the effects of channel fading on the *Bit Error Rate* (BER) performance of a system. Typically, transmitter time diversity is obtained by transmitting the energy associated with a particular channel symbol over many symbol intervals. When the period over which the symbol energy is distributed is much larger than the average duration of a deep fade in the received signal power, each original transmitted symbol can be estimated by correlating the appropriately aligned received TS signal with the transmitted spreading sequence in the receiver. The TS correlation receiver uses the energy of the channel symbol not affected by the deep fade to estimate the original transmitted data symbol on a symbol-by-symbol basis for uncoded data symbols.

When the TS technique is used for uncoded systems operating in a Rayleigh flat-fading channel, improvements in the *Signal to Noise Ratio* (SNR) requirements are obtained by estimating and reconstructing channel symbols received during deep fades from the symbol energies not affected by the deep fades.

Forward Error Correction (FEC) codes designed for *Additive White Gaussian Noise* (AWGN) channels perform better when used in combination with TS than standard interleaving methods. This is due to the ability of the TS technique to break up correlated error bursts, along with the additional processing gain achieved by reconstructing channel symbols received during fades.

1.2 RESEARCH IN CONTEXT

"*Receiver-diversity techniques have been known for a long time to improve the fading-channel quality.*" - taken from [9].

Receiver-diversity is but one of many diversity techniques that can be used with significant effect to improve the performance of communication systems operating in fading channels. Some of the more prominent diversity techniques known for use in communication systems are discussed in Section 3.2.1. All these techniques impose serious constraints on systems that use them. These constraints

include: extensive bandwidth usage, high levels of receiver complexity, and restraints regarding the physical realization of systems incorporating multiple transmitter and/or receiver antennas. Nevertheless, these diversity techniques provide significant gains when combined with suitable coding techniques and are therefore actively researched. An investigation into the optimum combination of coding and diversity techniques was conducted by the RaDiCom[1] Group in the *Laboratory for Advanced Engineering* (LAE) (now RE at UP[2]) and is documented in [10]. Findings in this report indicate that the combination of diversity techniques and error correction coding provide the optimum system performance. These findings are confirmed by results in [9], where it is stated that robust communication systems can be obtained by combining diversity techniques with FEC codes designed for the AWGN channel. This topic will be discussed in more detail in Chapter 5. All these findings emphasizes the need for an efficient, low complexity diversity technique that can be integrated successfully with existing coding techniques.

The TS technique, designed to provide signal diversity in Rayleigh flat-fading channels, answers in the aforementioned requirements of a diversity scheme. The baseline TS technique used in this project was originally proposed and patented by [1]. Further research on the functioning and benefits of this technique was conducted by [6, 7]. The emphasis of this work fell on the basic principles of the TS technique and the search for suitable time spreading sequences received a great deal of attention. The following important observations regarding the TS technique can be made from the results in [6, 7]:

- The TS technique suffers from a BER performance floor at high SNRs.
- *Inter Code Interference* (ICI) severely limits the performance of the TS technique in fading channels for $\overline{E}_b/N_0$ levels above 10 dB.

Additional research by the author also indicated that:

- The TS technique is dependent on sufficiently long spreading sequences to obtain adequate transmitter time diversity. Longer spreading sequences does however require more processing power in both the transmitter and receiver structures.
- TS integrated with FEC coding promises considerable gains in SNR requirements for fading mobile communication channels due to its ability to provide signal diversity, while breaking up correlated error bursts.

The objective of this project is to address the aforementioned inefficiencies identified within the original TS technique in order to improve its BER performance in fading channels, while minimizing

[1] Radio and Digital Communication
[2] Research Enterprises at University of Pretoria (Pty) Ltd

the computational power required to implement the technique. The statistical properties of the TS technique regarding bit error occurrence and Gaussianizing of fading channels are investigated. This knowledge is used by the author when coding strategies and the integration thereof with TS are proposed and analyzed.

While previous work on the TS technique emphasized the ability of the technique to reconstruct data symbols received during periods of deep fades, this dissertation analyzes the technique from the perspective of transmitter signal diversity. This makes it possible to relate this technique to other coding and diversity techniques proposed in the literature, highlighting the advantages of using the TS technique.

1.3 UNIQUE CONTRIBUTIONS

The basic principles of the TS technique, with special emphasis on spreading sequence design and the use of different spreading sequences are documented in [1, 6, 7]. This paved the way for the author to make several contributions in this dissertation towards the implementation of a viable TS modem. Although the TS technique was initially proposed by the advisor for this project, the contributions documented here were all generated by the author. The most important contributions include:

- The introduction of a new *Amplitude Correction-Inter Code(Sequence) Interference Cancellation* (AC-ICIC) module that improves the overall BER performance of the modem. This technique was developed by the author from other techniques not entirely suited for the TS system. The technique completely eliminates the BER performance floor occurring at high $\overline{E}_b/N_0$ levels in fading channels and enables the TS technique to provide gains equivalent to multiple order diversity techniques at a fraction of the system complexity. Furthermore, the TS technique obtains these gains without the usual increase in required transmission bandwidth associated with existing time and frequency diversity techniques.

- The introduction of a channel estimation technique specifically adapted for the TS system by the author that permits the use of coherent demodulation in the receiver structure. This channel estimation technique is integrated with the TS technique and the *Inter Code(Sequence) Interference Cancellation* (ICIC) module. The channel estimation technique allows for a more realistic simulation of the proposed TS system, since perfect carrier phase recovery need not be assumed, as was the case in [6], p 53. This addition brings the TS technique one step closer to being a physically realizable system.

- A new technique to increase the effective time diversity offered by relatively short fundamental spreading sequences. This technique makes it possible to obtain the same signal diversity from

shorter spreading sequences, reducing the number of computations associated with TS in the transmitter and receiver by a factor k, where k is defined as the temporal expansion factor.

- The integration of FEC coding strategies with the TS technique.
- A thorough analysis of a TS modem in a Rayleigh flat-fading channel with the emphasis on issues regarding the integration with FEC coding strategies.
- Several simulation results including error performance statistics, channel estimation techniques, BER graphs under different channel conditions, etc.
- The generation of a complete set of simulation software objects required to develop and test the TS system.

The contributions made in this dissertation regarding the improvement of the existing TS technique are best summarized as follows:

- At a BER of $P_e = 10^{-6}$, the new uncoded TS system, in a Rayleigh flat-fading channel, requires only 11.5 dB more transmitted signal power than a coherent *Phase Shift Keying* (PSK) system in an AWGN channel. This result is in contrast with the original TS system which suffered from a BER performance floor occurring at $P_e = 10^{-2.5}$, which implies that it can not perform better than $P_e = 10^{-2.5}$, even if the SNR is increased to infinity.
- Using a $R_c = 2/3$ rate convolutional code with the new TS system, its performance can be improved to within 1 dB from that of an uncoded *Phase Shift Keying* (PSK) system in AWGN at a BER of $P_e = 10^{-6}$.
- Also, at a BER of $P_e = 10^{-3}$, the new uncoded and coded TS systems require 12 and 16 dB less transmitted signal power to perform at the same level as a standard coherent PSK modem in a Rayleigh flat-fading channel.
- The new uncoded TS system is also shown to perform similar to an uncoded 3^{rd} order diversity system using coherent PSK in a Rayleigh flat-fading channel. Comparative results from [3] and [4] are used as performance reference.
- When compared to coded PSK systems with infinite interleaver depth in a Rayleigh flat-fading channel. The $R_c = 2/3$ rate coded TS system requires 14 dB less transmitted signal power to ensure a BER of $P_e = 10^{-6}$. Comparative results for a 8-state $R_c = 2/3$ rate 8-PSK Ungerboeck coded system, taken from [9], is used as performance reference.

The theoretical results presented in the aforementioned references are however derived assuming perfect carrier phase recovery and maximal-ratio diversity combination and does therefore not reflect

the implementation losses associated with practical systems. The gains obtained from using the TS technique become even more apparent when these implementation losses are taken into account.

The efficient method by which the TS technique transforms a Rayleigh flat-fading channel to a Gaussian channel is evident from the substantial performance gains obtained when the TS technique is combined with a standard $R_c = 2/3$ rate convolutional code designed for the AWGN channel.

The following presentations and publications have emanated from the research conducted during the completion of this dissertation:

Keynote presentation:

S.A. Swanepoel and L.P. Linde, "A Time Spread Technique with Interference Cancellation for fading Mobile Communication channels," in *Proceedings of IEEE AFRICON '99*, pp. 131-134, Sept. 1999.

Publications:

S.A. Swanepoel and L.P. Linde, "Performance evaluation of a Time Spread diversity technique with for Rayleigh flat-fading channels channels," in *SAIEE Journal*, submitted for review.

1.4 RESEARCH OUTLINE

Apart from the introductory and concluding chapters, this dissertation consists of five chapters and an appendix in which aspects regarding the TS technique and its enhancements are discussed. The TS technique is aimed at improving the performance grade of digital communication systems operating over a fading channel. This requires a thorough understanding of the flat-fading mobile communications channel. Chapter 2 gives some background to the different channel effects associated with a fading communication channel and some of the parameters used to characterize this channel are discussed. Since a physical channel can not be used to evaluate the performance of the TS technique, a suitable statistical channel model must be used. The flat-fading Rayleigh channel model that is used in this dissertation is described. Deviations from the ideal channel model is explained and justified. This chapter gives a broader perspective to the effects associated with a fading channel and places the specific channel model that is used in this project in context.

Chapter 3 is concerned with the description of the basic TS technique analyzed in [6], where TS is described as a method to reconstruct data symbols received during deep fades. This dissertation

attempts to analyze the TS technique from a wider perspective and examines the technique from the time diversity perspective. Furthermore, this chapter briefly describes different classes of spreading sequences that could be used for time spreading. Temporal expansion of a spreading sequence in time can increase the time diversity obtained from a short fundamental spreading sequence. This observation is described as a unique contribution. Next, the transmitter and receiver structures of a basic TS system is described for later reference. The final section of this chapter discusses the origin of ICI and justifies the investigation of ICIC methods to eliminate this phenomena.

Chapter 4 emphasizes the importance of accurate channel state information in coherent receivers and ICIC structures. The use of pilot symbols to estimate the effects of a fading channel is described in detail. The origin and extent of ICI in TS systems are discussed as a first step towards finding effective ICIC strategies. These ICIC strategies are similar to techniques used in the *Code Division Multiple Access* (CDMA) environment to cancel the effects of *Multi-User Interference* (MUI). A brief summary is given of some applicable MUI cancellers used in the CDMA environment. With good channel estimates provided by the *Pilot Symbol Aided Modulation* (PSAM) technique, several ICIC strategies are proposed for implementation in the TS receiver. The identification and implementation of these ICIC strategies are one of the main contributions of this dissertation and improves the TS system performance markedly.

One of the side benefits of the TS technique is its ability to transform a Rayleigh flat-fading channel into a Gaussian channel and to randomize correlated symbol error bursts. These properties, when integrated with FEC codes designed for AWGN channels, can provide substantial BER performance gains. Chapter 5 describes a low complexity method to integrate FEC coding and time spreading. The transparency of the TS technique allows for a soft decision Viterbi decoder to be used as a *Maximum Likelihood Sequence Estimator* (MLSE). The Viterbi algorithm is used to decode the convolutional FEC code and is described in Section 5.3.3. A brief overview of a strategy, where the TS technique is used in conjunction with a turbo coding scheme, concludes the chapter.

A simulation study conducted to evaluate the TS technique under various circumstances is documented in Chapter 6. This chapter begins by illustrating some important TS signals in the time, frequency and signal space domains. The fading channel model is verified by calculating various statistical and frequency domain parameters based on the simulated channel output signals. This is followed by a large number of BER results depicting the performance of the PSAM technique. The performance of the TS technique in combination with ICIC and integrated error correction coding is evaluated by calculating BER results. This chapter consolidates all the topics covered in this dissertation and gives some concluding results and discussions on the viability of the TS technique for use in practical systems.

Chapter 7 summarizes the research that has been done in this dissertation, and highlights the most outstanding results. Proposals for future research is made, based on results and topics discussed in this dissertation.

Details on the implementation of the statistical fading mobile channel model that is used in this dissertation is documented in Appendix A.

The Borland C++ Builder source code and Matlab M-files developed during the course of this dissertation is available in Adobe®-*.pdf* format from the *Center for Radio and Digital Communication* (CRDC) in the Department of Electrical and Electronic and Computer Engineering at the University of Pretoria.

CHAPTER TWO

MOBILE COMMUNICATION CHANNELS

2.1 CHAPTER OVERVIEW

Some important characteristics of a mobile digital communication channel are discussed in this chapter. The objective of the TS technique is to improve the performance of a communication system operating in mobile channels directly, and indirectly through integration with error correction coding techniques. A thorough understanding of the phenomena associated with mobile channels are therefore crucial in the understanding and evaluation of the TS technique. The focus of this chapter is on the Rayleigh flat-fading channel, which has very specific characteristics, and served as the platform for testing the TS technique and its enhancements. References on mobile channel characteristics and the simulation model implementations thereof include [11, 12, 13, 14, 15, 3].

2.2 SMALL-SCALE MULTIPATH PROPAGATION

Small-scale fading describes the rapid fluctuations in a radio signal occurring over a small period of time or travel distance. The effects of large-scale path loss effects may be ignored when adequate power control strategies are implemented. Fading occurs when two or more versions of the same transmitted signal arrive at the receiver at slightly different times. The three most important effects associated with multipath propagation in a radio channel are:

- Rapid signal level changes over a small time interval or travel distance.
- Random frequency modulation due to varying Doppler shifts on different multipath signals.
- Time dispersion caused by multipath propagation delays.

The signal at the antenna of a receiver at any point in space may consist of a large number of plane waves having randomly distributed amplitude and phase values, with random angles of arrival. These multipath components combine vectorially in the receiver antenna and cause the received signal to distort or fade. Even when the receiver is stationary, the received signal may fade due to movement of surrounding objects.

2.2.1 FACTORS INFLUENCING SMALL-SCALE FADING

The severity of the aforementioned effects are determined by the following physical factors:

- **Multipath propagation** - The presence of reflecting objects and scatterers in a channel creates a constantly changing environment. This results in replicas of the transmitted signal reaching the receiver at different times, each replica with different degrees of attenuation and phase distortion. The vector sum of these transmitted signal replicas result in a time dispersed received signal with random phase and rapid changes in the signal level. Time dispersion of the transmitted signal may lead to severe *Inter Symbol Interference* (ISI) in a digital communication system. Depending on the time dispersion characteristics of the mobile channel, it may result in frequency selective fading, where portions of the received signal spectrum are severely attenuated.

- **Speed of the mobile** - Relative movement between the transmitter and receiver antennas result in random frequency modulation due to different Doppler shifts on each of the multipath components.

- **Speed of surrounding objects** - Moving objects in the radio channel may induce time varying Doppler shifts on the different multipath components. If the speed of the receiver exceeds the speed of the objects, this effect may be ignored.

- **Transmission bandwidth of the signal** - If the transmitted signal bandwidth is greater than the coherence bandwidth of the multipath channel, the received signal will be distorted, but its signal strength will not fade much over a local area (i.e., the small-scale fading will not be significant). The coherence bandwidth of a multipath channel is related to its specific structure and is a measure of the maximum frequency difference for which the signal amplitudes at the channel output are still strongly correlated. If the transmitted signal has a small bandwidth compared to the coherence bandwidth of the channel, the amplitude of the signal will change rapidly, but the signal will not be distorted in time.

2.2.2 DOPPLER SHIFT

When a receiver is moving directly towards the corresponding transmitter, the apparent transmitted frequency as observed by the receiver is f_d higher than the actual transmitted frequency. The inverse

applies when the receiver is moving directly away from the transmitter. The apparent change in frequency, or Doppler shift, is given by f_d, where

$$f_d = \frac{v}{\lambda} \quad [Hz] \tag{2.1}$$

and v is the relative speed between the receiver and transmitter, with λ the wavelength of the transmitted radio signal. When the receiver and transmitter are moving towards each other, the Doppler shift is positive, as opposed to a negative Doppler shift when the relative movement between receiver and transmitter are in opposite directions. Different received multipath components may experience different Doppler shifts, resulting in the random modulation of the transmitted signal, as observed by the receiver.

2.3 PARAMETERS OF MULTIPATH MOBILE CHANNELS

The power delay profile of a multipath channel determines many of its parameters. Power delay profiles are obtained from channel sounding measurements and are mostly represented as plots of relative received power versus excess delay relative to a fixed time delay reference.

2.3.1 TIME DISPERSION PARAMETERS

In order to compare different multipath channels, some parameters have been chosen to grossly quantify the multipath channel. The mean excess delay ($\bar{\tau}$), is the first moment of the power delay profile and the *Root Mean Square* (RMS) delay spread (σ_τ), is the square root of the second moment of the power delay profile. The maximum excess delay (X dB), is defined to be the time delay during which the multipath energy falls X dB below its maximum. Since the power delay profile and the magnitude frequency response of a channel are related by a Fourier transform, the RMS delay spread and coherence bandwidth of a channel are inversely proportional.

2.3.2 COHERENCE BANDWIDTH

Coherence bandwidth B_C, is a statistical measure of the range of frequencies over which a channel can be considered to have equal gain properties. In this frequency range, any two frequency components show strong amplitude correlation properties.

There exists a loose inverse relationship between the RMS delay spread (σ_τ) and the coherence bandwidth. In general, spectral analysis techniques and system simulations are however required to determine the exact impact that time varying multipath has on a particular transmitted signal.

2.3.3 DOPPLER SPREAD AND COHERENCE TIME

Doppler spread B_D, is a measure of the spectral broadening caused by the time rate of change of the mobile radio channel. If a pure sinusoidal signal is transmitted over a fading channel, the received signal would have spectral components in the range ($f_c - f_d$ to $f_c + f_d$), where f_d is the Doppler shift in Hertz.

The time domain dual of Doppler spread is Coherence time T_C. The fading channel impulse response is essentially time invariant over the statistical time parameter T_C. A popular equation, taken from [11], relating the Coherence time T_C and the maximum Doppler shift f_m, is

$$T_C = \sqrt{\frac{9}{16\pi f_m^2}} \quad [s]. \tag{2.2}$$

2.4 TYPES OF SMALL-SCALE FADING

Depending on the relation between different signal parameters (such as bandwidth, symbol period, etc.) and channel parameters (such as RMS delay spread and Doppler spread), different transmitted signals will undergo different types of fading. While multipath delay spread leads to time dispersion and frequency selective fading, Doppler spread leads to frequency dispersion and time selective fading. The two propagation mechanisms are independent of each other and are summarized in Fig. 2.1. The different types of small scale fading effects are discussed in the following sections.

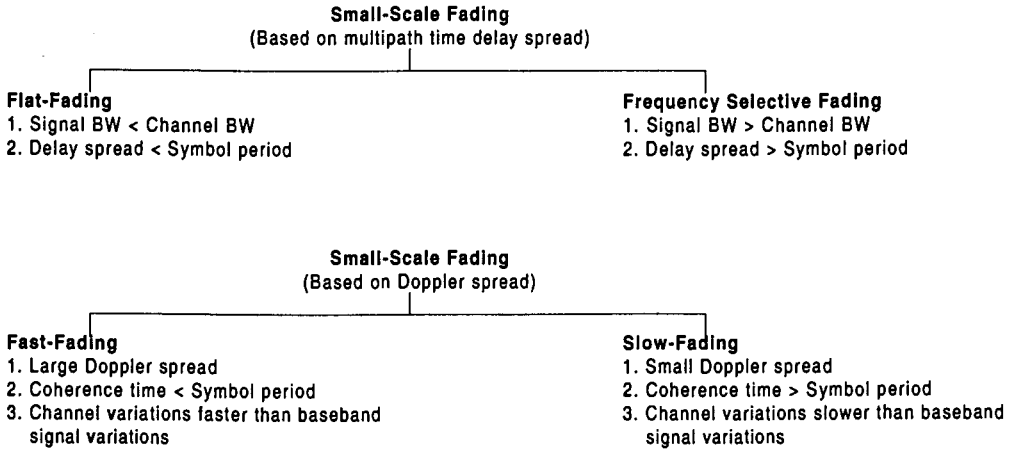

Figure 2.1: Types of small-scale fading.

2.4.1 FLAT-FADING

Flat-fading occurs due to the time dispersion of a transmitted signal. If a mobile communication channel has a constant gain and linear phase response over a bandwidth *greater* than the bandwidth of the transmitted signal, the received signal will exhibit the effects of flat-fading. With flat-fading, the spectral characteristics of the transmitted signal are preserved at the receiver. However, the strength of the received signal varies in time due to fluctuations in the channel gain, caused by multipath propagation. The characteristics of a flat-fading channel in terms of its impulse response $h(t)$, and frequency response $H(f)$, are best summarized in Fig. 2.2. In a flat-fading channel, the recipro-

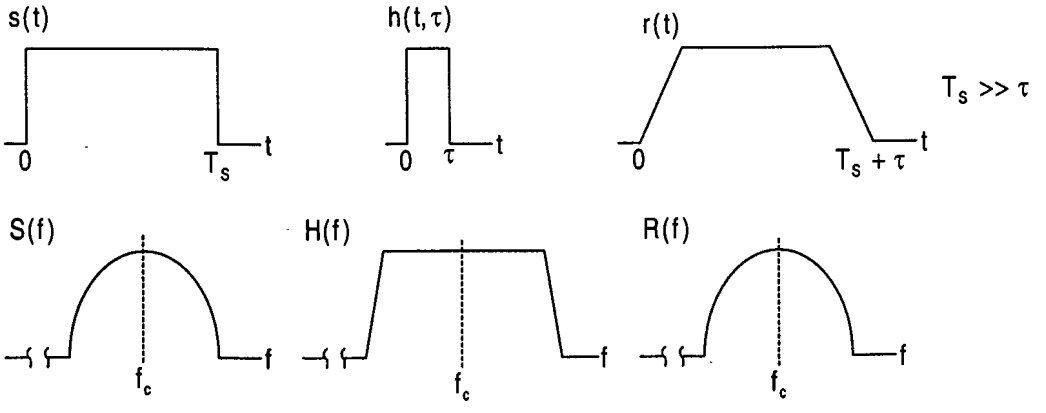

Figure 2.2: Flat-fading channel transfer characteristics.

cal bandwidth of the signal is much larger than the multipath time delay spread of the channel and $h_b(t,\tau)$ can be approximated as having no excess delay (i.e., a single delta function with $\tau = 0$). The distribution of the instantaneous gain of a flat-fading channel is often modelled as a Rayleigh distribution. This implies that the instantaneous area of the delta function in the channel's impulse response, measured at different times, has a Rayleigh distributed *Probability Density Function* (PDF).

Flat-fading occurs when the following conditions are met:

$$B_S << B_C \tag{2.3}$$

and

$$T_S >> \sigma_\tau, \tag{2.4}$$

where T_S is the reciprocal bandwidth (symbol period) and B_S is the bandwidth, respectively, of the transmitted signal, and σ_τ and B_C are respectively the RMS delay spread and coherence bandwidth of the channel. The effect of a flat-fading channel on a signal is described mathematically by (4.4).

Referring to Fig. 2.2, the amplitude of $s(t)$ is affected by time varying attenuation levels. Since

the channel has no excess delay, $\tau = 0$ no time dispersion of the transmitted signal occurs. In the frequency domain, although varying in time, the gain of the channel's frequency transfer function $H(f)$ remains constant over the entire bandwidth of the transmitted signal $S(f)$. Thus, no frequency selective fading occurs in the Rayleigh Flat-Fading channel and $R(f)$ represents an amplitude scaled version of $S(f)$ at any given time. Note that $H(f)_{max}$, the channel gain over the signal bandwidth, varies as a function of time according to a Rayleigh distributed amplitude PDF.

2.4.2 FREQUENCY SELECTIVE FADING

A channel induces frequency selective fading in a transmitted signal, only if the channel has a constant amplitude gain (not a function of f) and linear phase response over a bandwidth *smaller* than the transmitted signal bandwidth. Under these conditions, the reciprocal bandwidth of the transmitted signal is smaller than the multipath delay spread of the channel impulse response. Frequency selective fading occurs due to time dispersion of the transmitted signal and induces ISI in digital communication systems.

Viewed in the frequency domain, the channel becomes frequency selective where the channel gain $H(f)$ is different for different frequency components. Frequency selective fading is caused by multipath delays approaching or exceeding the symbol period of the transmitted symbols. For frequency selective channels

$$B_S > B_C \tag{2.5}$$

and

$$T_S < \sigma_\tau, \tag{2.6}$$

Different equalizer structures are used in practice to eliminate the effects of frequency selective fading. These equalizers attempt to compensate for ISI induced by the frequency selective fading channel by combining the different delayed versions of the original signal in an optimal way. Equalizer structures are designed to adapt to changing channel conditions.

2.4.3 FAST FADING

In a fast fading channel, the channel impulse response changes rapidly within each symbol period. This implies that the coherence time of the channel is smaller than the symbol duration of the transmitted signal. Fast fading causes frequency dispersion, which leads to signal distortion. A signal undergoes fast fading if

$$T_S > T_C \tag{2.7}$$

and

$$B_S < B_D, \tag{2.8}$$

where T_C is the coherence time and B_D, the Doppler spread of the channel. It is important to note that fast or slow fading is independent of flat- or frequency selective fading. Thus, the fading rate of the channel gives no information about it being a flat- or frequency selective fading channel. In practice, fast fading only occurs at very low data rates or in systems where the relative movement between the transmitter and receiver are extremely fast.

2.4.4 SLOW FADING

The channel impulse response of a slowly fading channel changes at a rate much lower than the transmitted baseband signal. It may be assumed that this channel is static over one or several reciprocal signal bandwidths. In the frequency domain, this implies that the Doppler spread is much narrower than the transmitted signal bandwidth. The conditions for a channel to be classified as slow fading are

$$T_S << T_C \tag{2.9}$$

and

$$B_S >> B_D. \tag{2.10}$$

2.5 THE SLOW, FLAT-FADING CHANNEL

In this section, the flat-fading radio channel with slowly fluctuating channel effects and Rician or Rayleigh distributed signal envelopes are discussed. This channel is used to evaluate the TS technique and its enhancements and is discussed in more detail. The three important characteristics of this channel, namely its fading rate, instantaneous frequency transfer function and signal envelope probability distributions are discussed in the following subsections.

2.5.1 FADING RATE AND FREQUENCY TRANSFER FUNCTION

The terms slow and flat-fading have been discussed in Sections 2.4.1 and 2.4.4. To summarize, each frequency component within the bandwidth of a signal transmitted through a flat-fading channel experiences the same time varying attenuation due to channel effects. Thus, the instantaneous magnitude frequency transfer function $|H(f)|$ of the flat-fading channel is flat across the transmitted signal bandwidth and the rate at which channel effects change are much slower than the rate at which the baseband transmitted signal changes.

2.5.2 STATISTICS OF THE FADING SIGNAL ENVELOPE

2.5.2.1 RAYLEIGH FADING DISTRIBUTION

The Rayleigh distribution is commonly used to describe the statistical time varying nature of the received envelope of a flat-fading signal. It is known that the sum of two quadrature Gaussian noise signals obey the Rayleigh distribution, which has a PDF given by

$$p(r) = \begin{cases} \frac{r}{\sigma^2} \exp\left(-\frac{r^2}{2\sigma^2}\right) & (0 \leq r \leq \infty) \\ 0 & otherwise, \end{cases} \tag{2.11}$$

where σ is the RMS value of the received signal amplitude before envelope detection, assuming a constant envelope sinusoidal signal was transmitted. The probability that the envelope of the received signal is smaller than a certain value R, is given by the corresponding *Cumulative Distribution Function* (CDF)

$$P(R) = \int_0^R p(r)dr = 1 - exp\left(-\frac{R^2}{2\sigma^2}\right). \tag{2.12}$$

This expression is used when the theoretical duration of an average fade below R is derived and will be referred to in Section 2.5.2.3.

2.5.2.2 RICIAN FADING DISTRIBUTION

A Rician distributed signal envelope is observed when there is a dominant, non-fading signal component present in the received fading signal. This is normally due to a *Line Of Sight* (LOS) propagation path and results in the random multipath signals being superimposed on the non-fading signal. This has the effect of adding a *Direct Current* (DC) component to the random multipath attenuation value. In the limit, as the LOS signal becomes weaker, the signal envelope PDF tends to having a Rayleigh distributed envelope (see (2.11)). The Rician distribution is given by

$$p(r) = \begin{cases} \frac{r}{\sigma^2} e^{\left(-\frac{r^2+A^2}{2\sigma^2}\right)} I_0\left(\frac{Ar}{\sigma^2}\right) & (A \geq 0, r \geq \infty) \\ 0 & otherwise. \end{cases} \tag{2.13}$$

The Rician factor K, defined as the ratio between the deterministic signal power and the variance of the multipath signal components, is given by

$$K = 10 \log_{10} \frac{A^2}{2\sigma^2} \quad dB, \tag{2.14}$$

where A denotes the peak amplitude of the non-fading signal component. From (2.14) it is evident that for $K \to -\infty$, the Rician distribution becomes equal to the Rayleigh distribution given in (2.11). Fig. 2.3 depicts the signal envelope PDFs for values of $K = -\infty$ dB (Rayleigh) and $K = 6$ dB.

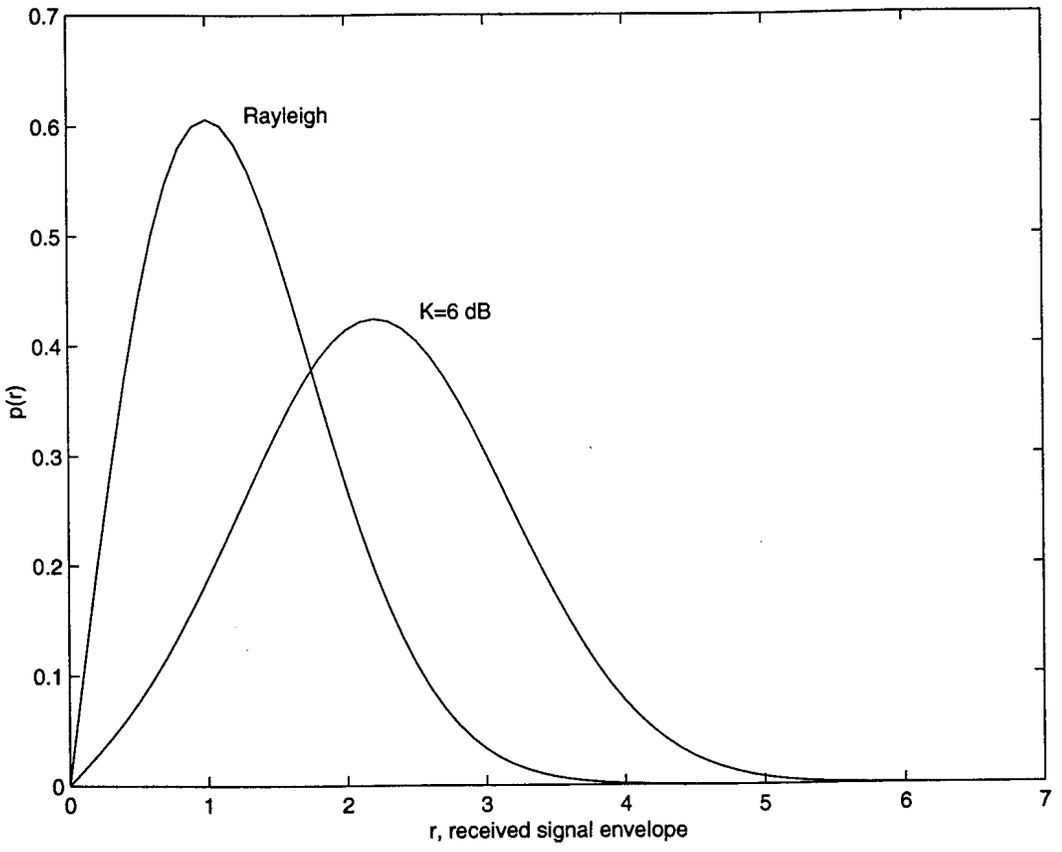

Figure 2.3: Signal envelope PDF's for different values of K, with the variance of the multipath, $\sigma^2 = 1$.

2.5.2.3 LEVEL CROSSING RATE AND AVERAGE FADE DURATION

The *Level Crossing Rate* (LCR) is defined as the expected rate at which the Rayleigh fading envelope, normalized to the RMS signal level, crosses a specified level ρ, in a positive-going direction. The number of level crossings per second is given by

$$N_R = \int_0^\infty \dot{r} p(R, \dot{r}) d\dot{r} = \sqrt{s\pi} f_m \rho e^{-\rho^2}, \tag{2.15}$$

where f_m is the maximum Doppler shift induced by the channel and $\dot{r}$ is the slope of the signal envelope. The average fade duration is defined as the period of time for which the received signal is below a certain level (normalized level ρ). For the Clarke Doppler spectrum discussed in Section 2.6.1, the average fading duration below ρ is given by

$$\bar{\tau} = \frac{e^{\rho^2} - 1}{\rho f_m \sqrt{2\pi}}. \tag{2.16}$$

This parameter gives an indication of the number of consecutive symbols severely affected by fading bursts. This is important to the TS technique as it determines the amount of time diversity required to effectively combat the effects of deep signal fades.

2.6 STATISTICAL FADING CHANNEL MODEL

The TS technique analyzed in this dissertation is evaluated using an adapted statistical channel model originally proposed by Clarke and discussed in [11]. This model assumes a fixed transmitter with a vertically polarized antenna. The field at the receiver is assumed to comprise of N azimuthal plane waves, each with arbitrary phases and angles of arrival, with equal average amplitudes. The equal average amplitude assumption only holds when there is no LOS signal component present. The adapted channel model is shown in Fig. 2.4 and is implemented as two multiplicative lowpass Gaussian processes influencing the in-phase and quadrature-phase components of the transmitted signal respectively. The LOS parameter allows for the presence of a specular path and determines the power ratio between the specular path and the multipath components of the received signal. Information on the normalization of the channel parameters to ensure a unity channel gain is given in Appendix A.

The multiplicative fading process as implemented in Fig. 2.4 can be described mathematically as

$$s'(t) = a(t)s(t)e^{j\psi(t)}, \tag{2.17}$$

where $\psi(t)$ is a uniformly distributed phase angle and $a(t)$ is a Rayleigh or Rician distributed amplitude attenuation variable.

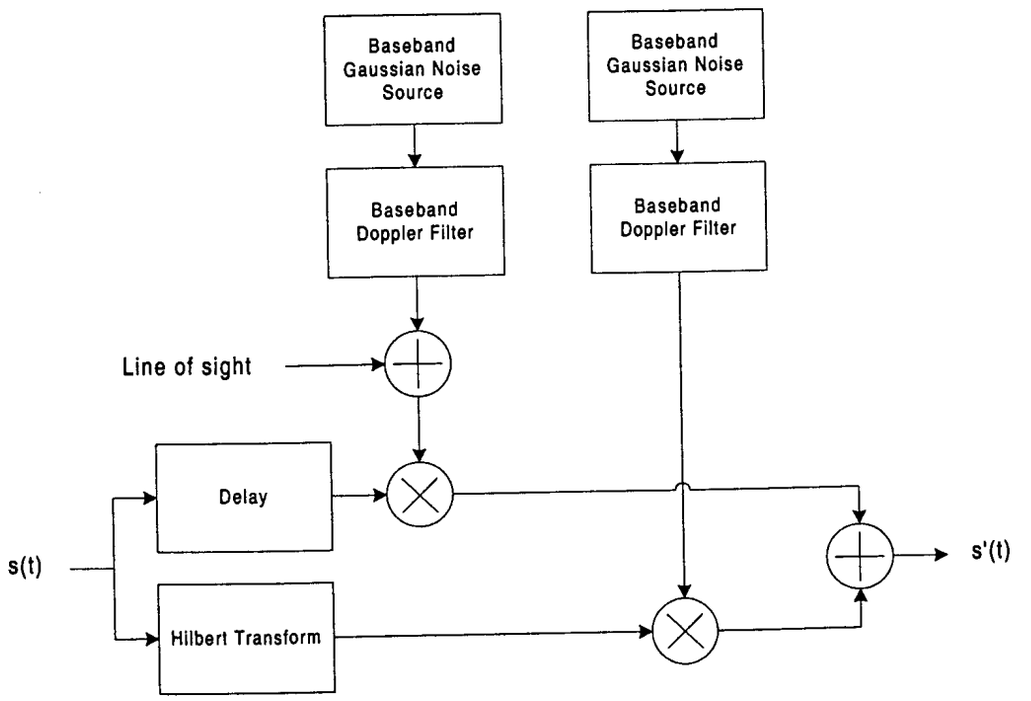

Figure 2.4: Modified Clarke fading channel model without additive white Gaussian noise.

2.6.1 DOPPLER POWER SPECTRUM

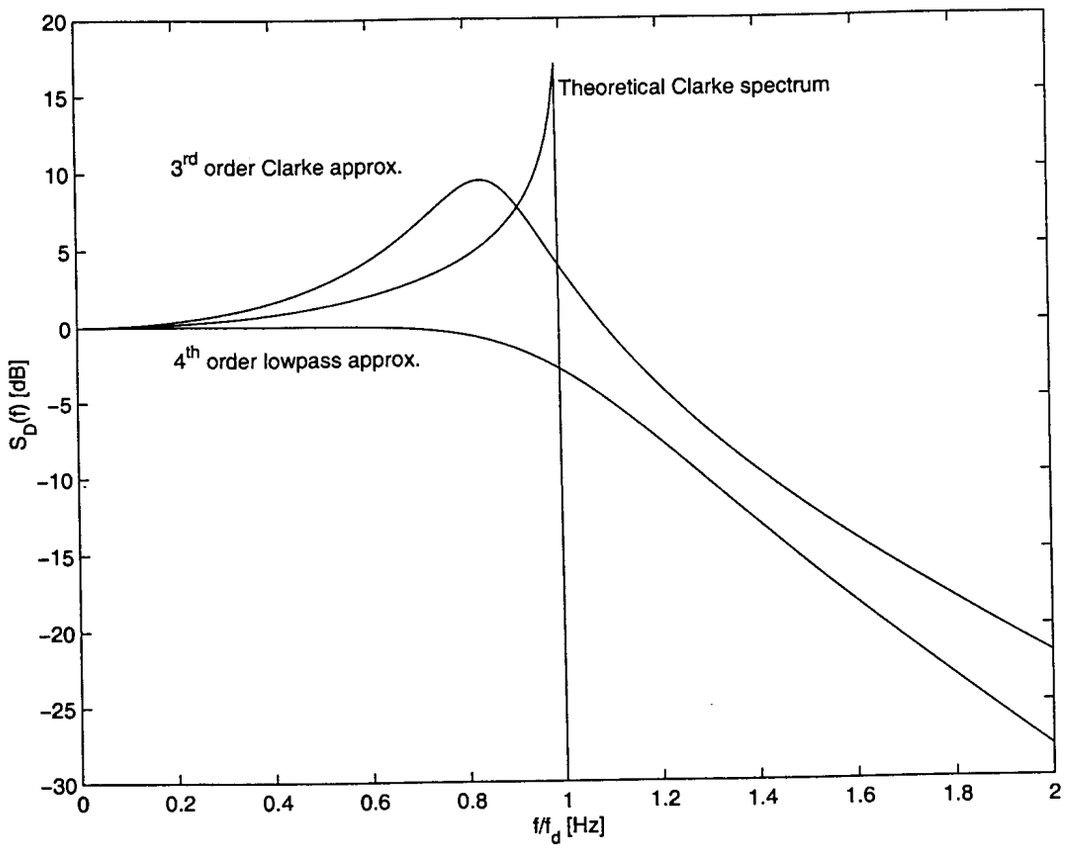

Figure 2.5: Theoretical Clarke Doppler spectrum with a superimposed 3^{rd} and 4^{th} order approximation.

Under the specific assumptions of a vertical $\lambda/4$ antenna and a uniform phase distribution over 0 to 2π, the spectrum of the fading process in the Clarke model is given by

$$S(f) = \frac{1.5}{\pi f_m \sqrt{1 - \left(\frac{f - f_c}{f_m}\right)^2}}, \tag{2.18}$$

(2.18) gives the familiar U-shaped Doppler power spectrum. It is difficult to obtain this spectrum accurately in software simulators, but according to [12], it can be approximated with reasonable accuracy by a *Low Pass Filter* (LPF) process with $f_{3dB} = f_m$, where f_m is the maximum Doppler shift. This approximation affects the average fade duration below specified signal thresholds and other higher order statistics of the fading process. Since parameters such as the average fading duration plays a role in the performance of the TS system, this was not acceptable.

A more accurate 3^{rd} order approximation of the Doppler spectrum, was proposed by [14] (see Fig. 2.5). This, and other methods of approximating the Doppler power spectrum is discussed in Section

A.2. The altered Doppler spectra does however have an effect on the duration of fade crossings and other higher order fade statistics. This needs to be taken into account when theoretical fade durations are compared with the measured simulation values.

2.7 SUMMARY

This chapter provided some background information on the mobile communication channel and commenced by giving a general description of the small-scale radio propagation path. The effects associated with multipath propagation were briefly mentioned and reasons for neglecting large-scale propagation effects were given. Some factors influencing the severity of small-scale fading effects were discussed and the most important parameters describing these effects were mentioned. The Rayleigh flat-fading channel that was used to evaluate the performance of the TS technique and its enhancements were discussed in detail. The emphasis of this discussion fell on the fading signal's envelope PDF and fading statistics, which plays an important role in the performance of the TS system. A theoretical expression for the average duration of a fade below a specified level was given (see Section 2.5.2.3). This is an important parameter, determining the performance of the TS technique in flat-fading channels. Finally, the model for the Rayleigh flat-fading channel used in this dissertation was described. This model was adapted from the original model proposed by Clarke [11]. Additional information regarding the implementation of the channel model is given in Appendix A.

CHAPTER THREE

THE TIME SPREAD CONCEPT

3.1 CHAPTER OVERVIEW

The improved TS technique described in this dissertation is based on the TS system proposed by [6, 1, 7]. This chapter gives some background to the TS technique and describes some of the academic contributions made during the completion of this dissertation. The diversity principles used by the TS technique to limit the effects of flat-fading in a radio channel is explained in the first section of this chapter. Since suitable spreading sequences plays an important role in the performance of the TS technique, the second section deals with the design and selection of these sequences. A family of genetic spreading sequences have been proposed by [6], p 32, that showed potential for use in a TS system. These sequences are limited in length, thus limiting their time diversity properties. A technique to increase the time diversity obtained from these sequences are proposed in Section 3.4. Section 3.5 describes the structure of a basic TS transmitter without any enhancements, while the following section describes the accompanying TS receiver structure. The chapter concludes with a brief summary of the most important characteristics of the TS technique.

3.2 SIGNAL DIVERSITY OBTAINED THROUGH TIME SPREADING

3.2.1 SIGNAL DIVERSITY

When dealing with the effects of flat-fading, an alternative to increased transmitted power is the use of multiple-receiver techniques, categorized under the name diversity [3, 16, 17]. Known diversity techniques include: space, frequency, direction-of-arrival, polarization, time, and multipath diversity. The standard approach to diversity is based on the fact that, with several diversity branches, be it space, frequency or time diversity, the probability that the signal will fade on all branches simultaneously can

be made small. Another approach would be to observe that under fairly general conditions, a channel affected by fading can be turned into an AWGN channel by increasing the number of diversity branches. This is confirmed by the central limit theorem which states that the sum of a sufficient number of statistically independent random variables with identical probability distributions approaches a Gaussian distribution [18]. Since diversity techniques are aimed at combating the effects of fading on a communication system, it should be clear that the relative advantage obtained from a diversity scheme will become lower as the channel moves away from a Rayleigh fading towards a Rician fading channel.

All diversity techniques rely on the fact that the same information is transmitted on different diversity branches, where each branch ideally suffers from an independent fading process. Different diversity branches can be obtained using one of, or a combination of, the following techniques:

- **Spatial diversity** - Multiple transmitter and/or receiver antennas transmit and receive the same information. These antennas are placed at different physical locations thereby creating independent diversity branches. It is often a complex task to obtain sufficient spatial diversity to ensure statistically independent diversity branches, especially in portable transceivers.
- **Frequency diversity** - Different carrier frequencies are used to transmit the same information, creating different diversity branches. The carriers should be separated by at least one multiple of the channel's coherence bandwidth B_C [Hz]. Good diversity is obtained from this technique, but the increase in the effective signal bandwidth is undesirable.
- **Time diversity** - With conventional time diversity techniques the same information is transmitted in different times slots that are separated by a period greater than the channel's coherence time T_C [s]. This method increases the effective signal bandwidth and introduces delays in the signal. While the TS technique also introduces delays in the system. Ignoring the slight bandwidth increase required by channel estimation techniques, TS does not increase the original information signal bandwidth requirements.

The large number of diversity techniques gives rise to an even larger number of possible implementations which falls beyond the scope of this dissertation. Good references on diversity techniques with the emphasis on spatial diversity can be found in [16, 5, 19].

3.2.2 DIVERSITY COMBINING

Important to any diversity technique is the method by which the signals from the different diversity branches are combined. The three most popular diversity combining techniques are:

- **Selection combining** - Here, only the branch with the best instantaneous SNR is selected as input to the remaining part of the receiver. This technique requires *Channel State Information*

(CSI) at the receiver but is not optimal since usable information regarding the fading signal is discarded.

- **Equal gain combining** - The signals from all the diversity branches are summed with equal weights to form a composite signal used in the remaining part of the receiver and no CSI is needed. This is a suboptimal method for combining the different diversity branches, since all the branches contributes the same amount of additive noise in the receiver while their contributions to the desired signal power are not equal.

- **Maximal-ratio combining** - A linear combination of the weighted signals from each diversity branch is used as input to the rest of the receiver. The signals from each diversity branch are weighted according to the instantaneous SNR of that branch. This method maximizes the overall average SNR, but requires CSI for all the diversity branches.

3.2.3 TIME SPREAD DIVERSITY

With the TS technique, the energy of each data symbol is spread in time over a period much longer than T_C, the coherence time of the channel. This implies that, while part of the data symbol energy may be lost due to a deep fade, a large part is unaffected by the fade and the original data symbol can be estimated from the remaining signal energy. The term data symbol is used instead of logical bit, since the input to the TS module in the transmitter may be any *Pulse Amplitude Modulation* (PAM) symbol. This is different from [6], where only binary data symbols are considered for use with the TS technique.

The basic TS receiver makes no distinction between portions of the received signal affected by fading and portions not affected by fading. The basic TS receiver can therefore be approximated by an equal gain diversity combining system (see Section 3.2.2). A more complex TS receiver is described in Section 4.5.4. This receiver structure selectively weighs the TS symbols with the inverse of the fading depth before estimating the original data symbol. This technique implements a system that approximates a maximal-ratio combining diversity receiver.

The TS technique distributes the data symbol energy uniformly in time using a spreading sequence. The term sequence and code are used interchangeably and refers to a set of elements (chips) making up a code or sequence. Each data symbol's energy is spread in time by transmitting an orthogonal spreading sequence, weighed by the data symbol's phase and amplitude, instead of the original data symbol. The spreading sequence consists of N chips, each with a duration equal to the original data symbol. Thus, an original data symbol with duration T_S, is transmitted over a period of $N.T_S$ [s] with the energy per chip equal to $1/N$ times the energy of the original data symbol energy, E_S carried by each original data symbol. Since a new data symbol must be transmitted every T_S seconds, the chips

from N - 1 previous spreaded data symbols tend to overlap in time. This process is illustrated in Fig. 3.1. The figure shows the spreading sequences associated with each data symbol. The polarity and amplitude scaling of each spreading sequence is determined by its corresponding data symbol. These overlapping sequences from different data symbols accumulate to form a composite signal that is transmitted over the radio channel after carrier modulation.

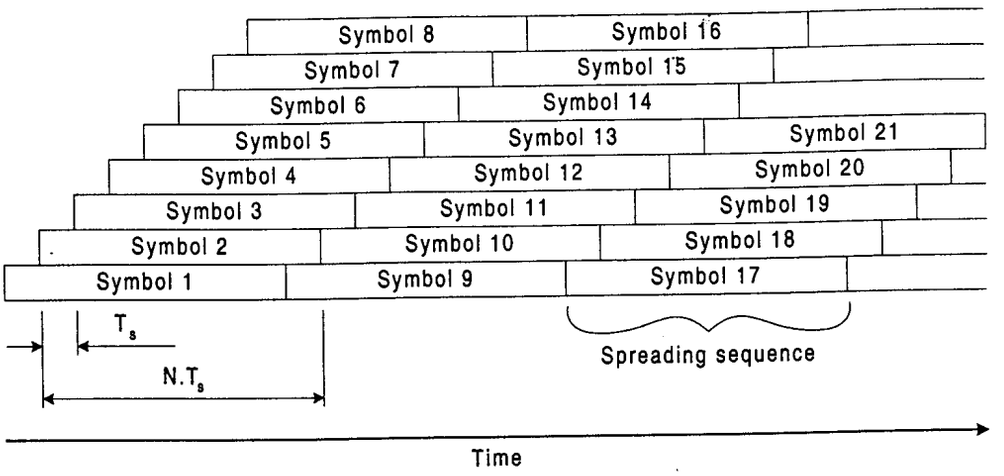

Figure 3.1: TS concept of overlapping spreading sequences.

In the TS receiver, the signal corrupted by fading and noise is applied to a cross-correlator that estimates the original transmitted data symbols by correlating the received signal with the known spreading sequence. The TS technique makes use of a only one spreading sequence to distribute the energy from every data symbol in time. Since the spreading sequences overlap in time, it must exhibit very good *Aperiodic Auto-Correlation* (AAC) properties to prevent ICI from occurring between the sequences associated with nearby data symbols. Effective spreading sequences are extremely important to ensure the success of the TS technique. Some popular spreading sequences and their correlation characteristics are discussed in the next section. From these, the complex spreading sequences proposed by Dukic [20] are shown to be best suited for use with the TS technique.

3.3 TIME SPREAD SEQUENCES

It is mentioned in Section 3.2.3 that effective spreading sequences are crucial to the performance of a TS system. Ideally, suitable spreading sequences must have the following important characteristics:

- The spreading sequence must distribute the data symbol energy uniformly over the entire sequence duration.

- The correlation properties of the spreading sequence must be such that no ICI occurs in the cross-correlation process.
- The cross-correlation characteristics of spreading sequences used for TS purposes must have a low sensitivity for the effects of fading.

From [6], p 39, the Dukic spreading sequence family [20], originally designed for *Radio Detection And Ranging* (RADAR) applications, are most suitable for use in a TS system and will receive the focus of this section. Other sequences that will be mentioned briefly (from [6], p 22) are ordinary binary sequences, numerically synthesized sequences, *Frank Zadoff Chu* (FZC) sequences and *Constant Amplitude Zero Auto-Correlation* (CAZAC) spreading sequences.

In reference [6], p 19, has developed a *Figure Of Merit* (FOM) to compare different sequences with each other when evaluating the suitability of a particular spreading sequence for use in a TS system. First, an ICI factor (ICI in [6], pp 18) is defined as

$$ICI_{max} = 2\sum_{i=0}^{N-1}\left|\sum_{j=0}^{i} c_i c_j^*\right| \quad ; \; i \neq j. \tag{3.1}$$

This corresponds to the maximum possible non-normalized ICI that may occur due to sequence overlap. (3.1) resembles the sum of the modulus of the sidelobes of the AAC function of a sequence. The *Figure Of Merrit* (FOM) is then defined as the difference between the maximum AAC peak and the ICI_{max} value.

$$M = \frac{\sum_{i=0}^{N-1} c_i c_j^* - ICI_{max}}{N}, \tag{3.2}$$

where M denotes the minimum effective correlation peak in the receiver, normalized by the sequence length. Error free communication is only possible when $M > 0$. Since M gives an indication of the noise margin after correlation in the receiver, it is desirable that M be as large as possible. With M being normalized by the sequence length, it can be used as a measure to compare the different spreading sequences of different lengths on an equal base.

Finally, the *Normalized Fade Sensitivity Factor* (NFSF), taken from [6], p 49, is defined to give an indication of the performance of different spreading sequences in a fading channel. This is an important performance criteria for sequences used by a TS system since the TS system must be designed to perform optimal in a fading environment.

$$NFSF = \frac{\sum_{i=0}^{N-1}\sum_{j=0}^{i} |\mathrm{Re}\{c_i c_j\}|}{N^2} \quad ; i \neq j. \tag{3.3}$$

The NFSF does not take into account the ability of longer sequences to span isolated fades more effectively than shorter sequences. It does however allow for the comparison of different sequences,

based on their inherent sensitivity to fading. Since the NFSF gives an indication of the sensitivity of a spreading sequence to fading, it is desirable that NFSF be as low as possible.

3.3.1 BINARY SPREADING SEQUENCES

Binary sequences such as Gold and Kasami sequences exist which show good *Cross Correlation* (CC) as well as periodic *Auto-Correlation* (AC) properties, but poor AAC values. Barker sequences are known to have the best AAC properties of all binary spreading sequences. Barker sequences exhibits AAC sidelobes no greater than $1/N$, with N the sequence length. Binary Barker sequences of seven different lengths up to a length of thirteen are known. The time-energy distribution capabilities of these sequences are therefore limited. Techniques used to improve the time diversity obtained from spreading sequences will be discussed in Section 3.4. The FOM according to (3.2), for Barker sequences of length 3, 5, 7, 11 and 13 are greater than zero. These sequences can therefore be used in TS systems, but since their noise margins are very low, fading and AWGN would render them useless. Since Barker sequences are the optimal binary sequences as far as AAC properties are concerned, it may be concluded that no other binary *Pseudo Noise* (PN) sequence will have a better FOM. Binary PN sequences are therefore not suitable for use in TS systems.

3.3.2 NUMERICALLY SYNTHESIZED SEQUENCES

A Genetic Algorithm by which sequences with elements taken from a specified set of values and good correlation properties can be found, are described in [6], p 32. This algorithm produces sequences with good FOM values, indicating suitability for TS use.

The process of finding long spreading sequences are however very time consuming and divergent, thus only sequences with lengths up to fifteen were generated (see Table 3.1). However, short spreading sequences provide very little time diversity and are therefore not suitable for use in a TS system. The technique described in Section 3.4 has been found to provide an effective method by which the potential time diversity rendered by short spreading sequences can be considerably increased. Following this procedure, spreading sequences generated by numerical synthesis could indeed be used effectively in TS systems.

3.3.3 *FRANK ZADOFF CHU* (FZC) SEQUENCES

FZC sequences, [21, 22] exhibit perfect periodic AC properties and are a class of *Generalized Chirp Like* (GCL) sequences, [23]. FZC sequences are complex spreading sequences, thus each sequence has a real and imaginary part. Although FZC sequences exhibit perfect periodic AC properties, their AAC functions show correlation sidelobes apart from the main lobe. These correlation sidelobes are small relative to the correlation peak, but nevertheless result in the degradation of a TS system's

Table 3.1: Numerically Synthesized Sequences taken from [6], pp 32.

Length	Sequence Elements	FOM	Location Method
4	1,1,2,-2	1.00	Exhaustive Search
5	1,2,2,-2,1	2.40	Exhaustive Search
6	1,-2,1,2,1,1	0.67	Exhaustive Search
7	2,2,1,-1,-1,2,-2	1.29	Genetic Algorithm
8	1,-2,2,-1,-1,1,2,1	0.63	Genetic Algorithm
9	-1,2,-2,2,2,-2,-2,-2,-1	1.33	Genetic Algorithm
10	-1,1,-2,2,-2,-2,2,2,1,1	0.40	Genetic Algorithm
11	-2,-2,-1,-2,-2,2,2,-2,1,-2,2	1.82	Genetic Algorithm
13	1,1,1,1,1,-1,-1,1,1,-1,1,-1,1	0.08	Genetic Algorithm
15	-1,1,2,1,-2,-1,2,-1,2,-1,-1,-1,-2,-1,-1	0.27	Genetic Algorithm

performance. This performance degradation is shown in [6], pp 72. From this we conclude that FZC sequences are not ideally suited for TS applications. It will however be shown that the use of ICIC techniques can significantly improve the sequence performance in AWGN and fading.

3.3.4 CAZAC SEQUENCES

CAZAC sequences are a family of complex spreading sequences for which the real part of its periodic AC function is perfect. Like the FZC sequences, the AAC function of this family of sequences also exhibits correlation sidelobes which degrades the performance of a TS system employing these sequences. ICIC strategies can be used to improve the performance of these sequences, when used in a TS system.

3.3.5 DUKIC SEQUENCES

Dukic sequences are a class of complex spreading sequences that were originally designed for use in Spread-Spectrum Radar applications [20]. These sequences can not be used in CDMA systems, because unlike FZC, CAZAC and binary Gold or Kasami sequences, there is only one Dukic sequence for a specific sequence length. Thus different sequences of the same length can not be assigned to different users for user separation purposes. What makes the Dukic sequence family attractive for use in TS systems is the fact that the real part of its AAC function is perfect. Since the AAC function of a Dukic sequence exhibits no sidelobes, no ICI occur when these sequences are used in a TS system operating in AWGN. This property makes Dukic sequences superior to all other spreading sequences when applied in a TS scenario. The superior performance of Dukic sequences in the TS scenario is confirmed by BER results presented in [6], pp 77. Thus, the Dukic spreading sequences are the

sequence family of choice for use in the TS system described in this dissertation. The correlation properties and generation of the Dukic sequences will be discussed in the following sections.

3.3.5.1 CORRELATION PROPERTIES

The real part of the AAC function for a Dukic sequence is a δ function. To evaluate the AAC function of a Dukic sequence, let $C(k)$, $k = 1, 2, 3, ..., N$, be the N complex valued elements of the sequence, with $C(k) = 0$ for all other values of k. The real part of the AAC function of a Dukic sequence of length N is given by:

$$\begin{aligned} U &= \mathrm{Re}\left\{\mathrm{AAC}\left(C(k)\right)\right\} \\ &= \mathrm{AAC}\left(\mathrm{Re}\left\{C(k)\right\}\right) + \mathrm{AAC}\left(\mathrm{Im}\left\{C(k)\right\}\right). \end{aligned} \tag{3.4}$$

This process is illustrated in Fig. 3.2 for a length $N = 64$ Dukic spreading sequence. Observe from Fig. 3.2 that the AACs of the real and imaginary part sequences, although not perfect, add to give a perfect real part AAC function for the Dukic sequence. This occurs because the AAC sidelobes of the real part and imaginary part Dukic sequences are negatives of each other and therefore cancels out completely when summed. This property enables the TS receiver to perfectly recover each transmitted data symbol from the overlapping spreading sequences in the absence of noise and fading.

3.3.5.2 SEQUENCE GENERATION

The Dukic sequence is derived from the condition that the real part of its AAC function should be a δ function. For a length N sequence, this condition can be written as [20]:

$$\sum_{i=0}^{N-1}\sum_{k=0}^{N-1} z^{-(i-k)}\mathrm{Re}\left\{\exp[j(\psi_i - \psi_k)]\right\} = 0 \quad , i \neq k. \tag{3.5}$$

This leads to $N-1$ equations with N unknowns. Substituting $\Delta_i = \psi_i - \psi_k$, a system with $N-1$ equations and $N-1$ unknowns is obtained which can easily be solved for small values of N. The solution for $N = 4$ is given by:

$$\Delta_1^{(1)} = 0, \quad \Delta_2^{(1)} = \pi/2, \quad \Delta_3^{(1)} = \pi. \tag{3.6}$$

Assuming $\psi_1 = 0$, the other values of ψ can be obtained from

$$\psi_{i+1} = \psi_i + \Delta_i, \quad i = 1, 2, 3, ..., N-1. \tag{3.7}$$

And the N complex elements of the Dukic sequence are given by

$$C(k) = \exp(j\psi_k), \quad k = 1, 2, 3, ..., N \tag{3.8}$$

with $j = \sqrt{-1}$.

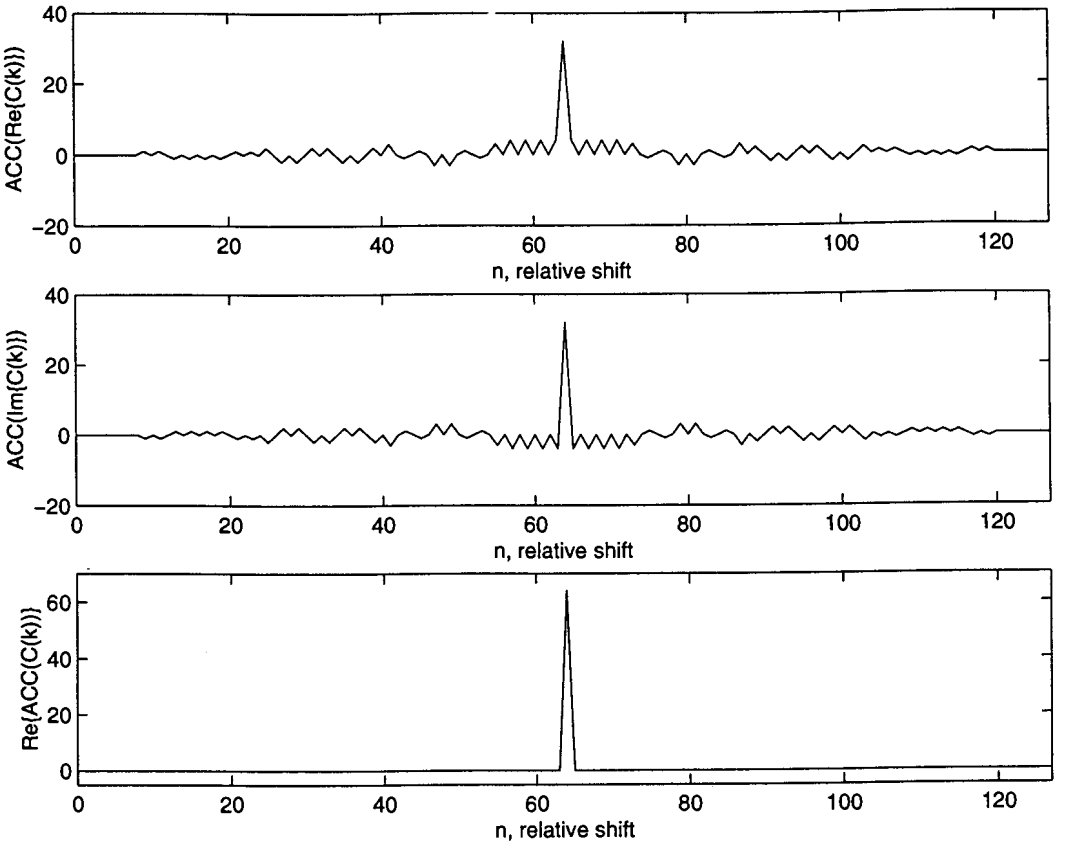

Figure 3.2: Real part AAC function composition for a $N = 64$ Dukic sequence.

With one of the solutions $\Delta_i^{(1)}, i = 1, 2, 3, ..., N-1$, given by (3.6), it is possible to obtain the vector $\Delta_i^{(2)}, i = 1, 2, 3, ..., 4N-1$, which is the solution of the system with $4N-1$ equations. The vairable $\Delta_i^{(2)}$ is related to $\Delta_i^{(1)}$ by the following equations:

$$\begin{aligned} \Delta_i^{(2)} &= 0, & i &= 1, 3, 5, ..., 2N-1 \\ \Delta_{2i}^{(2)} &= \Delta_i^{(1)}, & i &= 1, N-1 \\ \Delta_{2N}^{(2)} &= \pi/2 \\ \Delta_{4N-i}^{(2)} &= \pi - \Delta_i^{(2)}, & i &= 1, 2N-1 \end{aligned} \tag{3.9}$$

(3.10)

By repeated use of (3.10) it is possible to obtain solutions for very long code sequences. Note that only sequences of length $N = 2^{2i}, i = 1, 2, 3, ...$ can be obtained using this method.

3.4 IMPROVED TIME DIVERSITY

When the channel fading rate is very slow compared to the channel symbol rate, very long spreading sequences are necessary to obtain sufficient time diversity. Long spreading sequences on the other

hand, necessitates very large correlator structures in the TS receiver. This is not desirable since it increases the receiver size and complexity.

An efficient method by which the time diversity of a spreading sequence can be increased, while limiting the size of the correlator structures in the TS receiver, is described in the following paragraphs. This technique is documented as one of the main contributions made by this dissertation, since it significantly reduces the implementation complexity required by the TS technique.

The time diversity obtained from a short spreading sequence can be increased by expanding the sequence in time. The temporal expansion is obtained through zero-interpolation i.e., by inserting zero amplitude elements between successive original sequence elements. This process is illustrated in Fig. 3.3 for a length $N = 8$ sequence. Examining Fig. 3.3, it is clear that an ordinary spreading sequence

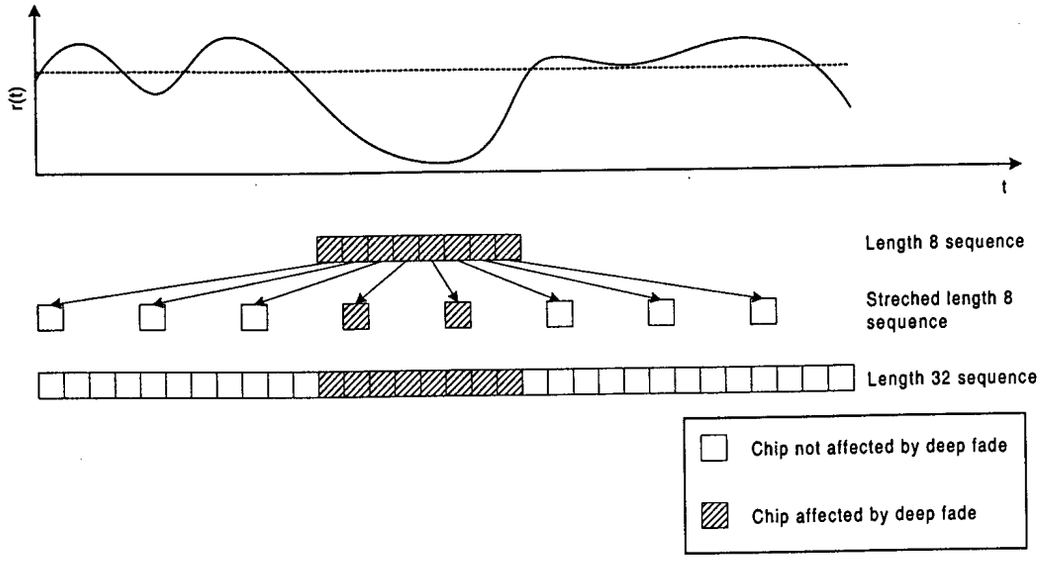

Figure 3.3: Increased sequence diversity obtained by stretching existing $N = 8$ TS sequence to a $N = 32$ sequence.

of length $N = 8$, would be ineffective against a fade such as that shown in the figure, since the entire sequence is attenuated during the fade. For a length $N = 32$ sequence, as shown at the bottom of Fig. 3.3, 75% of the sequence is unaffected by the fade. Thus, the original transmitted data symbol can be estimated from the remaining part of the sequence with a high degree of accuracy. The correlation process in the TS receiver would however require 32 multiplications and additions.

The same time diversity obtained from a length $N = 32$ sequence, can be obtained by temporal expansion of an ordinary length $N = 8$ sequence. The expansion process illustrated in Fig. 3.3

requires three zero-amplitude sequence elements to be inserted between every two elements of the length $N = 8$ sequence. This results in a sequence with the *same* temporal span than a length $N = 32$ sequence, but with *four* times less multiplications and additions needed in the correlator of the TS receiver structure. Note that only 25% of the stretched spreading sequence is affected by the deep fade, the same percentage as for the length $N = 32$ sequence. Thus, none of the gains obtained from time spreading were compromised by stretching a short spreading sequence to increase its time diversity. The latter is confirmed by simulation results in Section 6.8, Figures 6.18 to 6.20. Note that, unlike interleaving techniques that merely shuffles the order of symbols in time to create some time diversity on codeword level, the TS technique temporarily expands each symbol. This introduces time diversity on symbol level.

In general, a spreading sequence of length N can be expanded in time to have the same temporal span than a length $k.N$ sequence by inserting $k - 1$, zero-amplitude sequence elements between every two successive sequence elements of the original sequence(called primary sequence values). As mentioned in the previous paragraph, this results in k-times less multiplications and additions needed in the TS receiver's correlator structure. Note that an extremely short sequence can not be stretched indefinitely to increase its temporal span, since this would limit the TS technique's ability to Gaussianize the Rayleigh fading channel. This is discussed in Section 3.2.1, where it is reiterated that the Central Limit Theorem only holds when a sufficiently large number of statistically independent random variables are summed. By expanding a spreading sequence that is too short, the sequence has very little elements and provides too little statistically independent random variables to effectively Gaussianize the Rayleigh fading channel. This phenomena is confirmed by simulation results in Chapter 6.

An important added advantage of using the expanded TS sequences instead of long non-expanded sequences, is that the number of quantization levels required in the system's transmitter and receiver structures are also divided by k. This makes it possible to use less expensive DAC and ADC devices when implementing the TS system. Using less quantization levels reduces the number of resources required for mathematical operations and increases the speed with which they can be executed.

Fading affects the amplitudes of the individual elements in a spreading sequence. This distorts the correlation properties of the spreading sequence (code) and results in nearby time spreaded data symbols to interfere with each other. Intuitively, less sequence elements that overlap in time results in less ICI. When using a shorter expanded spreading sequence instead of a normal spreading sequence, less spreading sequence elements overlap in time. It will be shown in Chapter 6 that this indeed improves the performance of a TS system under certain conditions (see Figures 6.18 to 6.20).

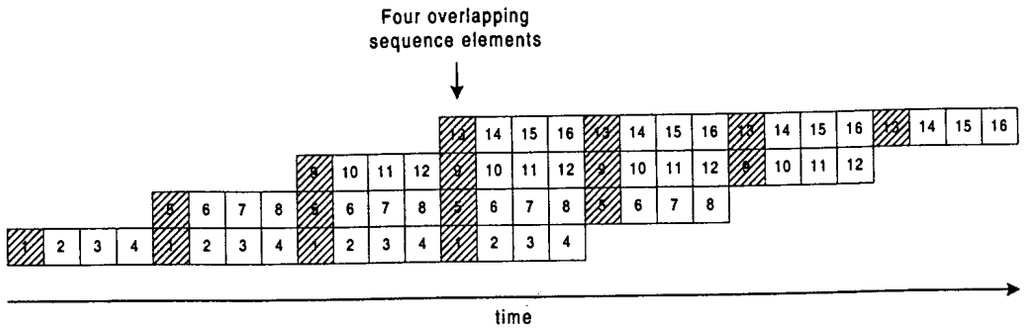

Figure 3.4: Less overlapping sequence elements for an four times expanded length $N = 4$ TS sequence.

Fig. 3.4 illustrates the effect of expanding an ordinary length $N = 4$ sequence to obtain the time diversity properties of a length $N = 16$ sequence. Note that the maximum number of overlapping sequence elements are equal to four, the length of the non-expanded sequence. Thus, by stretching a spreading sequence in time, the same time diversity can be obtained as for a long spreading sequence, but now with less ICI. Note that in Fig. 3.4, sequence elements with the same numbers belong to the same sequence and are associated with a specific data symbol. Henceforth, expanded spreading sequences will be described by their name, fundamental sequence length x and expansion factor y, according to *Sequence name-x-y*.

3.5 TIME SPREAD TRANSMITTER

The basic TS transmitter is described in this section. Refer to Chapters 4 and 5 for descriptions of the adaptations needed to support channel estimation and FEC coding in this basic TS transmitter. Fig. 3.5 illustrates the building blocks of the basic TS transmitter.

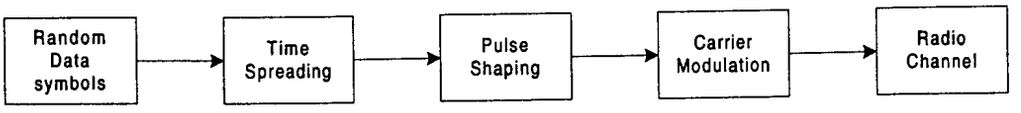

Figure 3.5: The basic TS transmitter.

3.5.1 RANDOM DATA SYMBOLS

Random data symbols originating from any data source may be applied to the TS module. Complex spreading sequences are used in a balanced spreading structure. Thus, the same data symbol must

be applied to both the in-phase and quadrature-phase branches of the TS module. Consequently, only one-dimensional *Pulse Amplitude Modulation* (PAM) symbols can be applied to the spreading module of a TS system employing complex spreading sequences. The use of higher order modulation techniques such as Q^2PSK may be considered to allow the use of multi-level and/or multi-phase symbols with the TS technique [24]. Alternatively, real valued spreading sequences can be used which makes it possible to apply any multi-level and/or multi-phase symbol to the TS module.

3.5.2 TS MODULE

The TS module performs the time spreading in the transmitter of a TS system. The basic building block of this module is a multiply and accumulate function with a delay element. When sequentially linked together, these building blocks form a multiply and accumulate buffer as illustrated in Fig. 3.6. When a complex spreading sequence is used, two of these structures operate in parallel, both receiving the same input symbol, but spreading with the real and imaginary part of the TS sequence respectively (see Fig. 3.7). The output of each delay element in Fig. 3.6 is given by the following general expression:

$$a'_k = a_k + s_n.\mathrm{Re}\{C_k\} \quad ,k = 1,2,3,...,N \tag{3.11}$$

where a'_k represents the new output value of the k^{th} delay element, a_k the current delay element output value, s_n the symbol applied to the TS module at that instant and $\mathrm{Re}\{C_k\}$ the real value of the k^{th} sequence element. The same applies to the quadrature-phase branch of the TS module, where the imaginary part of the complex spreading sequence is used instead.

After each new input symbol period, the value of s_n changes and the contents of the delay line is shifted one element to the right according to

$$\begin{aligned} a_1 &= 0 \\ a_k &= a'_{k-1} \quad ,k = 2,3,4,...,N. \end{aligned} \tag{3.12}$$

Here, a'_N is the output of the TS module that is applied to the baseband pulse shaping filter. This multiply, accumulate and shift structure resembles a *Finite Impulse Response* (FIR) filter implementation, where each new symbol represents an impulse that excites the filter. The output of one branch in the TS module is given by

$$b_n = \begin{cases} \sum_{k=1}^{n+1} s_{n-k-1}.c_k & ,n < N \\ \sum_{k=1}^{N} s_{n-k-1}.c_k & ,n \geq N, \end{cases} \tag{3.13}$$

where c_k is a real or imaginary element of either a complex or non-complex spreading sequence. To simplify notation for stretched spreading sequences, let N denote the length of the stretched sequence.

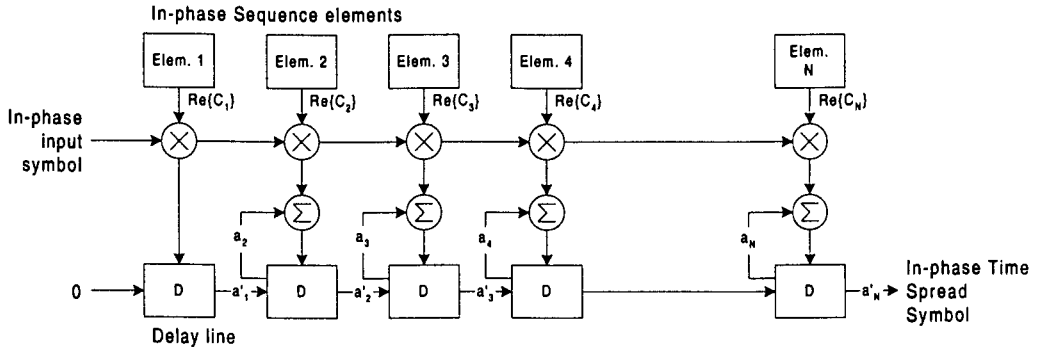

Figure 3.6: In-phase multiply and accumulate buffer of the TS transmitter module.

When a non-complex spreading sequence is used, the TS structure may be implemented in several ways:

1. The same spreading sequence may be used on both the in-phase and quadrature-phase branches of the TS module, with the same data symbol used as input to both branches. This would allow the application of M-PAM symbols to the TS module, where $M \geq 2$.

2. Only the in-phase branch of the TS module is used. This would also allow the application of M-PAM symbols to the TS module, where $M \geq 2$.

3. When using the same real valued spreading sequences on both the in-phase and quadrature-phase branches of the TS system, different data symbols can be applied to each branch. This would allow the use of any *M-Quadrature Amplitude Modulation* (QAM) signal constellation as input to the TS module.

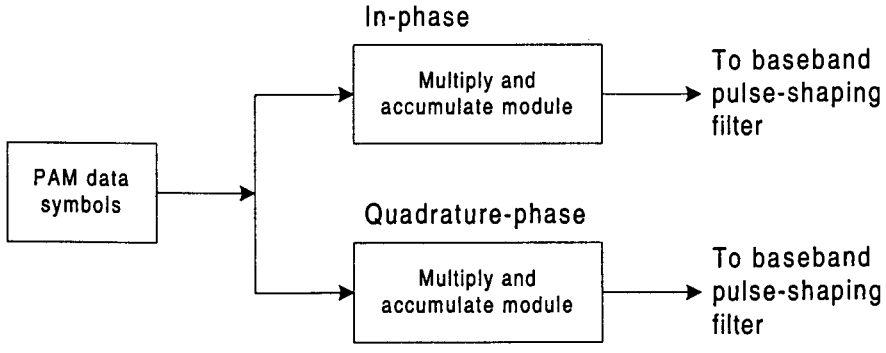

Figure 3.7: A TS module with two parallel multiply, accumulate and shift structures employing complex spreading sequences.

3.5.3 PULSE SHAPING

The output of each TS module is converted to impulses that are applied to a *Finite Impulse Response* (FIR) pulse shaping filter aimed at conserving transmission bandwidth by limiting the baseband signal bandwidth of the in-phase and quadrature-phase signals separately. The pulse shaping filter also acts as one part of a matched filter pair aimed at maximizing the peak symbol SNR after matched filtering in the receiver. A popular matched filter pair that limits the transmission bandwidth, while ensuring maximum eye pattern openings in the receiver, are the square root Nyquist filter pair. The impulse response $h(t)$, of the square root Nyquist filter is given by

$$h(t) = \frac{\sin\left(\frac{\pi(1-\alpha)t}{T_S}\right)}{\pi t\left(1-\left(\frac{4\alpha t}{T_S}\right)^2\right)} + \frac{4\alpha\cos\left(\frac{\pi(1+\alpha)t}{T_S}\right)}{\pi T_S\left(1-\left(\frac{4\alpha t}{T_S}\right)^2\right)} \tag{3.14}$$

and the frequency transfer function $H(f)$ for this filter is given by

$$H(f) = \begin{cases} 1 & ,|f| < \frac{1-\alpha}{2T_s} \\ \cos\left[\frac{2\pi T_s}{4\alpha}\left(|f| - \frac{1-\alpha}{2T_s}\right)\right] & ,\frac{1-\alpha}{2T_s} \leq |f| \leq \frac{1+\alpha}{2T_s} \\ 0 & ,|f| > \frac{1+\alpha}{2T_s}. \end{cases} \tag{3.15}$$

T_s denotes the symbol period and α, the spectral roll-off factor of the Nyquist filter. The parameter α determines the bandwidth of the signal occupied beyond the Nyquist frequency $1/2T_s$, which is called the excess bandwidth. When $\alpha = 1$, the excess bandwidth, expressed as a percentage of the Nyquist frequency, is 100%. For $\alpha = 0.5$ the excess bandwidth is 50%. Fig. 3.8, depicts the impulse and frequency responses for a square root Nyquist filter with a roll-off factor $\alpha = 1$. Note that $h(t)$ and $H(f)$ are normalized so that $h(0) = 1$ and $H(0) = 1$, respectively.

3.5.4 CARRIER MODULATION

Depending on the configuration of the TS module, as described in Section 3.5.2, the outputs of the two square root Nyquist matched filters in the in-phase and quadrature-phase branches of the TS transmitter are modulated onto two orthogonal *Intermediate Frequency* (IF) carrier frequencies. These two modulated carrier signals are then summed before being translated to a *Radio Frequency* (RF) frequency for transmission over the radio channel. The output of a typical TS transmitter employing complex spreading sequences is given by

$$x(t) = y^I(t)\cos(2\pi f_{IF}t) + y^Q(t)\sin(2\pi f_{IF}t), \tag{3.16}$$

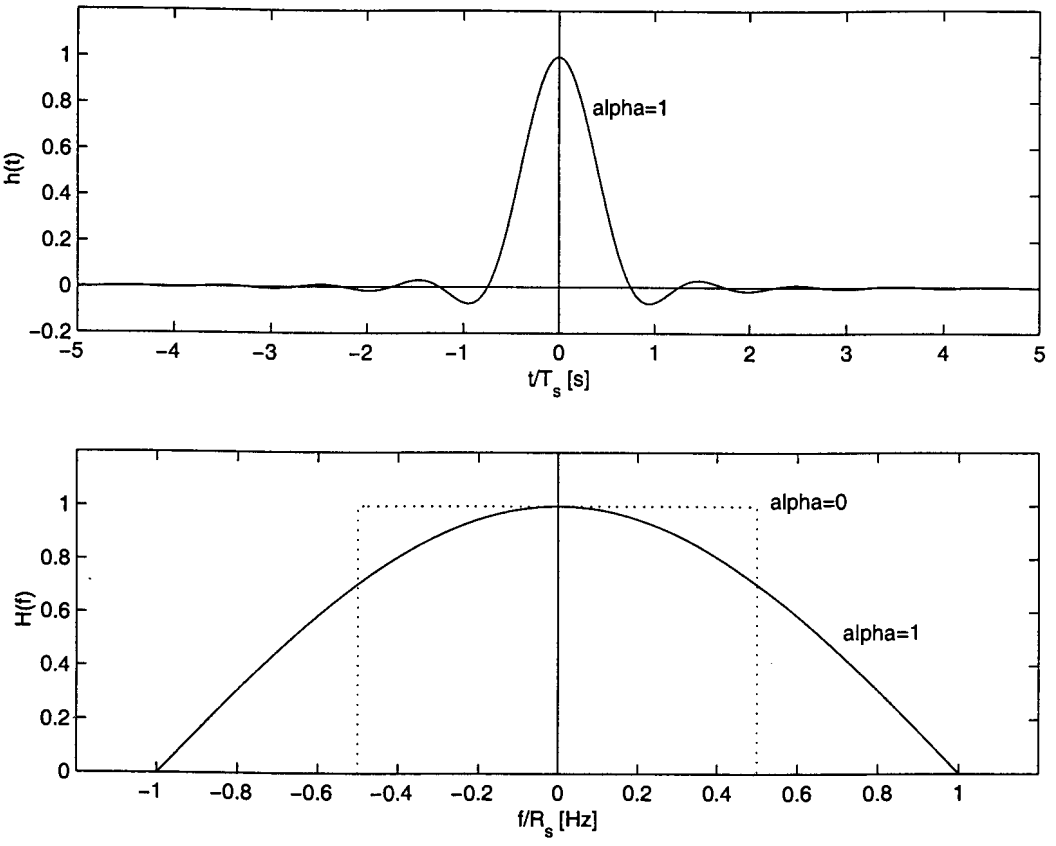

Figure 3.8: Impulse response $h(t)$, and frequency response $H(f)$, of a square root Nyquist filter with $\alpha = 1$.

where

$$y^I(t) = h(t) \otimes \sum_{n=0}^{K} b_n^I \delta(t - nT_s) \tag{3.17}$$

$$y^Q(t) = h(t) \otimes \sum_{n=0}^{K} b_n^Q \delta(t - nT_s) \tag{3.17b}$$

and either b_n^I or b_n^Q is used (see (3.13)), depending on which spreading sequence is used in the TS module and whether the in-phase or quadrature-phase branch is considered. Fig. 3.9 illustrates the modulation process with all the relevant signal names indicated on the figure. It is important to note that, since the duration of each TS symbol is equal to the duration of the unspreaded data symbols on each branch, the introduction of the TS technique causes no increase in the bandwidth requirements of the system. In other words, if TS is introduced to a system employing *Binary Phase Shift Keying* (BPSK) modulation, it would not alter the bandwidth requirements of the original system.

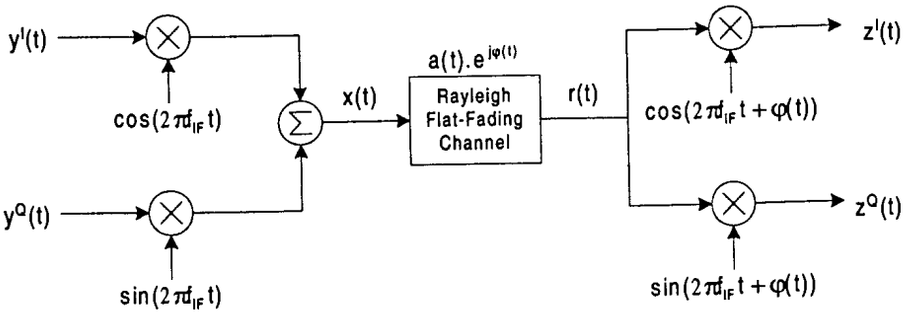

Figure 3.9: The TS modulation and demodulation modules with all the relevant signal names. Refer to Section 3.6.1 for definitions of the channel signals and symbol names.

3.6 DATA RECOVERY FROM FADED TIME SPREAD SYMBOLS

The basic TS receiver without PSAM, ICIC or FEC is discussed in this section. A block diagram of the basic TS receiver can be seen in Fig. 3.10. The receiver is subdivided into four modules namely: Demodulation, Matched Filtering and Sampling, Time Despreading and a Decision Device. It is assumed that the received signal is already translated down to an IF carrier frequency, thus no pre-filtering and RF stages of the receiver is considered.

The first module demodulates the TS signal situated on an in-phase and quadrature-phase IF carrier pair to two baseband signals. The second module consists of two matched filters and an ideal sampling circuit. Thirdly, the sampled baseband signals are applied to the time despreading module. Finally, the output of the time despreading correlators are applied to a decision device that decides which data symbol was transmitted.

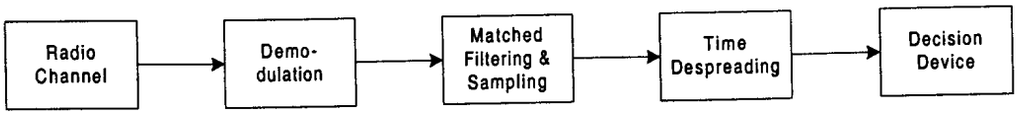

Figure 3.10: The basic TS receiver.

3.6.1 DEMODULATION

The input to the demodulation module is translated down from the RF-TS signal that was transmitted over the radio channel. After down-translation, the received TS signal is situated at an IF carrier frequency. Assume that the RF frequency is much higher than the IF frequency. Thus, if a *Local Oscillator* (LO) with a frequency of $f_{LO} = f_{RF} - f_{IF}$ is used, the two spectral images of the received TS signal after down-translation would be situated at f_{IF} and $f_{RF} + f_{LO}$. If a suitable filter

is used to remove the spectral image of the received TS signal at $f_{RF} + f_{LO}$, the expression for the received signal on the IF carrier would be

$$r(t) = a(t)e^{j\psi(t)}x(t) + n(t), \tag{3.18}$$

where $a(t)e^{j\psi(t)}$ is the complex channel gain, $x(t)$ is given by (3.16) and $n(t)$ is an AWGN term. Assuming perfect phase recovery, the normalized in-phase and quadrature-phase signals on the two branches of the demodulation module are given by

$$\begin{aligned} z^I(t) &= a(t)\left\{y^I(t) + y^I(t)\cos(4\pi f_{IF}t + 2\psi(t)) + y^Q(t)\sin(4\pi f_{IF}t + 2\psi(t))\right\} \\ &\quad + n^I(t) \end{aligned} \tag{3.19}$$

$$\begin{aligned} z^Q(t) &= a(t)\left\{y^Q(t) - y^Q(t)\cos(4\pi f_{IF}t + 2\psi(t)) + y^I(t)\sin(4\pi f_{IF}t + 2\psi(t))\right\} \\ &\quad + n^Q(t) \end{aligned} \tag{3.19b}$$

where $n^I(t)$ and $n^Q(t)$ are two AWGN terms. A block diagram illustrating the demodulation process with all the relevant signal names can be seen in Fig. 3.9. The assumption of perfect phase recovery implies that the phase distortion, $\psi(t)$ induced by the fading channel, is known at all times. This assumption is very important since it allows perfect coherent demodulation. It is shown in Chapter 4 that this is a very optimistic assumption which can only be approximated in physical systems through the use of e.g., pilot signal assisted demodulation techniques.

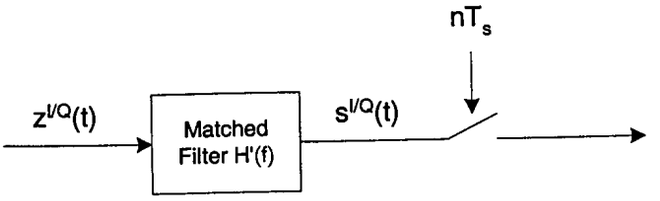

Figure 3.11: A block diagram of the matched filter and sampling module for either the in-phase or quadrature-phase branch of the TS receiver.

3.6.2 MATCHED FILTERING AND SAMPLING

It is explained in Section 3.5.3 that the pulse shaping filters in the TS transmitter is part of a matched filter pair. A block diagram of the matched filter and sampling module in the TS receiver can be seen in Fig. 3.11. The matched filters in the receiver also serve as lowpass filters that remove the double frequency terms at the outputs of the demodulation module, given by (3.19). Square root Nyquist filters are used as pulse shaping filters in the transmitter of the TS system. The impulse response $h'(t)$, and frequency transfer function $H'(f)$, of the matching filters in the receiver are given by [18]

$$h'(t) = h(-t) \tag{3.20}$$

and

$$H'(f) = H^*(f), \tag{3.21}$$

where $h(t)$ and $H(f)$ are given by (3.14) and (3.15) respectively.

Note that the delays introduced by the matched filters are not taken into account in (3.20) and (3.21). The impulse response of a square root Nyquist filter is time symmetrical, thus $h(t) = h(-t) = h'(t)$. To illustrate the effect of a square root Nyquist matched filter pair with a roll-off factor of $\alpha = 1$, the eye diagram obtained for a BPSK modulation system after matched filtering with the aforementioned filter pair is shown in Fig. 3.12.

When perfect symbol timing recovery is assumed, the outputs of the matched filters are sampled at the exact instant when the eye pattern, shown in Fig. 3.12, is maximally open. Referring to Fig. 3.12, the sampling instances would be at $t = 0, 1, 2, \ldots$. The sampled outputs of the in-phase and quadrature-phase branches of the matched filter module are then applied to the time despreading module that is discussed in the next section.

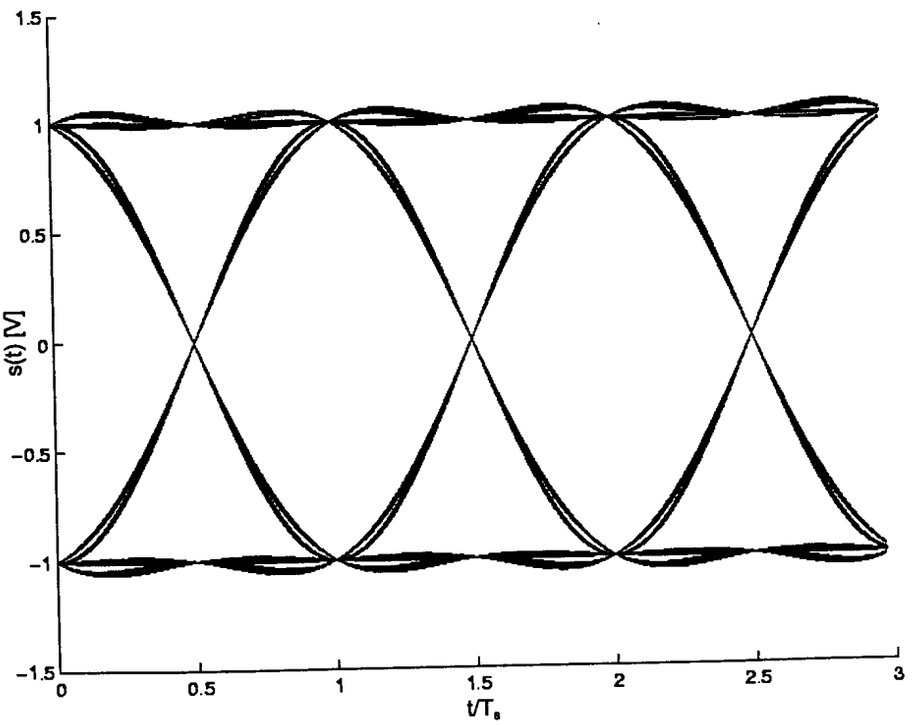

Figure 3.12: Eye diagram at the output of a square root Nyquist filter with $\alpha = 1$, for a BPSK modulation system.

3.6.3 TIME DESPREADING MODULE

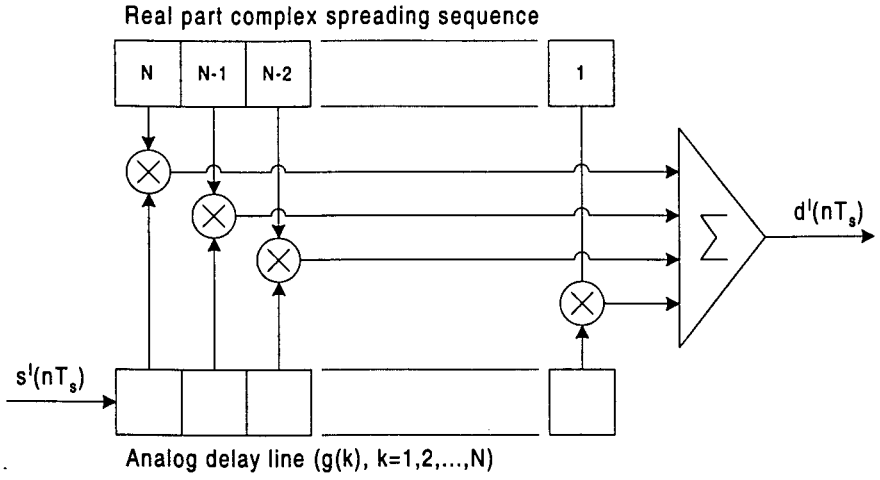

Figure 3.13: The implementation of (3.22) as part of the time despreading module.

The inputs to the time despreading module are the sampled in-phase and quadrature-phase outputs of the matched filters $s^{I/Q}(t)$, discussed in the previous section. Despreading is performed by correlating the received TS symbols with the spreading sequence employed in the transmitter. The type of correlation process used depends on the spreading sequence used in the transmitter of the TS system. There are three possible configurations of the time despreading module:

1. When a complex spreading sequence with desirable real part AAC properties are used, a complex correlation between the complex TS symbols (in-phase and quadrature-phase symbols) and the complex spreading sequence is performed. The real part of this complex correlation output is then used as an estimate of the original transmitted data symbol.

2. When a non-complex spreading sequence is used on the in-phase branch of the TS system only, the correlation between the received TS symbols and the spreading sequence gives an estimate of the transmitted data symbol.

3. When different symbols are applied to the in-phase and quadrature-phase branches of the TS transmitter, separate correlations of the non-complex spreading sequence with the respective TS symbols on the two branches of the TS receiver give estimates of the two transmitted data symbols.

Only the first configuration will be discussed in this section, since the second and third configurations are trivial derivatives of the time despreading module using complex spreading sequences.

The real part of the CC function of a complex spreading sequence can be simplified to the CC value of

the real part sequence and the in-phase TS symbols plus the CC value of the imaginary part sequence and the quadrature-phase TS symbols. The equation for the CC function $d^I(nT_s)$, of the real part sequence with the in-phase TS symbol stream $s^I(nT_s)$, is given by

$$d^I(nT_s) = \sum_{k=1}^{k=N} \mathrm{Re}\{C(k)\}\, g^I((N-k+1)T_s) \tag{3.22}$$

and the CC function $d^Q(nT_s)$, of the imaginary part sequence with the quadrature-phase TS symbol stream $s^Q(nT_s)$ is given by

$$d^Q(nT_s) = \sum_{k=1}^{k=N} \mathrm{Im}\{C(k)\}\, g^Q((N-k+1)T_s), \tag{3.23}$$

where $g^I(mT_s)$ and $g^Q(mT_s)$, $m = 1, 2, 3, ..., N$, are the elements of the in-phase and quadrature-phase analog delay lines, respectively. The in- and quadrature-phase TS symbols are shifted into the in- and quadrature phase delay lines g^I and g^Q on each new symbol time instant. The implementation of (3.22) can be seen in Fig. 3.13. The same structure is used to perform the correlation in the quadrature-phase branch of the TS receiver, except that the imaginary part of the complex spreading sequence is used instead. The real part of the CC between the received complex TS symbols and the complex spreading sequence is given by

$$U(nT_s) = d^I(nT_s) + d^Q(nT_s). \tag{3.24}$$

When a temporally expanded spreading sequence with an expansion ratio of $1 : l$ is used, every l^{th} element of the delay line is used in the correlation and only the elements of the non-expanded sequence need to be stored in the spreading sequence buffer. Referring to Section 3.4, this greatly reduces the number of computations needed for time despreading in the TS receiver.

3.6.4 DECISION DEVICE

The output of the time despreading module is applied to a decision device that determines the corresponding data symbol that has been transmitted. When bipolar data symbols are used, the decision device is a simple comparator that gives outputs according to

$$a_{out}(nT_s) = \begin{cases} 1 & U(nT_s) \geq 0 \\ -1 & U(nT_s) < 0, \end{cases} \tag{3.25}$$

where a_{out} is the output of the decision device and U is the output of the time despreading module at a specific sampling instant. The extension of (3.25) to multilevel symbols is trivial. If the transmitted data was encoded, the decision device could be replaced by any soft input decoder. For instance, if the data at the TS transmitter was convolutionally encoded, a MLSE decoder can replace the decision device. This is an attractive feature of the TS system that will be discussed in more detail in Chapter 5.

When a non-complex spreading sequence is used with multi-dimensional data symbols, the in-phase and quadrature-phase outputs of the time despreading module are simultaneously applied to a decision device that determines which symbol was transmitted.

3.7 INTER CODE INTERFERENCE

The correct detection of data symbols transmitted by a TS system is highly dependent on the correlation properties of the time spreading sequence employed, as discussed in Section 3.2.3. After a data symbol is detected using the time despreading module, $N-1$ sequence elements, belonging to the detected symbol, remain in the complex delay line of the time despreading module. Note that N is the number of elements in the non-expanded spreading sequence. These $N-1$ remaining sequence elements overlap with sequence elements from data symbols that must still be detected. The remaining sequence elements may cause interference during the detection of symbols. When a spreading sequence with perfect AAC properties is used, the sequence elements from previously detected data symbols remaining in the correlation buffer cause no interference when detecting new data symbols, because their correlation with the spreading sequence is zero.

The amplitude and phase values of the transmitted TS signal are distorted when it traverses the fading radio channel. This influences the correlation properties of the spreading sequence used to obtain time diversity and results in partial correlation between overlapping spreading sequences from nearby data symbols. The partial CC of overlapping sequences cause a form of ICI between the spreading sequences/codes from overlapping data symbols. This phenomena degrades the performance of a TS system in a fading channel and will be addressed in Chapter 4, where some ICIC strategies are documented which eliminates this problem.

3.8 SUMMARY

This chapter commenced by describing some signal diversity techniques used to limit the effects of fading on a signal transmitted over a fading radio channel. The principles of the TS technique were discussed and it was shown to exhibit some of the characteristics associated with signal time diversity techniques. Section 3.2.3 highlighted the dependence of the TS technique on spreading sequences with good AAC properties to distribute the energy of each data symbol in time. It was shown that, unlike traditional time and frequency diversity techniques, this form of time diversity can be obtained without any increase in the original transmitted signal bandwidth.

It was explained that the correlation properties of spreading sequences play an important role in deter-

mining the performance of the TS system. Due to the strict requirements set for selecting spreading sequence families that may be used in a TS system, only a few spreading sequences exist that can be used for TS purposes. From these, the Dukic spreading sequence [20], was identified to be the best suited for TS systems.

As mentioned earlier, it is difficult to obtain spreading sequences with adequate correlation properties that are long enough to provide a sufficient amount of temporal diversity. The computational power required to process very long spreading sequences also make the implementation of TS technique less tractable. Section 3.4 described a novel technique whereby the time diversity obtained from a short spreading sequence can be increased significantly. The development of this technique constitutes an important contribution made by this dissertation. This technique not only allows the use of short spreading sequences in TS systems, but also reduces the computational power required in the receiver and transmitter of a TS system in terms of the number of calculations and the degree of accuracy required when doing floating point multiplications, etc. It is shown in Chapter 6 that the increased time diversity obtained from this technique does not reduce the performance of the TS technique.

The structure of a basic TS transmitter and receiver were described theoretically. It has been pointed out by [6] that even under perfect carrier phase recovery conditions, the TS system suffers from a performance degradation in fading channels due to the distortion of the spreading sequence's correlation properties by the fading channel. This performance degradation results in an irreducible BER performance floor that can not be improved by increasing the transmitter power. Efficient techniques to reduce this BER floor have been developed and are discussed in Chapter 4.

CHAPTER FOUR

INTERFERENCE CANCELLATION

4.1 INTRODUCTION

Fading distorts the envelope and phase of a signal transmitted over a mobile radio channel. Since radio spectrum is a limited natural resource, modulation and coding techniques attempt to make the best possible use thereof. Higher order modulation techniques however, needs good symbol phase synchronization measures to operate effectively. While FEC coding schemes provide significant gains in the required $\overline{E}_b/N_0$ values needed to obtain a certain BER level, coherent reception is required for effective operation.

Various techniques have been proposed in the literature that permit coherent reception of signals in fading communication channels. The use of *Transparent Tone In Band* (TTIB) methods to provide estimates of the received signal envelope and phase properties have been analyzed in several papers and books [11, 25, 26, 27, 28]. This technique has also been used in analog modulation schemes as described in [29], to provide frequency and phase references for coherent demodulation.

In recent years a technique called PSAM was the topic of many research papers [30, 31, 32, 33, 34, 35, 36, 37]. This technique provides estimates of the fading effects in a mobile channel and makes pseudo coherent detection over fading channels possible. CSI is obtained from known symbols inserted in the symbol stream of the transmitter. This technique has several advantages over the more conventional pilot tone methods. It is also of particular interest that PSAM has been included in the Wideband-CDMA proposal for the 3^{rd} generation mobile communications standard [38].

Although PSAM is primarily used to allow coherent demodulation in systems operating over fading channels, the pilot symbols can additionally provide channel state information to *Maximum Likelihood* (ML) FEC decoders. This topic has been studied in [32, 37, 39].

The cross-correlation properties of overlapping spreading sequences from different data symbols are degraded when transmitted over a mobile channel exhibiting correlated fading properties. This chapter describes a technique, called ICIC, that similar to MUI cancellation in CDMA systems, that is applied in the TS receiver to limit the effects of ICI. PSAM plays an important role in the ICIC process and gives estimates of the amplitude fading effects on the received TS symbols.

4.2 PILOT SYMBOL AIDED MODULATION

In a PSAM system, the transmitter periodically inserts known symbols in the original data symbol stream. The receiver, employing PSAM techniques, then estimates the amplitude and phase distortions caused by the fading channel from these pilot symbols. These estimates are used to allow coherent demodulation of the data symbols in the receiver. Unlike other pilot signal techniques, the PSAM transceiver module does this without changing the transmitted pulse shape and/or peak-to-average power ratio of the transmitted signal. Processing of the pilot symbols at the transmitter and receiver are not computationally intensive. The mathematical description of the PSAM technique that follows has been adapted from [30].

4.2.1 GENERAL DESCRIPTION

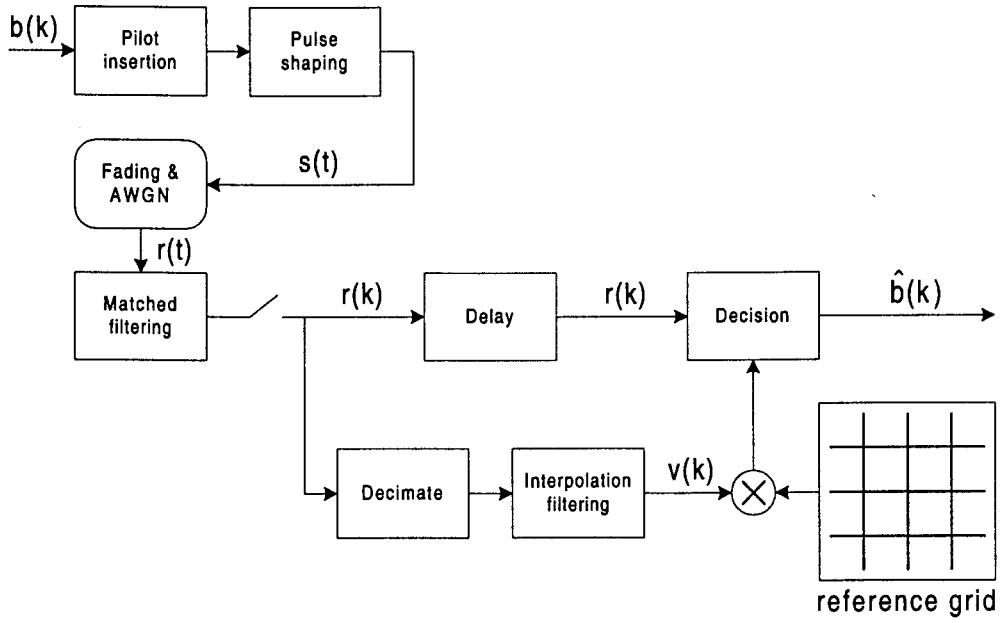

Figure 4.1: Block diagram of a PSAM system.

In a standard PSAM system, known symbols are periodically inserted in the transmitted symbol

stream before pulse shaping, the composite signal is then transmitted over the flat-fading radio channel after pulse shaping and carrier modulation. The block diagram of a PSAM transceiver can be seen in Fig. 4.1.

After matched filter detection and optimal symbol sampling, the symbol stream is split into two. The reference branch extracts the pilot symbols and interpolates them to generate an estimate of the channel state for each data symbol. It then scales and rotates the reference decision grid according to the estimated phase and amplitude values, before feeding the modified decision boundaries to the decision device in the data branch. In the mean time, the extracted data symbols are delayed to compensate for the interpolation delay in the reference branch. This formulation is similar to the model where the receiver normalizes the received data symbols by dividing them with the estimates from the reference branch. However, the aforementioned description is mathematically more tractable.

A consequence of this technique is the delay introduced by the interpolation process. In order to obtain enough samples for a good channel estimate, the receiver must wait and buffer pilot symbol samples for several PSAM frames.

4.2.2 TRANSMITTED SIGNAL

The transmitted signal has a complex envelope given by

$$s(t) = A \sum_{k=-\infty}^{\infty} b(k)p(t - kT_s), \tag{4.1}$$

where T_s is the symbol duration, $b(k)$ is the k^{th} symbol, A is an amplitude factor, and $p(t)$ is a symbol pulse shape with

$$\int_{-\infty}^{\infty} |p(t)|^2 dt = 1. \tag{4.2}$$

The symbols are formatted into frames of length M in which the pilot symbols, inserted at times $i = kM$, have a known value of $\tilde{b}$. In physical systems, the pilot symbols are randomized by a PN sequence to avoid the transmission of periodic pulses, generating line components in the signals *Power Spectral Density* (PSD). This however does not effect the analysis of the PSAM system, and is consequently not implemented. Fig. 4.2 illustrates the structure of the transmitted signal with the periodically inserted pilot symbols.

4.2.3 BANDWIDTH INCREASE

In order to support real time transmission of data, the symbol period of the original data symbols must be decreased when pilot symbols are inserted. This causes an increase in the required transmission bandwidth. If the pilot symbols are used to sample the fading process at the Nyquist rate (twice the

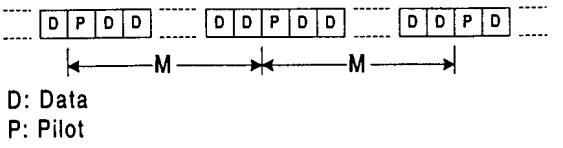

Figure 4.2: PSAM transmitted frame structure.

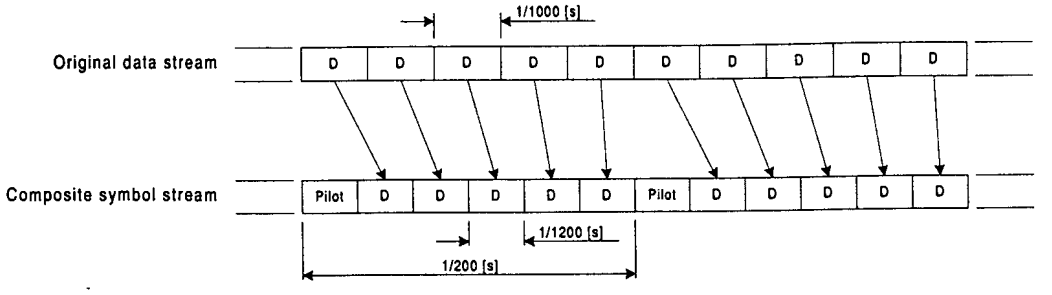

Figure 4.3: Effect of inserting pilot symbols on signal bandwidth.

frequency of the highest frequency component, f_m, of the fading process) the minimum increase in single sided transmission bandwidth of the signal amounts to f_m, if an ideal Nyquist filter is used for pulse shaping.

For example, assume that the maximum Doppler spread in a channel is 100 [Hz]. This would require the channel to be sampled at a minimum of 200 [samples/s] to ensure perfect signal reconstruction. If the data rate for a system is 1000 [symbols/s], one channel sample must be taken for every five data symbols. This process is illustrated in Fig. 4.3 and would require the composite symbol stream to operate at 1200 [symbols/s], since an extra symbol needs to be transmitted for every five data symbols in real time. If ideal Nyquist filtering ($\alpha = 0$) was used in the original system, a single sided signal bandwidth of $1/2T_s = 500$ [Hz] would have sufficed. With the insertion of pilot symbols the required bandwidth would be $1/2T_s' = 600$ [Hz], which is 100 [Hz] wider than the required bandwidth of the original data signal. In general terms, the insertion of one pilot symbol for every $M-1$ data symbols causes the required signal bandwidth to increase by a factor $M/(M-1)$.

4.2.4 ENERGY DISSIPATION IN PILOT SYMBOLS

Pilot symbols inserted for channel estimation purposes carry no information, although they are dissipating transmitter power. This fixed amount of energy dissipated by pilot symbols are not a function of any channel parameter and causes an additional X dB offset in the BER graph of a system when compared to an ideal system not employing pilot symbols. When the energy transmitted per pilot symbol is equal to the average energy transmitted per data symbol, at a rate of one pilot symbol for

every $M-1$ data symbols, the loss in effective $\overline{E}_b/N_0$ caused by the pilot symbol insertion is given by:

$$\begin{aligned} X &= 10\log_{10}\left(\frac{E_{data}(M-1)+E_{pilot}}{M}\right) - 10\log_{10}\left(\frac{E_{data}(M-1)}{M}\right) \text{ dB} \\ &= 10\log_{10}\left(\frac{M}{M-1}\right) \text{dB}, \end{aligned} \tag{4.3}$$

where E_{data}, the average data symbol energy, equals E_{pilot}, the energy transmitted per pilot symbol.

4.2.5 FADING CHANNEL EFFECTS

Although discussed in Chapter 2, the fading channel effects are briefly summarized in this section for notation purposes. The output of a flat-fading channel is given by

$$r_c(t) = c(t)s(t) + n_c(t), \tag{4.4}$$

where $n_c(t)$ is an AWGN term with power spectral density N_0 in both real and imaginary components. No frequency offset f_o is taken into account, thus $c(t)$ only resembles the fading process in the channel. In order to use the notation in [30], $c(t) = g(t)$ since no frequency offset is present, where $g(t)$ is the complex Gaussian fading process with variance σ_g^2 and Doppler spread f_D. The AC function for the complex channel gain can be written as:

$$R_c(\tau) = \sigma_g^2 \tilde{R}_c(\tau), \tag{4.5}$$

where $\tilde{R}_c(\tau)$ is the unit power equivalent of the channel's AC function. The analysis is not limited to a specific AC function, but when the Clarke spectrum is assumed, $\tilde{R}_c(\tau)$ is given by

$$\tilde{R}_c(\tau) = J_0(2\pi f_D \tau), \tag{4.6}$$

which has the typical U-shaped power spectrum given by (2.18) and illustrated in Fig. 2.5.

In the simulation study, the 3^{rd} order approximation of the Clarke spectrum, illustrated in Fig. 2.5, is used and its AC function is mathematically calculated for use in the TS system.

The difference between the AC functions for the ideal Clarke spectrum and the 3^{rd} order approximation can be seen in Fig. 4.4. Note that the sharper frequency cutoff of the ideal Clarke spectrum results in a much wider AC function.

4.2.6 PSAM RECEIVER

The receiver detects the pulses using a matched filter with complex impulse response $p^*(-t)/\sqrt{N_0}$. The normalization of the additive noise is done for notational convenience in the derivations that follow. It is assumed that no ISI occurs for the input symbols, which implies that no receiver timing

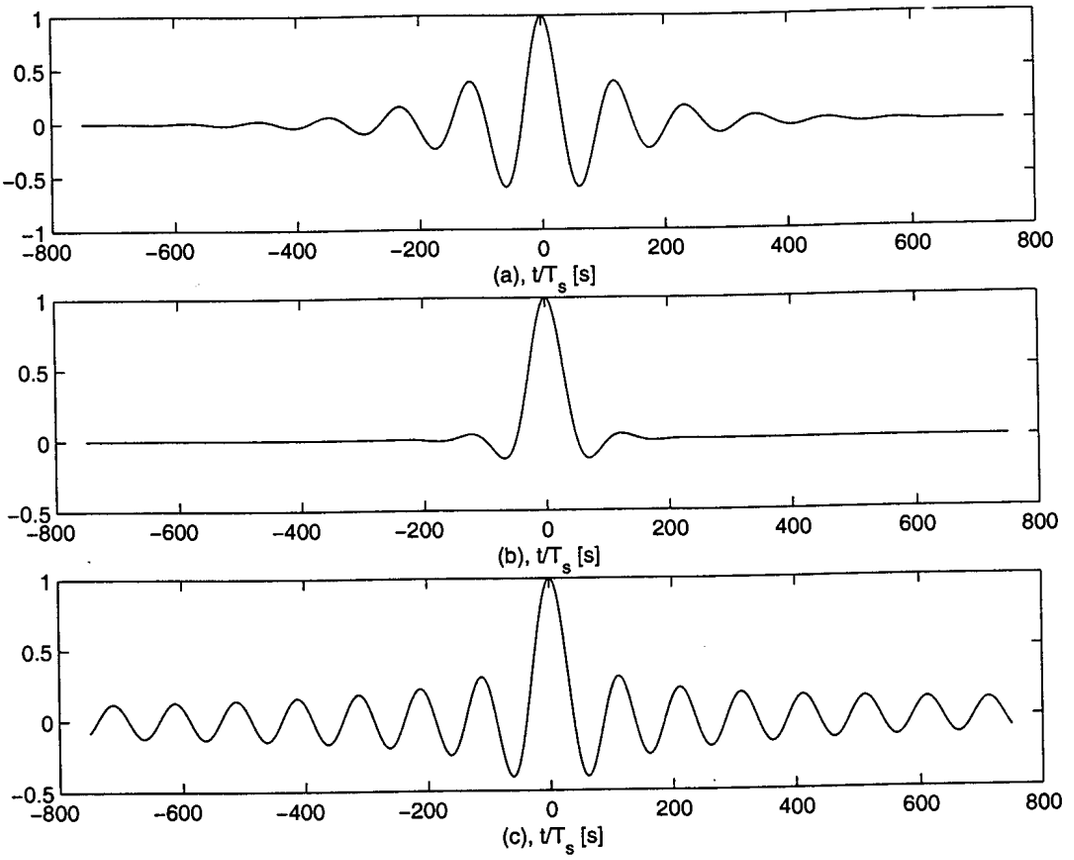

Figure 4.4: Normalized channel impulse response AC functions for different Clarke spectrum approximations. (a) 3^{rd} order approximation, (b) 4^{th} order LPF approximation, (c) Theoretical Clarke spectrum. The fading rate in (a) to (c) is equal to 1% of the channel symbol rate.

errors are present and that the fading is slow enough not to cause any significant distortion of the symbol pulses.

The ratio q, is defined as the pilot power to data power ratio:

$$q = \frac{\tilde{b}^2}{(M-1)E\left[|b|^2\right]}, \tag{4.7}$$

where the expectation is taken over data symbols only and M is the number of symbols in a frame. With n bits per symbol and $M-1$ data symbols per frame, the received energy per data bit is:

$$E_b = \frac{\sigma_g^2 A^2}{n(M-1)}|\tilde{b}|^2\left(\frac{1+q}{q}\right). \tag{4.8}$$

The symbol-spaced samples $r(kT_s)$ of the matched filter output are given by

$$\begin{aligned} r(k) &= \frac{Ac(kT_s)}{\sqrt{N_0}}b(k) + n(k) \\ &= u(k)b(k) + n(k), \end{aligned} \tag{4.9}$$

where the Gaussian noise samples $n(k)$ are white with unit variance and the symbol gain $u(k)$, defined here has a variance of:

$$\begin{aligned}\sigma_g^2 &= \frac{1}{2}E\left[|u|^2\right] \\ &= \gamma_b \frac{n(M-1)}{|\tilde{b}|^2}\frac{q}{1+q},\end{aligned} \tag{4.10}$$

where $\gamma_b = \overline{E}_b/N_0$.

Consider $b(0)$ to be a pilot symbol with the detection of $b(k)$, $-\lfloor M/2 \rfloor \leq k \leq \lfloor (M-1)/2 \rfloor$. The channel state estimator calculates an estimate of the symbol gain $u(k)$ using the K nearest pilot samples:

$$v(k) = \sum_{k=-\lfloor K/2 \rfloor}^{\lfloor K/2 \rfloor} h^*(i,k)r(iM). \tag{4.11}$$

Note that the coefficients $h(i,k)$ depend on the position k within the frame. The estimator error $e(k)$, is defined as

$$e(k) = u(k) - v(k), \tag{4.12}$$

where $v(k)$ and $u(k)$ denotes the symbol gains as before.

4.2.7 FRAME SYNCHRONIZATION

An important aspect regarding any PSAM technique is the method by which the receiver determines the position of the pilot symbols in the received symbol stream. This topic was studied extensively in [40] and [41]. Although perfect frame synchronization is assumed in all systems evaluated in this dissertation, this topic is discussed here for completeness sake.

Two methods, of which one is a ML estimation method, are described in [40]. In both instances, each pilot symbol is an element of a maximal length sequence with good periodic AC properties. Both synchronizers compute a weighted correlation coefficient for the incoming symbols versus the maximal length pilot sequence. This ensures fast and accurate acquisition at high SNR's, and requires low computational complexity in the synchronization module. It was shown in the literature that for a fixed acquisition time, the ML estimator must be used while the hypothesis testing method provides a fixed probability of correct acquisition. The method of ML estimation for frame synchronization is discussed in more detail in the following sections.

The ML estimator is a fixed sample size estimator with a performance that varies significantly as a function of the input SNR. This estimator will give an estimate of the pilot symbol position even when no signal is present. The synchronizer uses a fixed observation interval of length $L = N_S N_P$,

starting at $n = 0$. Define a vector of sampled matched filter outputs,

$$\mathbf{x} = [x_0, x_1, x_2, ..., x_{L-1}]^T, \tag{4.13}$$

where N_P is the number of symbols in a frame and N_S is the number of elements in the pilot symbol sequence. The frame synchronization problem is to estimate $\mu \in [0, L-1]$ which corresponds to the start of a frame. In the absence of a-priori information, the beginning of the frame (i.e., the location of the first pilot symbol, p_0) appears with equal probability in any of L positions in $\mathbf{x}$. Therefore, the ML estimate of μ is the minimum error probability synchronizer. This is given by

$$\hat{\mu} = \underset{\mu \in [0, L-1]}{\text{Argmax}}\, f(\mathbf{x}/\mu), \tag{4.14}$$

where $f(\mathbf{x}/\mu)$ is the conditional PDF of $\mathbf{x}$ given μ.

It has been shown by [40] that using only a vector of pilot spaced observation vectors $\mathbf{x}_P(\mu_2)$, for $\mu_2 = 0, 1, 2, ..., N_P - 1$ and $\mu = \mu_1 N_P + \mu_2$, greatly reduces the computational complexity of the ML receiver, while not reducing the estimator performance significantly.

The effect of frequency offset is not taken into account in this dissertation, thus the synchronizer problem reduces to

$$\hat{\mu} = \underset{\mu \in [0, L-1]}{\text{Argmax}} \left| \left([\mathbf{T}^{\mu_1}]^T \mathbf{p} \right)^H \mathbf{x}_P(\mu_2) \right|^2 - \zeta \parallel \mathbf{x}_P(\mu_2) \parallel^2 \tag{4.15}$$

when only pilot spaced samples are used. The matrix $\mathbf{T}$ is a circular shift matrix defined as

$$\mathbf{T} = \begin{bmatrix} 0_{1,1} & 1_{1,2} & 0_{1,3} & \cdots & 0_{1,N_S} \\ \vdots & 0_{2,2} & \ddots & & \vdots \\ \vdots & \vdots & & 1_{N_S-2,N_S-1} & 0_{N_S-2,N_S} \\ 0_{N_S-1,1} & 0_{N_S-1,2} & \cdots & 0_{N_S-1,N_S-1} & 1_{N_S-1,N_S} \\ 1_{N_S,1} & 0_{N_S,2} & \cdots & \cdots & 0_{N_S,N_S} \end{bmatrix}, \tag{4.16}$$

where, for example, $\mathbf{T}[1, 2, 3]^T = [2, 3, 1]^T$ and $\mathbf{T}^T[1, 2, 3]^T = [3, 1, 2]^T$. Vector $\mathbf{p}$ is the pilot symbol vector and ζ is a data correction term averaged over all data vectors, defined as

$$\zeta = \frac{\left[\sum_{d \in \Omega_d} |d|^2 e^{-\frac{E}{N_0}|d|^2} \right]}{\left[\sum_{d \in \Omega_d} e^{-\frac{E}{N_0}|d|^2} \right]}, \tag{4.17}$$

where Ω_d denotes the data symbol constellation.

Although this synchronizer is only approximately optimal at low SNRs, simulation studies by [40] showed that it performs well over a large range of SNRs. The synchronization problem is beyond the scope of this dissertation and will therefore not be implemented in the simulation evaluation of the TS technique. Thus, perfect symbol and frame synchronization will be assumed under all circumstances.

4.2.8 OPTIMUM INTERPOLATION

Various interpolation filters are described in the literature. Two examples are the lowpass filter used by [32] and the approximately Gaussian filter described in [31]. These filters give plausible but arbitrary results and allow for a great deal of improvement. A Wiener filter is used in [30] to minimize the variance of the estimation error e, from (4.12). This interpolation technique shows great improvement on earlier methods and is discussed in the following paragraphs.

Define $\mathbf{r}$ as a vector of length K, consisting of a set of pilot samples $r(iM)$, $-\lfloor K/2 \rfloor \leq i \leq \lfloor K/2 \rfloor$ and $\mathbf{h}(k)$ as the corresponding set of filter coefficients for the k^{th} position in the frame. Then the symbol gain estimate is given by

$$v(k) = \mathbf{h}^{\dagger}(k)\mathbf{r}, \tag{4.18}$$

where $\dagger$ denotes the complex conjugate transpose. Now the interpolation error is given by

$$e(k) = u(k) - \mathbf{h}^{\dagger}(k)\mathbf{r}. \tag{4.19}$$

The $K \times K$ AC matrix for the pilot symbol vector $\mathbf{r}$ is:

$$\mathbf{R} = \frac{1}{2}E[\mathbf{r}\mathbf{r}^{\dagger}] \tag{4.20}$$

and the $M-1$ length K covariance vectors are:

$$\mathbf{w} = \frac{1}{2}E[u^{*}\mathbf{r}]. \tag{4.21}$$

Then the variances of interest are given by

$$\begin{aligned} \sigma_v^2(k) &= \mathbf{h}^{\dagger}(k)\mathbf{R}\mathbf{h}(k) \\ \sigma_{uv}^2(k) &= \mathbf{w}^{\dagger}\mathbf{h}(k) \\ \sigma_e^2(k) &= \sigma_u^2 - 2\mathrm{Re}[\sigma_{uv}^2(k)] + \sigma_v^2(k). \end{aligned} \tag{4.22}$$

It is shown in [42] that an optimum estimate is obtained if the coefficient vector $\mathbf{h}$ is selected to satisfy

$$\mathbf{R}\mathbf{h}(k) = \mathbf{w}(k). \tag{4.23}$$

The estimation error variance then attains its minimum value and

$$\begin{aligned} \sigma_v^2(k) = \sigma_{uv}^2(k) &= \mathbf{w}^{\dagger}(k)\mathbf{R}^{-1}\mathbf{w}(k) \\ \sigma_e^2(k) &= \sigma_u^2 - \sigma_v^2. \end{aligned} \tag{4.24}$$

In the case under consideration, there exists explicit expressions for components of the arrays $\mathbf{R}$ and $\mathbf{w}(k)$ and we may write

$$R_{ik} = \gamma_b n(M-1)\frac{q}{1+q}\tilde{R}_c((i-k)MT) + \delta_{ik}, \tag{4.25}$$

where δ_{ik} is the Kronecker delta, and

$$w_i(k) = \gamma_b \frac{n(M-1)}{\tilde{b}^*} \frac{q}{1+q} \tilde{R}_c((iM-k)T) \tag{4.26}$$

with * indicating the complex conjugate of $\tilde{b}$. The optimum interpolation filter coefficients are then given by

$$\mathbf{h}(k) = \mathbf{R}^{-1}\mathbf{w}(k). \tag{4.27}$$

The interpolation filter coefficients can be calculated numerically if the AC function of the channel fading process is known. Fig. 4.5 illustrates these filter coefficients calculated for different SNRs. The interpolation filter has 19 taps and the filter coefficients for the first symbol in a five symbol frame is shown. Here the first symbol in the frame resembles a pilot symbol. Note how the filter impulse response widens as the SNR decreases. This corresponds to a narrower filter bandwidth (Noise Equivalent Bandwidth) and therefore an increase in SNR in the channel estimation module of the receiver. From Fig. 4.5, the interpolation filter is focused towards limiting the noise entering the interpolation process at low SNRs, while it is focused towards more accurate channel sample interpolations at higher SNRs. This clearly illustrates the SNR dependency of the interpolation filter. In a practical system, a single set of filter coefficients would typically be selected at the most likely SNR operating point for the system. This would make the interpolation filter suboptimal at SNRs other than the selected SNR. Note that the interpolation filter coefficients are also dependent on the position of the desired channel estimate within the symbol frame. Thus for a seven symbol frame, there would be seven sets of K coefficient interpolation filters.

4.2.9 EFFECTS OF DIFFERENT PSAM CONFIGURATIONS

There are a number of parameters and configurations that determine the performance of a PSAM system which will be discussed briefly in the following sections.

4.2.9.1 EFFECT OF INTERPOLATION POSITION

The position of the symbol within the frame determines the estimation error and the BER performance of a PSAM system. [30] has shown that the effect of interpolation position is small and only visible at very high SNRs, where the effect is not masked by AWGN. It was shown in [30] that for normal operating conditions with a frame size of five symbols and K greater than seven, the effect of the interpolation position is negligible.

4.2.9.2 EFFECT OF PILOT SYMBOL AMPLITUDE AND SPACING

The frame size, or pilot symbol spacing M, has an optimum value. There is a trade-off between wasting energy in pilot symbols and not sampling the fading process often enough to ensure good

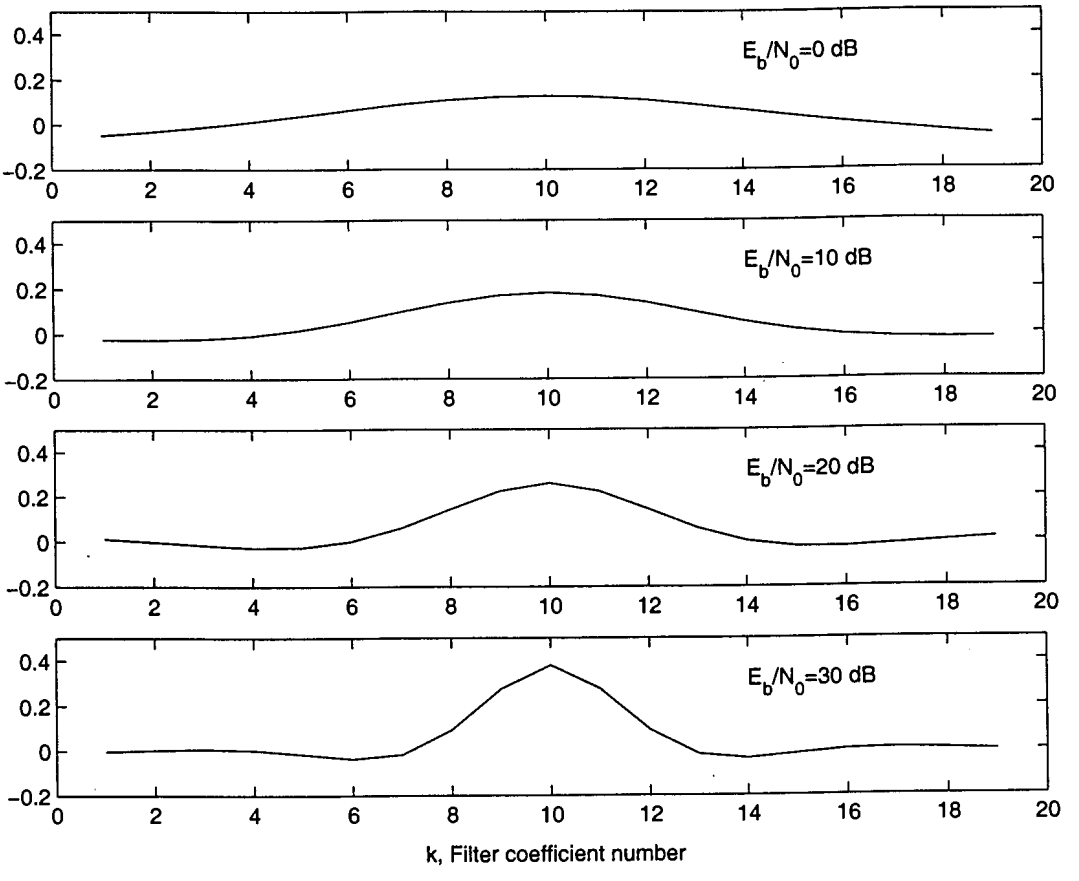

Figure 4.5: Interpolation filter impulse responses at different SNRs for a 19-tap, 5-symbol frame interpolation filter optimized for a fading rate of 1% of the channel symbol rate. The y-axis represents the filter coefficient amplitudes.

channel estimation. This goes for the pilot symbol energy levels as well. When high energy pilot symbols are used, the pilot symbol SNR is good and good channel estimates are obtained. Too high pilot symbol levels however, results in a waste in average transmitted power, leading to a reduction in average BER performance for the system. Intuitively the optimum pilot symbol energy level should be equal to the average data symbol energy with the pilot symbol insertion frequency equal to twice the bandwidth of the fading process of the mobile channel it is intended to sample.

4.2.9.3 EFFECT OF INTERPOLATOR SIZE

The number of interpolator coefficients plays a significant role in the performance of a PSAM system. With reference to Fig. 4.5, the interpolation filter impulse response for low SNRs does not stretch far enough to encapsulate all the significant estimation coefficients. This is not true at $\overline{E}_b/N_0 = 30$ dB, where the tail ends of the interpolation filter impulse response contain virtually no significant coefficient values for a filter with 19 taps at a fading rate of 1% of the channel symbol rate.

4.2.9.4 OPTIMIZED INTERPOLATION FILTER COEFFICIENTS

The interpolation filter coefficients are, among other parameters, dependent on the average SNR of the channel. This implies that there exists an optimum set of filter coefficients for every average SNR. This would require the interpolation filter coefficients to be recalculated at every new average SNR, or alternatively, a large number of pre-calculated coefficients would need to be stored in the receiver. This is not an acceptable solution, and the interpolation filter is instead loaded with a set of coefficients optimized at the most likely average SNR operating point. A third alternative is to use an adaptive interpolator as described in [42]. Preliminary tests however indicated that this method results in suboptimal BER performances and the technique was subsequently not pursued.

4.3 PILOT SYMBOL AIDED TIME SPREAD MODULATION

The simulation tests conducted in [6], pp 53, assumed perfect knowledge of the fading process affecting the transmitted TS signal. This assumption allowed perfect coherent demodulation of the received TS signal. In the BER tests conducted by [6], the simulated BER results compared very favourably, and to a certain extent out performed the ideal theoretical BER results for a system employing BPSK modulation in a Rayleigh flat-fading channel. The results were however unrealistic since it is impossible to obtain perfect knowledge of the fading process of a physical system. It has been shown in [33], among others, that the use of PSAM can only bring the BER performance of a coherent physical system to within one dB of the ideal theoretical BER performance.

This section describes a strategy to integrate PSAM with the TS system described in [6]. The method relies strongly on the theory documented in Section 4.2 and frequent references are made to this section. The TS transmitter with PSAM will be used throughout the discussions in the remainder of this dissertation. Different PSAM-TS receiver structures incorporating ICIC modules are described in Section 4.4.

4.3.1 GENERAL DESCRIPTION

The TS transmitter described in Section 3.5 remains unchanged except for the periodic insertion of pilot symbols in the TS symbol stream, prior to pulse shaping. After matched filtering, the receiver splits the symbol samples into two streams. The reference branch uses the pilot symbol samples to estimate the channel state while the data branch is delayed to compensate for the pilot symbol interpolation delay. The channel state estimates are then used to correct the phase of the received TS symbols before time despreading is performed as usual. At this stage, no attempt is made to correct the distorted amplitude levels of the TS system, this function is left to the TS despreading module.

4.3.2 TRANSMITTER

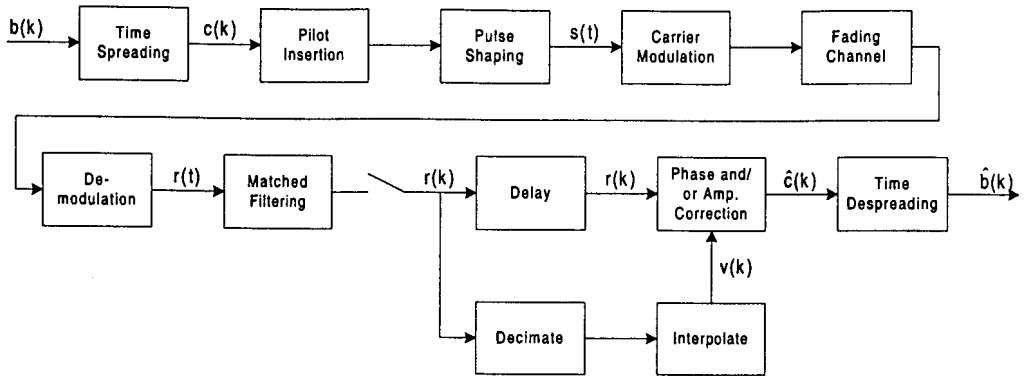

Figure 4.6: A basic TS system with PSAM.

A block diagram of a basic TS system, similar to that described in Chapter 3, but now with PSAM incorporated, is illustrated in Fig. 4.6. The signal frame structure and TS signal buildup can be seen in Fig. 4.3.3. Blocks with the same alphabetic letter resemble spreading sequence elements from the same data symbol. Although only illustrated in one dimension, the composite TS signal shown in Fig. 4.3.3 may be a complex signal if a complex spreading sequence is used. Pilot symbols are inserted periodically in the symbol stream emanating from the TS module. The length of the spreading sequence is N. This may be somewhat misleading, since one spreading sequence would typically span several PSAM frame lengths, as indicated by M.

4.3.3 TRANSMITTED SIGNAL

All signals in Fig. 4.6, apart from the modulated signal transmitted over the fading channel, are complex baseband signals. Different configurations of the TS system, determined by the type of spreading sequence and data symbols used, were discussed in Section 3.5.2 and may influence the nature of the composite transmitted PSAM-TS signal. In this section, only complex spreading sequences with one-dimensional data symbols are discussed. Since the basic functionality of PSAM is independent of the data symbols used, the theoretical description of a PSAM system given in Section 4.2 applies to the PSAM-TS system when the output of the TS module is regarded as the data source.

When phase modulated data symbols are used, it is a trivial task to determine the optimum amplitude of the pilot symbols, since all data symbols have the same amplitude levels, only with different phase angles. For hybrid phase- and amplitude modulated data symbols, the task of determining the optimum pilot symbol level is more difficult. For a M-QAM signal constellation, the average absolute[1]

[1] $y = |x|$

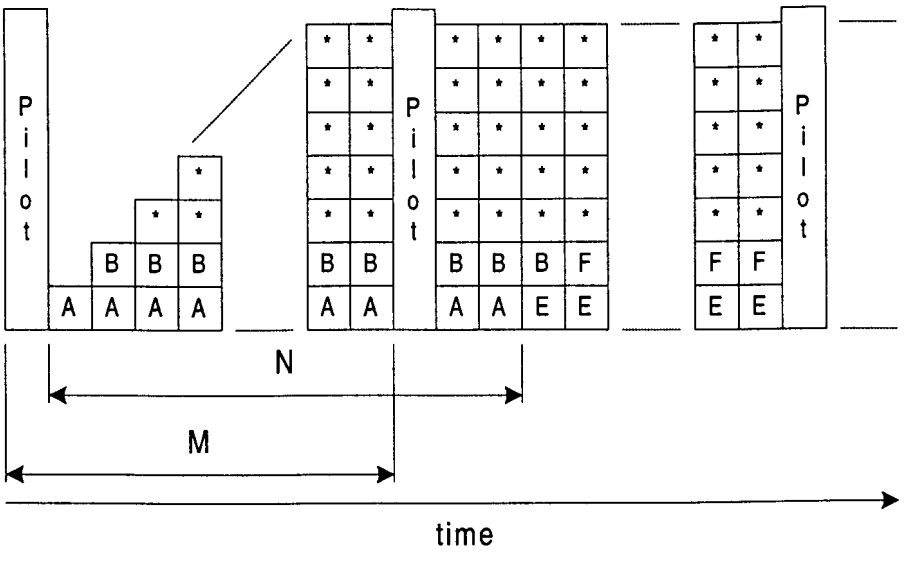

Figure 4.7: Signal frame structure of a TS system with PSAM.

data symbol energy must be calculated, from which the average absolute value data symbol level can be calculated. This average absolute data symbol level is also the optimum level for amplitudes of the pilot symbols that must be inserted into the data symbol stream. For relatively simple M-QAM signal constellations, the average absolute symbol level can be derived analytically since all the signal points in the signal constellation are known together with their probabilities of occurrence. The expression for the average absolute symbol level is given by

$$d_{Avg} = \sum_{i=1}^{M} p(\Omega_i) d_i, \tag{4.28}$$

where $p(\Omega_i)$ is the probability of occurrence of the i^{th} symbol in the Ω signal constellation and d_i is the absolute value of the i^{th} symbol amplitude.

When a Dukic spreading sequence (length N) with chip levels of $[-1, 0, 1]$ on both the real and imaginary axis is used, the complex signal constellation at the output of the TS module has $(2N+1)^2$ signal points with different probabilities of occurrence. Analytic calculation of the average absolute symbol level is very time consuming, thus it is rather calculated numerically by averaging over a large number of data symbols instead.

It was found experimentally that the average absolute symbol level for a length N Dukic sequence is equal to $\sqrt{N}$, when the symbol amplitude levels for the Dukic sequence are chosen from $[-1, 0, 1]$.

To summarize, the composite transmitted TS signal isidentical to the transmitted signal described

in Chapter 3.5, except that a pilot symbol with an energy level equal to the average TS symbol energy is now periodically inserted into the symbol stream prior to pulse shaping. In order to maintain real time transmission of data, the symbol period of the symbols in the composite PSAM-TS signal is reduced. This results in an increase in transmitted signal bandwidth as described in Section 4.2.3. All the principles regarding PSAM applies directly to a PSAM-TS system.

4.3.4 RECEIVER

The basic receiver for a PSAM-TS system is shown in Fig. 4.6. After demodulation, matched filtering and ideal sampling, as described in Section 3.5, the composite TS symbol stream $r(k)$, consisting of data and pilot symbols, are split into a data and a reference branch, respectively. The channel samples obtained from the pilot symbols are interpolated to give a channel estimate for each TS data symbol. The interpolated channel estimates are denoted by $v(k)$, and are calculated in accordance with (4.11). Unlike an ordinary PSAM system, only the phase of the appropriately delayed TS data symbols are corrected in accordance with the channel phase estimates. Referring to Fig. 4.6, the phase correction operation is described by

$$\hat{c}(k) = |r(k)|(\angle r(k) - \angle v(k)). \tag{4.29}$$

No attempts are made to correct the amplitudes of the TS data symbols affected by fading. This is left to the time despreading module that uses the time diversity of the TS signal to reduce the effects of signal envelope fading induced by the mobile channel.

Appropriate time despreading, as determined by the TS structure used in the transmitter, is used to despread the phase corrected TS symbol sequence. The output of the time despreading module gives an estimate $\hat{b}(k)$, of the transmitted data symbol $b(k)$.

4.3.5 INTERPOLATION FILTER

The interpolation filter used by the PSAM-TS receiver is identical to that described in Section 4.2.8 and is used to estimate the channel state between channel samples provided by the periodically inserted pilot symbols. The interpolation filter attempts to suppress the effects of AWGN, while providing accurate estimates of the fading process in the mobile channel.

4.4 ICIC BACKGROUND

4.4.1 PRIMARY INTERFERENCE SOURCE

The primary source of interference in a TS system was briefly mentioned in Section 3.7 and is discussed in more detail in this section. The spreading sequences from nearby data symbols overlap in time. These data symbols are resolved in the TS receiver by correlating the received TS signal

with the spreading sequence on each new symbol interval after pilot symbols, if present, have been removed. When a spreading sequence with perfect AAC properties is used, the original data symbol can be recovered perfectly without any interference from neighbouring data symbols in the absence of fading and AWGN.

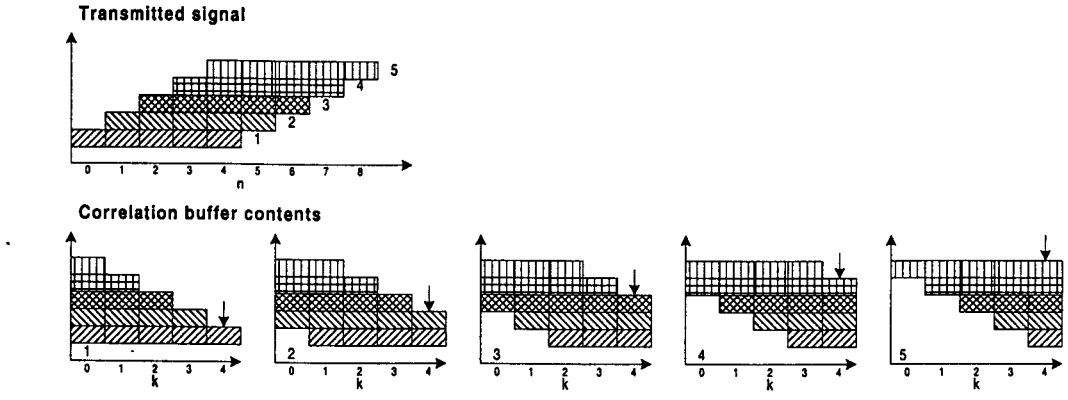

Figure 4.8: Received baseband TS signal and correlation buffer contents for a $N = 5$ spreading sequence TS system.

To illustrate the origin of ICI in a TS system, consider the transmission of five data symbols by a TS system using a length $N = 5$ spreading sequence. The graphical representation of this signal after matched filtering and ideal sampling, with the pilot symbols removed from the symbol stream, can be seen in Fig. 4.8. The sequence elements belonging to different data symbols are filled using different patterns. Also shown in Fig. 4.8, are the contents of the FIFO correlation buffer at different time instances, as the received TS signal is shifted through the buffer from left to right. At every time instant, the contents of the correlation buffer is correlated with the five element spreading sequence. The sequence marked with an arrow correlates perfectly with the spreading sequence in the receiver, while the cross- correlation terms from other spreading sequences are zero when a perfect spreading sequence is used. However, the overlapping sequence elements tend to interfere with the desired sequence when imperfect spreading sequences are used or, when fading is present in the radio channel. The interference from overlapping sequence elements reduces the noise margin of the TS system and results in an increased amount of symbol detection errors. For example, consider the detection of

symbol two in Fig. 4.8, the contents of the five correlation buffer elements are:

$$\begin{aligned} g(0) &= \mathbf{b_2c_0}+b_3c_1+b_4c_2+b_5c_3 \\ g(1) &= b_1c_0+\mathbf{b_2c_1}+b_3c_2+b_4c_3+b_5c_4 \\ g(2) &= b_1c_1+\mathbf{b_2c_2}+b_3c_3+b_4c_4 \\ g(3) &= b_1c_2+\mathbf{b_2c_3}+b_3c_4 \\ g(4) &= b_1c_3+\mathbf{b_2c_4} \end{aligned} \tag{4.30}$$

Then, the output of the time despreading module, implemented as a correlation function, is

$$U = b_2 = \sum_{k=0}^{4} g(k)c(k) \tag{4.31}$$

when a perfect normalized spreading sequence is used. When the amplitudes of the correlation buffer elements are corrupted by fading, the non-boldface terms in (4.30) will partially correlate with the spreading sequence $\mathbf{c}$ and appear as ICI terms in the correlation coefficient calculated for $\mathbf{g}$ and $\mathbf{c}$. Note that elements of the previously detected symbol, i.e. b_1, are also present in the correlation buffer.

4.4.2 INTERFERENCE CANCELLATION OBJECTIVES

The primary objective of the ICIC module is to remove all potential interference terms from the correlation buffer prior to the detection of a particular symbol. These interference terms originate from two sources namely:

1. The remainders of sequences associated with previously detected data symbols.
2. Sequences associated with data symbols that still have to be detected in the future, that are already partially shifted into the correlation buffer.

Different strategies to achieve these objectives are proposed in the sections to follow. Some background to the techniques used in *Multi-User* (MU)-detection systems employed in the CDMA environment are also given, since the interference problem in CDMA systems are closely related to the problem in the TS technique under discussion.

4.4.3 MU-DETECTION AND INTERFERENCE CANCELLATION IN THE CDMA ENVIRONMENT

MU detection and interference cancellation techniques for CDMA systems have been studied by many authors. Some references in this regard include [2, 43, 44, 45, 46, 47, 48, 49, 50]. Although not directly applicable to the interference problem in TS systems, the *Interference Cancellation* (IC)

strategies proposed for *Direct Sequence-Code Division Multiple Access* (DS-CDMA) systems provide some insight into the ICIC problem. An example of a popular IC technique is the successive IC scheme described by [2].

4.4.3.1 SUCCESSIVE MU-IC

Successive IC is a form of serial IC and stands in contrast with parallel IC schemes, where different users' signals are processed and detected simultaneously. Parallel IC structures can be very complex when compared to serial IC structures, which are in general more robust in performing MU-Detection and IC.

With successive IC, the approach is to successively cancel the interference caused by the strongest remaining user without exact knowledge of any of the individual users' signal power levels (see [2]). The strength of the received signal from each user is estimated from the outputs of a conventional correlation bank, instead of separate channel estimates for each user as is common practice. It is assumed that the spreading sequences from all users are known at the receiver. The flow diagram and functional block diagram in Fig. 4.9 illustrates the basic strategy followed by [2] in his proposed successive IC strategy.

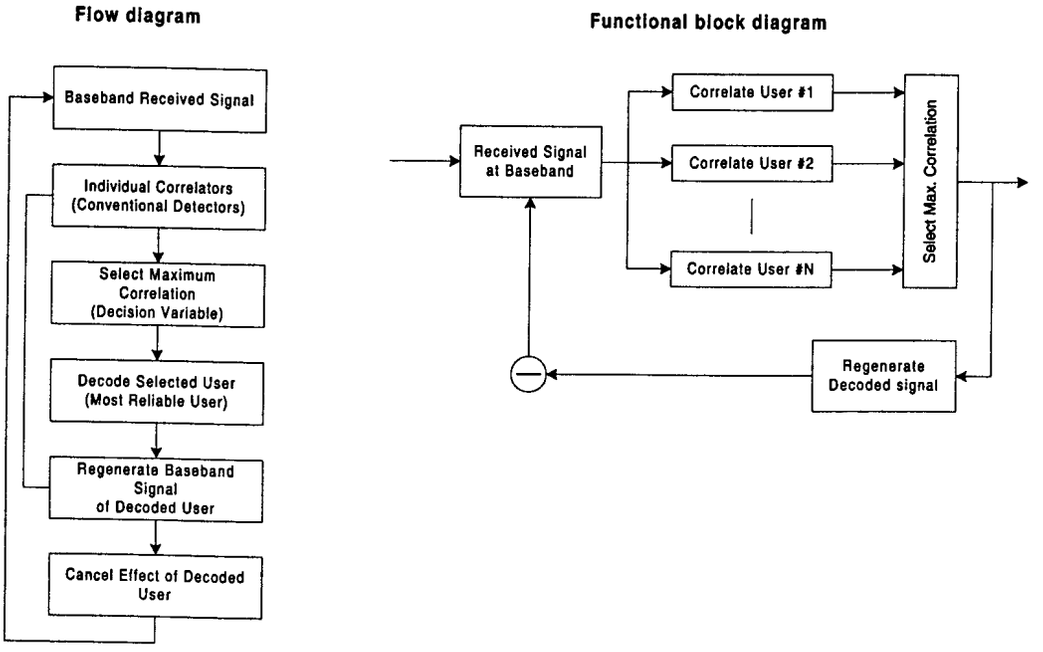

Figure 4.9: Successive MU-IC for CDMA, taken from [2].

The strongest user is decoded first and its effects cancelled from the received baseband signal. The

next strongest signal is then decoded and its effects are cancelled. The recursive decoding and cancellation are repeated until the weakest user signal is decoded.

Spreading sequences in a TS system overlap in time and can therefore not be decoded simultaneously. However, after slight modification, this successive IC strategy can also be utilized in a TS receiver, as is described in Section 4.5.3.

4.4.3.2 ADAPTIVE MU-IC STRATEGIES

In their paper, [44] mentions several adaptive IC structures and their shortcomings. Most of these receivers combine despreading and signal equalization in one structure. Consequently these structures are complex and slow to converge. Near-far effects also have a negative effect on the performance of these systems. Blind adaptation algorithms, which use training sequences at the beginning, and during transmission of data, have been proposed to overcome this problem. These algorithms however still need to switch between the blind adaptive algorithm and the standard decision feedback algorithms. The already complex structure of the TS system and good results obtained with other ICIC strategies, designed for the TS system, placed the investigation of adaptive IC algorithms beyond the scope of this dissertation.

4.5 PROPOSED ICIC STRATEGIES FOR TS SYSTEMS

The ICIC strategies described in this section rely on the TS systems to employing complex spreading sequences. The same principles can however be extended to systems that use non-complex spreading sequences.

4.5.1 REMAINDER SUBTRACTION ICIC

With this ICIC method, the remainder of the sequence associated with a particular data symbol is subtracted from the correlation buffer described in Section 4.4, after the symbol has been detected. There are two important aspects regarding this technique that must be emphasized:

1. The data symbol for which the remaining sequence elements are removed from the correlation buffer must be detected with a high degree of accuracy. For instance, if bipolar data symbols are used, a wrong decision on the polarity of the data symbol will result in a replica of the modulated sequence that was transmitted for that symbol to be added to the correlation buffer, instead of being subtracted. This will double the interference caused by the remainder of the sequence instead of completely eliminating its effect on data symbols that have to be detected.

2. The effect of fading on the transmitted data modulated sequence must be accounted for when reconstructing the modulated sequence for ICIC purposes in the TS receiver. It does not suffice

to subtract a perfect data modulated sequence from the correlation buffer, since it would not be an exact match of the sequence in the correlation buffer that has been subjected to fading. The latter emphasizes the importance of accurate fading estimation techniques in the TS system.

A PSAM-TS technique was proposed to provide estimates of the channel state associated with each TS symbol for phase correction as well as ICIC purposes (see Section 4.3). An estimate of the current data symbol is obtained by calculating the correlation coefficient between the contents of the correlation buffer and an appropriate spreading sequence. A block diagram of the functional modules giving inputs to the ICIC module is depicted in Fig. 4.10.

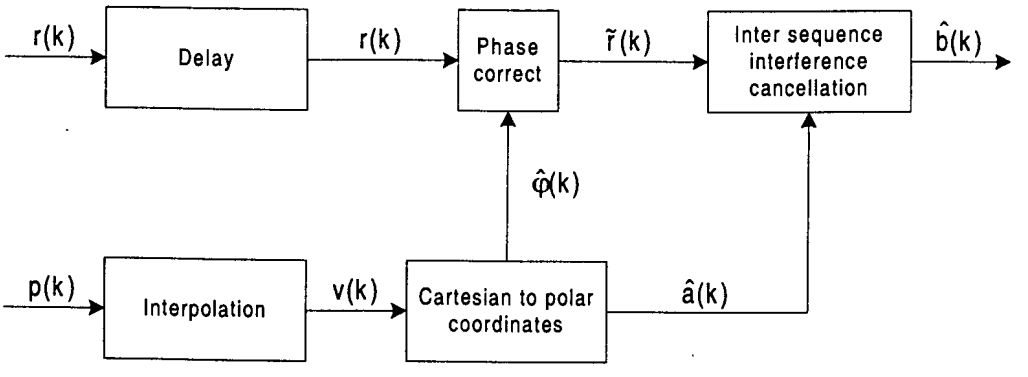

Figure 4.10: Block diagram of functional blocks giving inputs to the ICIC module.

The input to the ICIC module, $\tilde{r}(k)$, is the phase corrected TS symbol:

$$\tilde{r}(k) = |r(k)|(\angle r(k) - \hat{\psi}(k)). \tag{4.32}$$

The data symbol detection and ICIC procedures are performed in the following stages:
Stage 1: Determine the current data symbol

Determine the real part of the complex correlation function for the phase corrected TS symbols and the complex spreading sequence $\mathbf{c}$ at sampling instant k, i.e.

$$U(k) = \sum_{i=0}^{N-1} g(i)c^*(i), \tag{4.33}$$

where $g(i)$ is the i^{th} element of the complex FIFO correlation buffer and $c(i)$ is the i^{th} element of the complex spreading sequence. The value $U(k)$ is applied to a decision device that provides $\hat{b}(k)$, an estimate of the transmitted data symbol $b(k)$.

Stage 2: Cancel the effect of the detected symbol

The elements of the complex correlation buffer is updated according to the following algorithm at time $t = (k+1)T_s$:

$$g(i) = \begin{cases} g(i-1) - a(i-1)\hat{b}(k)c(i-1), & i = N-1, N-2, N-3, ..., 1 \\ \tilde{r}(k+1), & i = 0, \end{cases} \tag{4.34}$$

where $a(i)$ is the i^{th} element in the complex FIFO buffer containing the values of the channel estimates associated with each element $g(i)$. With perfect CSI and no AWGN, this procedure completely removes the remaining elements of the spreading sequence associated with $b(k)$ from the correlation buffer **g**. A detailed diagram of the corresponding ICIC module is illustrated in Fig. 4.11.

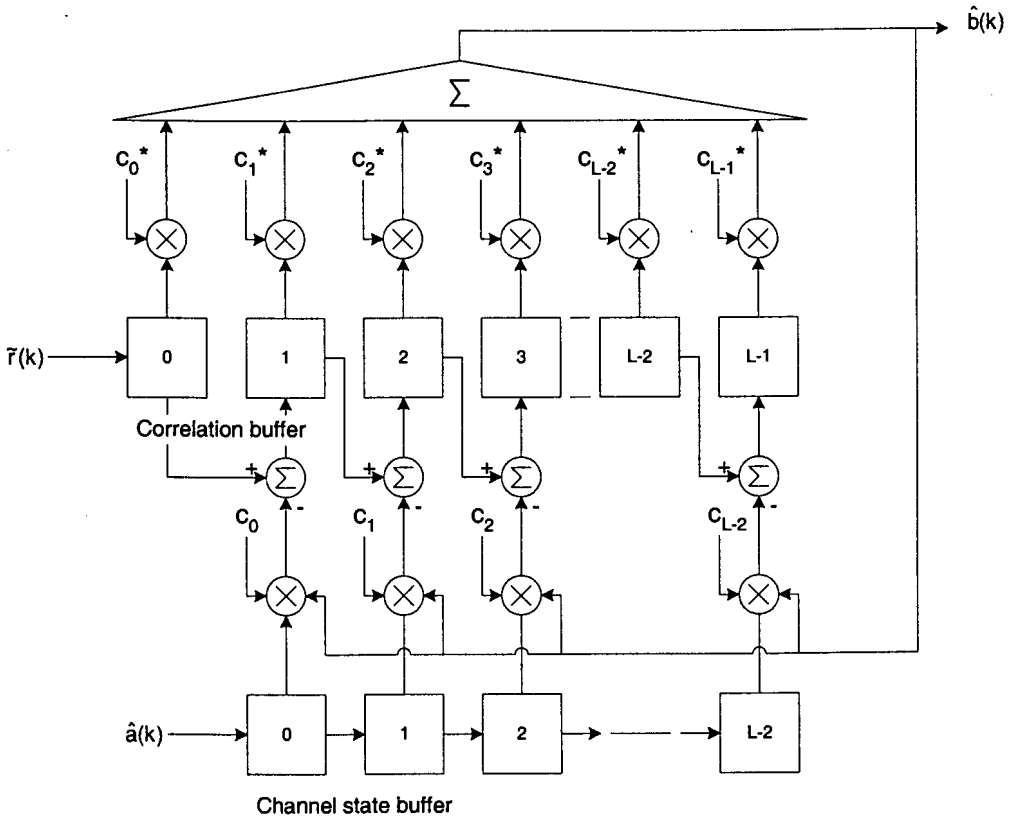

Figure 4.11: A detailed block diagram of the remainder subtraction ICIC algorithm. Symbol L corresponds to the effective number of elements in the TS sequence.

The primary element that limits the performance of the ICIC module is the presence of AWGN in the system. Noise gives rise to inaccurate channel estimates and corrupts the correlation properties of the spreading sequence which causes incorrect symbol decisions. This, combined with inaccurate

channel estimates, limits the performance of the ICIC module, making it impossible to completely remove the remainder of a particular spreading sequence from the correlation buffer.

With reference to (4.30), the majority of interference terms originates from spreading sequences corresponding to data symbols that have not been detected. These sequences can subsequently not be removed from the correlation buffer completely. The preliminary detection of future symbols and the subsequent elimination of their effects on the current data symbol is possible, but detection errors and accompanying incorrect cancellation efforts may result in even higher interference levels.

Note that the output of the ICIC module directly produces $\hat{b}(k)$, i.e. the soft estimate of the current data symbol. Therefore, no time despreading is necessary after ICIC has been performed since it is implicitly performed in the ICIC module.

4.5.2 NON DECISION BASED ICIC

Results showed that the performance of the aforementioned ICIC module can be improved, by using only data symbols that have a sufficient level of confidence in the ICIC process. This implies that only data symbols that fall well within the defined symbol regions are used for ICIC purposes. For instance, if $[-1, 1]$ data symbols were used, only symbols for which $|\hat{b}(k)| > \mu$ would be used for ICIC purposes. Where μ is a preset threshold level ranging between zero and the maximum symbol level in the TS receiver structure. This eliminated the possibility of incorrect ICIC actions due to incorrect data symbol decisions.

A non decision directed ICIC strategy is proposed as an alternative to the confidence level approach. This technique relies on the fact that the total energy of the TS symbols in the correlation buffer should decrease if an effective ICIC attempt is made. When bipolar data symbols are used, the sequence, distorted by fading, is both added and subtracted temporally from the correlation buffer, while the total energy in the buffer is measured for both scenarios. The process yielding the lowest total energy in the correlation buffer is regarded as the best ICIC attempt and the contents of the correlation buffer is updated permanently. Mathematically, this ICIC strategy can be simplified in order to determine U_- and U_+, according to (4.36), choosing the smallest value of the two, and updating the contents of the correlation buffer according to

$$g(i) = \begin{cases} g(i-1) \pm a(i-1)c(i-1), & i = N-1, N-2, N-3, ..., 1 \\ \tilde{r}(k+1), & i = 0, \end{cases} \tag{4.35}$$

where the decision to add (+) or subtract (-) is made, based on whether U_- or U_+ is the smallest.

$$U_\pm = \sum_{i=0}^{N-1} |g(i) \pm a(i)c(i)|^2 . \tag{4.36}$$

4.5.3 PARTIAL SUCCESSIVE ICIC

This ICIC strategy is based on the CDMA MU-IC scheme proposed by [2]. Joint detection and cancellation of all overlapping sequences in a TS system is not possible, since sequences overlap only partially. This results in an infinite number of sequences that would need to be detected simultaneously. To overcome this problem, only K symbols, excluding the current symbol, is jointly detected. The K symbols are only preliminary detected for IC purposes and subsequently still have to be decoded properly in future.

The recursive IC process taking place at each new data symbol interval is illustrated by the flow diagram in Fig. 4.12. The contents of the $N + K$ element correlation buffer is copied to a temporary

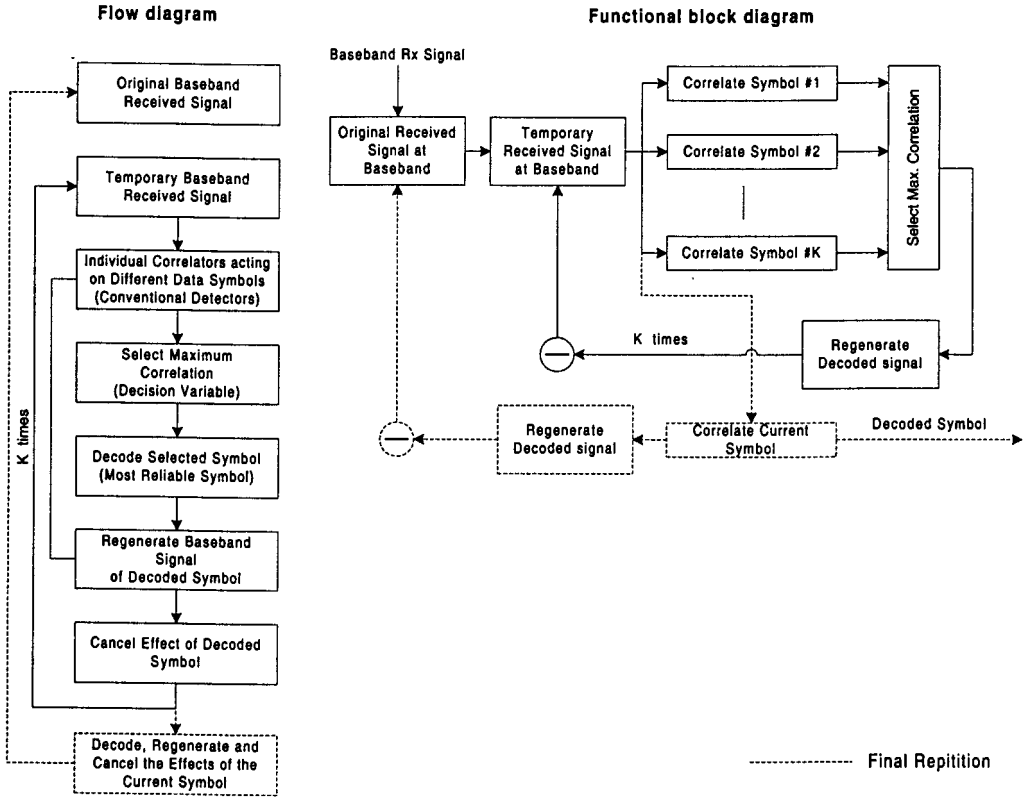

Figure 4.12: A functional flow and block diagram of the successive remainder subtraction ICIC algorithm.

buffer. The preliminary correlation metrics for each of the K symbols that must be detected during the next K symbol intervals are calculated. After decoding the symbol with the highest correlation peak (assumed to be the strongest remaining interferer), the faded sequence used to transmit this symbol is reconstructed and subtracted from the temporary correlation buffer. Again, the preliminary correlation metrics for the remaining symbols are calculated and the cancellation procedure of the

strongest interfering sequence is repeated until the weakest symbol has been detected. In the absence of noise, and with perfect CSI, K interfering sequences may be removed from the temporary correlation buffer. The current symbol is detected and decoded at this stage. Instead of cancelling its remainders from the temporary correlation buffer, it is removed permanently, since the final detection of the data symbol is complete.

It was found that attempts to cancel the remainders of all the data symbols from the correlation buffer resulted in a suboptimal performance. Thus, a minimum threshold for the correlation metric of a data symbol is set before it is used in the ICIC. This threshold reduced the probability of an incorrect ICIC attempt and improved the system performance. The value of this threshold was obtained through trial and error experiments and $\mu_{IC} = 0.5$ was found to be efficient for bipolar data symbols with unity amplitude.

4.5.4 MODIFIED REMAINDER SUBTRACTION ICIC

It was described in Section 4.3.4 that only the phase of the received TS symbols are corrected before time despreading and ICIC. This approach was followed after tests have shown that both amplitude and phase correction of the received TS symbols increased the BER of the system and only showed gains at high SNRs. This behaviour can be attributed to two phenomena:

1. During a deep fade, the instantaneous SNR for each TS and pilot symbol is below the average SNR value of the channel. The low instantaneous SNR results in less accurate channel estimates and subsequently less accurate phase and amplitude correction measures. Phase correction is crucial when coherent demodulation is attempted and can therefore not be neglected. However, attempts to correct the amplitude of TS symbols received during deep fades are not only inaccurate but may introduce additional noise to the already corrupted TS symbols. This observation would partially explain the poor performance of a TS system with symbol phase and amplitude correction under low SNR conditions.

2. Apart from introducing additional noise, amplitude correction measures during deep fades defeats the purpose of the TS diversity technique, which is to estimate data symbols from the time distributed symbol energies not affected by the fade.

Considering Fig. 3.3, the fading envelope of a signal not only fades below the average envelope level, but also rises above that value at certain times. The correlation properties of a spreading sequence are not only corrupted by signal fades below the average envelope level, but also by signal envelope surges above the average envelope level. During these envelope surges above the average level, the instantaneous SNR of the TS symbols are better than average. This would allow for more accurate channel estimates, resulting in good phase and amplitude correction measures. Implementing a selective amplitude correction method under no-noise conditions with perfect channel estimates would

result in a signal envelope shown in Fig. 4.13.

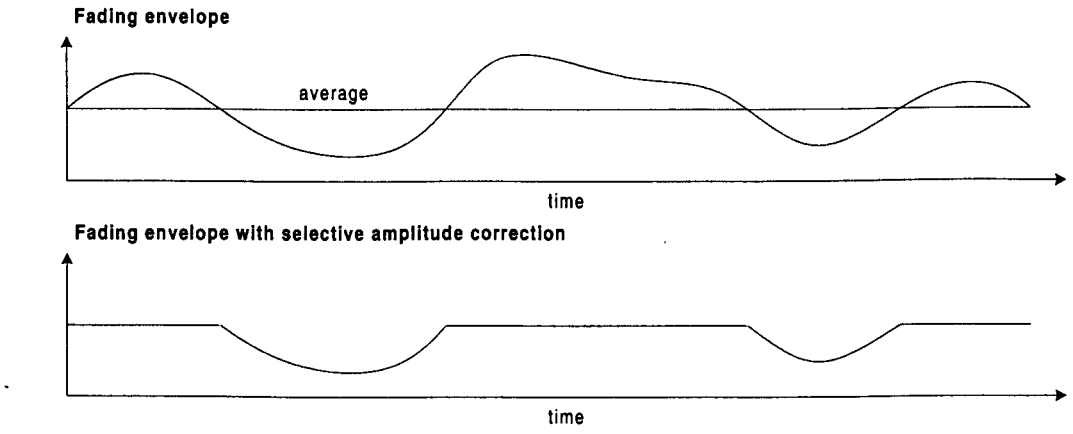

Figure 4.13: Effect of selective amplitude correction on a fading signal envelope under no-noise conditions.

The selective amplitude correction module can be implemented with good effect after the symbol phase correction module in Fig. 4.10. Note however that the fading envelope estimate $a(t)$, needs to be reset to unity during periods when the amplitude correction module was active, since it is assumed that the effects of fading have been eliminated completely during those periods.

This ICIC technique uses the available SNR per symbol more effectively than the standard ICIC method described in the previous section and achieves substantial improvements in the BER performance of the standard PSAM-TS system as can be seen in results depicted in Fig. 6.26.

4.6 SUMMARY

This chapter commenced by discussing the problem of obtaining accurate CSI for coherent detection and ICIC purposes. It was concluded from a literature study conducted on channel estimation techniques for the Rayleigh flat-fading channel, that PSAM was the best pilot signal aided channel estimation technique for coherent demodulation purposes. This chapter described the basic PSAM technique and the channel sample interpolation filter was emphasized, since it forms an integral part of any PSAM system. This discussion was followed by a description of the strategy followed to integrate the PSAM technique with the proposed TS system.

The MUI problem in DS-CDMA systems are closely related to the ICI problem in TS systems and a brief description of some of the MU-IC strategies employed in the DS-CDMA environment was

given. One of the main contributions of this dissertation is the development of several ICIC techniques to eliminate the ICI problem in TS systems. These techniques were discussed in the final sections of this chapter. Simulation results were generated to evaluate the different ICIC techniques under different channel conditions and with different system configurations. These results are presented in Chapter 6 and a discussion of the different results are provided.

CHAPTER FIVE

INTEGRATING ERROR CORRECTION CODING WITH THE TIME SPREAD TECHNIQUE

5.1 CHAPTER OVERVIEW

This chapter describes the integration of FEC coding techniques with the TS concept. The requirements for FEC codes to be used over a fading channel are briefly discussed. Then, the integration of a standard k/n-rate convolutional coding scheme with the existing TS system is described, and the emphasis is placed on the soft decision Viterbi decoder that is used to decode the encoded symbol stream at the output of the time despreading module. This is an exemplary chapter aimed at illustrating the performance and advantages gained when TS is combined with FEC techniques. Extensive research into different coding strategies falls beyond the scope of the dissertation and is left for future research. The chapter concludes with a short summary.

5.2 CODE REQUIREMENTS FOR USE IN TIME SPREAD MODEM

The error performance of a modulation code over a particular channel depends on several distance parameters and the path multiplicity of the code [51, 52]. For the AWGN channel, the error performance of the code depends primarily on its minimum squared Euclidean distance and path multiplicity characteristics. For the Rayleigh fading channel however, the error performance of the code strongly depends on its minimum symbol distance, minimum product distance, and path multiplicity. It depends on the minimum squared Euclidean distance to a lesser degree.

Receiver-diversity techniques have been known for a long time to significantly improve the quality of fading channels [9]. This topic was extensively investigated in [16, 5, 19] during recent years.

As mentioned in Chapter 3, the standard approach to diversity is based on the fact that, the probability that the received signal will fade on all branches simultaneously, can be made arbitrarily small by increasing the number of diversity branches. The approach taken in this dissertation (see Section 3.2.1) and [16, 5, 19] is philosophically different to this, since it is based on the observation that, under fairly general conditions, a channel affected by fading can be turned into an AWGN channel by increasing the number of diversity branches. As was mentioned earlier, the effect of TS is similar to the introduction of different diversity branches. Consequently, coding schemes designed to be optimal for the AWGN channel will perform asymptotically well on a fading channel with sufficient diversity introduced by the TS-technique. An advantage of this solution is its robustness, since changes in the physical channel has very little effect on the received signal.

As stated in [9], the problem of designing robust coding schemes for fading channels may be solved by the introduction of signal diversity. With this in mind, a simple yet effective coding scheme, based on a *Maximum Free Distance* (MFD) convolutional code, is proposed for integration with the existing TS technique described in previous chapters.

5.3 CODING STRATEGY FOR TIME SPREAD MODEM

5.3.1 TS TRANSMITTER WITH CODING

The FEC encoder is inserted in the TS transmitter directly after the binary data source, as can be seen in Fig. 5.1.

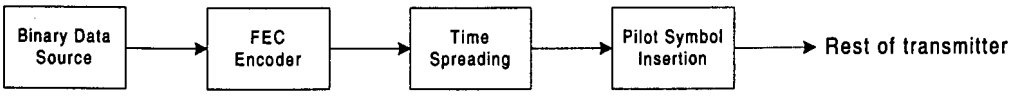

Figure 5.1: Integration of TS with FEC in the transmitter.

When more complex coding techniques, such as *Trellis Coded Modulation* (TCM) codes, are used, the TS module would be restricted to using non-complex spreading sequences, as multilevel/phase symbols can not be used in a TS system employing complex spreading sequences (see Chapter 3).

5.3.2 CONVOLUTIONAL ENCODING

A convolutional code is generated by passing the information sequence to be transmitted through a linear finite-state shift register. In general, the shift register consists of L (k-bit) stages and n linear algebraic function generators, as shown in Fig. 5.2. The input to the encoder, which is assumed to be

binary, is shifted into a shift register, k bits at a time. The number of output bits for every k input bits are n, resulting in a code rate of $R_c = k/n$. The parameter L is called the constraint length of the convolutional code.

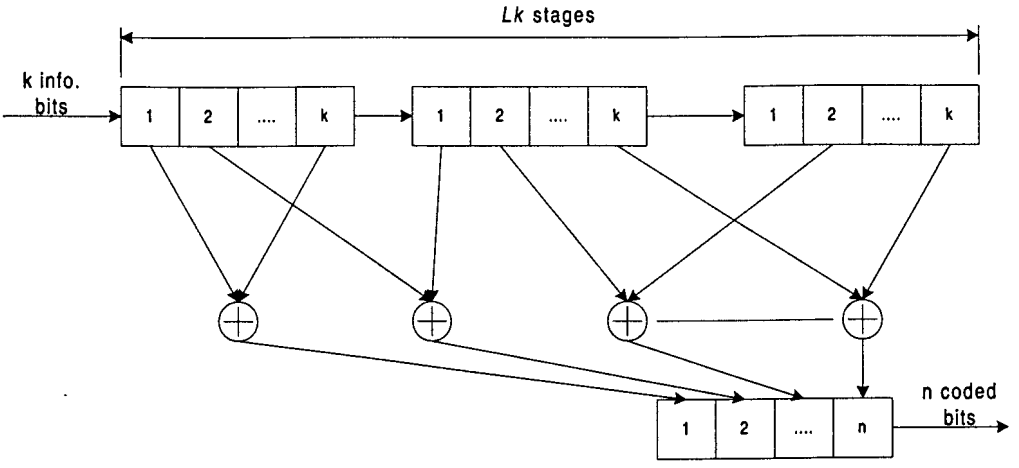

Figure 5.2: Convolutional encoder.

A common method of describing a convolutional code is to specify its generator matrix. As an alternative to specifying the generator matrix, the functional equivalent representation, namely a set of n vectors, corresponding to the n algebraic functions used to generate the n output bits, is given. Each vector has kL dimensions and contains the connections for generating the i^{th} output bit, where $i = 1, 2, 3, ..., n$.

The distance properties of a code determines its error correction capabilities. A compact and convenient method to illustrate the outputs of a convolutional encoder is the trellis diagram. The trellis diagram is a more elaborate structure showing the time-related transitions of a state diagram, which is only a graphical representation of the possible states of a convolutional code and its possible transitions from one state to another. For a certain input bit stream, the convolutional encoder follows a certain path through the trellis diagram. The minimum free distance d_{free} of a code is expressed as the minimum number of bits with which any path beginning and remerging with the all zero path differs from the all zero path in the trellis diagram. The parameter d_{free} plays an important role in the error correction capabilities of a code and must be maximized for optimal performance.

The convolutional $R_c = 2/3$ rate code [4] used in this dissertation has a constraint length of $L = 4$ and a d_{free} of 7.

The trellis diagram has $2^{k(L-1)} = 2^6 = 64$ states and the generator vectors for the three output bits in octal form are given by:

$$\begin{aligned} \mathbf{g}_1 &= 236_8 \\ \mathbf{g}_2 &= 155_8 \\ \mathbf{g}_3 &= 337_8 \end{aligned} \tag{5.1}$$

This code is optimal since it has the largest possible d_{free} for a given code rate R_c and constraint length L.

5.3.3 SOFT DECISION VITERBI DECODER

The soft decision Viterbi decoder is positioned in the TS receiver structure immediately after the time despreading and ICIC modules. No decoding or information extracting are made on the symbols before passing them to the Viterbi decoder since that would result in the loss of information and a consequent increase in average BER.

Unlike a block code that has a fixed length n, a convolutional coder is a finite state machine. Thus, the optimum decoder is a MLSE that makes decision based on a set of observations and not a single observation alone.

Suppose we observe a sequence of received symbols $r_1, r_2, r_3, ..., r_M$ where r_k, the received symbol at the k^{th} time interval, is given by

$$r_k = d_k + n_k \tag{5.2}$$

with d_k a symbol taken from the subset of possible transmitted symbols in the transmitted symbol sequence and n_k an AWGN sample. The joint PDF of $r_1, r_2, r_3, ..., r_M$ may be expressed as a product of M marginal PDFs, i.e.,

$$\begin{aligned} p\left((r_1, r_2, r_3, ..., r_M)|\mathbf{s}^{(m)}\right) &= \prod_{k=1}^{M} p(r_k|s_k^{(m)}) \\ &= \prod_{k=1}^{M} \frac{1}{\sqrt{2\pi}\sigma_n} \exp\left[-\frac{(r_k - s_k^{(m)})^2}{2\sigma_n^2}\right] \\ &= \left(\frac{1}{\sqrt{2\pi}\sigma_n}\right)^M \exp\left[-\sum_{k=1}^{M} \frac{(r_k - s_k^{(m)})^2}{2\sigma_n^2}\right] \end{aligned} \tag{5.3}$$

where s_k is one of the symbols in the subset of possible transmitted symbols and M is the number of outputs obtained from the demodulator. Given the received sequence $r_1, r_2, r_3, ..., r_M$, the detector determines the sequence $\mathbf{s}^{(m)} = \{s_1^{(m)}, s_2^{(m)}, ..., s_M^{(m)}\}$ that maximizes the conditional PDF $p(r_1, r_2, r_3, ..., r_M|s^{(m)})$. Such a detector is called a MLSE.

By taking the logarithm of (5.3) and neglecting the terms that are independent of $(r_1, r_2, ..., r_M)$, an equivalent MLSE which selects sequences that minimizes the squared Euclidean distance metric

$$D(\mathbf{r}, \mathbf{s}^{(m)}) = \sum_{k=1}^{M} (r_k - s_k(m))^2 \tag{5.4}$$

may be derived.

For the binary coding structure at hand, the total number of possible sequences in the trellis structure is equal to 2^M. If no simplification of the MLSE algorithm is applied, it requires that the metric for all 2^M sequences be calculated to find the most likely sequence $\mathbf{s}^{(m)}$ (i.e., the sequence that minimizes the squared Euclidean distance metric). The number of sequences in the trellis search may however be reduced by using the Viterbi algorithm [53] to eliminate less likely sequences as new data is received from the demodulator.

To explain the functioning of the Viterbi algorithm, consider the general trellis diagram shown in Fig. 5.3.

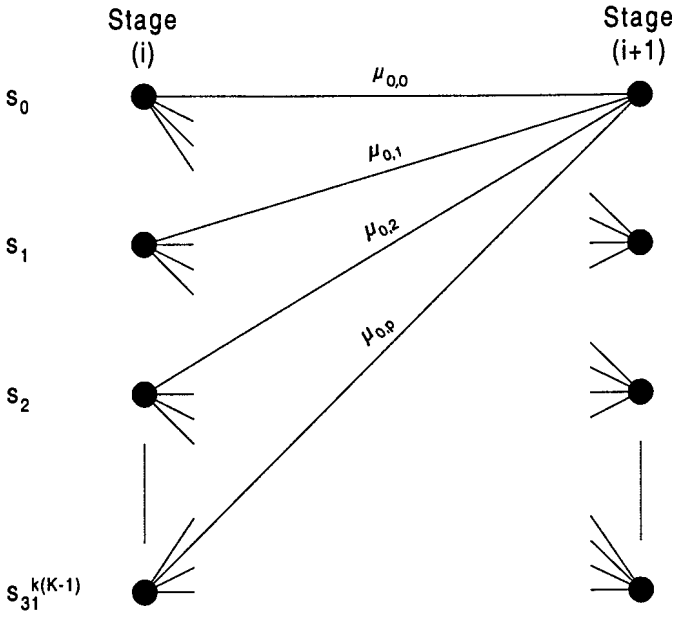

Figure 5.3: A general trellis structure.

Before the Viterbi algorithm is described, it is convenient to define the trellis notation illustrated in Fig. 5.3. $Stage(i)$ is the previous stage up to where the surviving trellis paths have been calculated, and $Stage(i+1)$ is the current stage for which certain branches in the trellis structure needs to be

eliminated in order to obtain the surviving paths up to $Stage(i+1)$. The parameter $\mu_{x,y}$ is the squared Euclidean distance metric for each branch in the trellis structure, where $x \in [0, 1, 2, ..., 2^{k(K-1)} - 1]$ indicates the number of the branch's final state and $y \in [0, 1, 2, ..., 2^k - 1]$ the number of the possible received code words for that branch. The convolutional code rate is k/n and the constraint length of the code is K. After each code word interval nT_s, each node (state) in the $(i+1)^{th}$ $Stage$ of the trellis diagram has one surviving path associated with it. This surviving path has a weight factor w_m, $m = 0, 1, 2, ..., 2^{k(K-1)} - 1$ that determines the likelihood of that path. The initial values of all path weights are set to zero.

During each code word interval nT_s, n analog symbols are received from the time despreading module to form a symbol vector $\mathbf{r}$. The branch metric $\mu_{x,y}$ is then calculated for each branch of node x and added to the weight factor of the surviving path associated with the begin-state of that branch. The branch metric is calculated according to

$$\mu_{x,y} = \sum_{l=0}^{n-1} (r_l - s_l^y)^2, \tag{5.5}$$

where r_l is the l^{th} received symbol and s_l^y is the l^{th} symbol associated with the y^{th} code word of node x. The parameter $\mu_{x,y}$ is then added to its corresponding surviving path metric w_m and the branch of node x with the smallest surviving path metric is concatenated to the corresponding surviving path associated with the branch's begin-state. Repeating this procedure for all the nodes in the $(i+1)^{th}$ $Stage$ of the trellis diagram leaves $2^{k(K-1)}$ surviving paths.

After approximately $C = 5$ memory intervals of n symbols each, the branches of the $2^{k(K-1)}$ surviving paths would have merged with a high probability at $C + 1 = 6$ stages back in the trellis structure. C denotes the constraint length of the Viterbi decoder. Thus, if the surviving paths are truncated to a length of $C + 1 = 6$ memory intervals, decisions made on the tail ends of the surviving paths would have a high degree of accuracy. Longer surviving paths will result in marginally better BER performances, but will also increase the decoder size and complexity.

5.4 INTEGRATED TS-TURBO CODING STRATEGY

Turbo Code (TC) was first introduced to the coding community in 1993 [54], and has ever since established itself as one of the most important breakthroughs in the error correction coding arena since the introduction of trellis coded modulation in 1982. TC was shown to provide substantial coding gains in AWGN and correlated fading channels under the condition that accurate CSI and adequate interleaving is available. The TC-TS-technique was developed through a joint effort of the author and Staphorst, where Staphorst was responsible for the implementation of the Turbo Coding

and Decoding algorithms. Work on the integrated TC-TS-technique falls beyond the scope of this dissertation and information provided in the following sections are only included to illustrate the transparency and versatility of the TS-technique. This section is aimed at describing the strategy to integrate TC with the existing TS technique addressed in this dissertation. Since its introduction in 1993, several variations of the original TC technique has been proposed in the literature. This section will only deal with the standard parallel concatenated TC technique and will treat the Turbo Encoder and Decoder as SISO devices that rely on the transparency of the TS technique for proper functioning.

5.4.1 TC-TS TRANSMITTER

The Turbo Encoder is integrated with the existing TS system in the same manner as the standard convolutional encoder (see Section 5.3.1). Binary symbols emanating from any source are Turbo Encoded and passed to the TS module.

Two half-rate systematic convolutional encoders are used as the constituent encoders in the parallel concatenated turbo encoder. Using all the bits at the outputs of the two encoders would result in a $R_c = 1/4$ rate code. The outputs of these two encoders are however punctured to obtain a $R_c = 1/2$ turbo code. The puncturing process involves the discarding of all the interleaved systematic code bits as well as every second parity bit from either of the two encoders respectively. This results in one systematic bit and one parity bit being transmitted for every one input bit. The parity bit is selected by the puncturing mechanism from one of the constituent encoders on a rotational basis. Thus with a $R_p = 4/5$ bit rate after pilot symbol insertion, the overall bit rate for the TC-TS system is $R_c = 2/5$. The frame size used in the turbo encoder amounts to 400 bits, of which 4 are padding bits, ensuring the correct termination of the convolutional code trellises.

5.4.2 TC-TS RECEIVER

The basic structure of the TS receiver with FEC decoding is not affected and only the soft decision Viterbi decoder is replaced by the turbo decoder. The soft outputs of the time despreading module serves as input to the turbo decoder in the same way as for the soft decision Viterbi decoder. All TC schemes are highly dependant on accurate CSI values and it is therefore necessary to re-estimate the CSI after time despreading. This is necessary since the TS technique effectively transforms the fading channel to a Gaussian channel, resulting in a different $\overline{E}_b/N_0$ after time despreading than is actually present in the channel. Due to TS it is no longer necessary to accurately estimate the fading process for CSI and only the average noise power need to be estimated. The output of the turbo decoder is an estimate of the original data which was encoded in the TC-TS transmitter.

5.5 SUMMARY

The TS technique is ultimately aimed at improving the performance of standard FEC coding techniques in a Rayleigh fading channel. This chapter was aimed at describing a technique to integrate the proposed TS diversity technique with a standard convolutional coding scheme. The convolutional encoder was discussed first and its generator functions and other specifications were given. The next section described a soft decision Viterbi decoder which serves as a MLSE to decode the convolutional code used in the system. The transparency of the TS technique with regards to the integration with coding techniques was finally illustrated by describing a strategy to employ a TC technique. The TC-TS transmitter and receiver were discussed briefly, with the emphasis on the integration of the parallel concatenated TC with the existing TS technique, rather than on the TC principle itself.

CHAPTER SIX

SIMULATION STUDY

6.1 CHAPTER OVERVIEW

This chapter begins by giving a description of the different TS transmitter and receiver configurations that have been used during the development and evaluation of the TS technique. The different building blocks implemented in the simulation software, that was employed to test the TS system under different channel and modem configurations, is briefly described. The simulated mobile channel used in this dissertation is verified by recording different signals in the time and frequency domains. The chapter continues by providing a large number of BER graphs that illustrate the performance of the TS technique under different channel conditions and with different transceiver configurations. Each set of results is discussed and explanations are given for certain system behaviours. The final section in this chapter illustrates the BER performances obtained by employing FEC techniques integrated with TS. This section confirms that substantial gains can be obtained by jointly using TS with FEC techniques. The chapter is concluded with a brief summary of the most important results presented in the chapter.

6.2 SIMULATION CONFIGURATION

All the simulation software used in this dissertation was written in Borland C++ Builder® and different building blocks were implemented as separate objects. These building blocks are briefly discussed in the following section. A number of functions, used in the analysis of the TS technique, were also implemented as M-files in Matlab®.

6.2.1 SIMULATION BUILDING BLOCKS

The most important building blocks in the simulation software used to evaluate the TS technique and its enhancements are listed below. These building blocks are implemented as generic C++ objects

and can be reused in other simulation configurations.

6.2.1.1 BINARY DATA SOURCE

This object generates a random binary data stream using a *Piece-wise Random Binary Sequence* (PRBS) generator. The object can produce outputs of both sampled and non-sampled data streams and is used in both the transmitter and receiver to generate a data stream. Given the same initial values, the data source produces the same output data stream. This property is used for reference purposes in the TS receiver, when the decoded data symbols are compared to the transmitted data symbols.

6.2.1.2 FIR FILTER

This object is used extensively throughout the transmitter and receiver structures. The object is especially used for pulse shaping and matched filtering purposes. The time spreading functionality in the transmitter is also implemented using this FIR object. The FIR object is initialized by specifying a set of filter coefficients stored in a binary file. When this set of coefficients is equal to the elements of a TS sequence, the object effectively implements the time spreading function.

6.2.1.3 CONVOLUTIONAL ENCODER

The convolutional encoder object forms part of the TS transmitter structure and convolutionally encodes a binary input data stream according to a set of generator polynomials. The code rate and set of polynomials is specified in an initialization file that is interpreted by the object.

6.2.1.4 NOISE GENERATOR

This object generates AWGN samples that have a specified mean μ and standard deviation σ. The object is used to generate AWGN samples in the implementation of the mobile communication channel. The object is also used in the generation of the in-phase and quadrature-phase fading components of the fading process in the mobile channel.

6.2.1.5 IIR FILTER

The IIR filter object is used in the mobile channel implementation to obtain the desired Doppler spectral shape for the lowpass fading processes.

6.2.1.6 RICIAN FADING CHANNEL

This object uses the Noise Generator and IIR Filter objects to implement a Rician Fading mobile channel with a Rician K parameter specified as one of the object parameters. This object is also used

to obtain a Rayleigh fading channel by setting $K = -\infty$ dB.

6.2.1.7 WIENER INTERPOLATION FILTER

The Wiener Interpolation Filter object samples the input symbol stream to extract the pilot symbols. These pilot symbols are then interpolated to give estimates of the fading amplitude and phase characteristics of the mobile channel. The coefficients for the Wiener Filter are stored in a matrix format in a binary file that is created using the *MakeOptWiener.m* Matlab function.

6.2.1.8 PSAM IC MODULE

This object implements the time despreading and IC module in the TS receiver. The object uses the fading channel estimates and received TS symbols as inputs and returns estimates of the transmitted data symbols.

6.2.1.9 SOFT DECISION VITERBI DECODER

This object implements the Soft Decision Viterbi Decoder used to decode the convolutionally encoded data symbols. The object is configured according to an initialization file that specifies the FEC code's code rate and Trellis structure.

6.2.1.10 CONVOLUTIONAL CODE TRELLIS GENERATOR

This functionality is implemented as a separate program and does not function as part of the main TS simulation. The program uses the generator polynomials of a convolutional code to generate it's Trellis structure. This Trellis structure is then stored in a file that is interpreted by the aforementioned Viterbi decoder object used to decode convolutional FEC codes.

6.2.2 TRANSMITTER SPECIFICATION

The transmitter structures described in Chapter 4 were used in the simulation evaluation of the TS technique. The technical detail concerning the spreading sequences that were used, viz pilot symbol insertion rate, FEC coding, etc., will be given in this section.

The following spreading sequences were used in the evaluation of the TS technique:

- Dukic sequences of lengths 64, 256 and 1024.
- Dukic sequences of lengths 16, 64, 256 and 1024 temporally expanded to obtain the same time diversity as a length 1024 sequence.

- Length 63 FZC sequences temporally expanded to obtain the same time diversity as a length 1008 sequence.
- One-dimensional genetic sequences of length 11, temporally expanded to a length of 165.

The pilot symbol insertion rate was set at one pilot symbol for every four TS symbols, with the pilot symbol level equal to the RMS TS symbol level. The pilot symbol rate was much higher than the required Nyquist sampling rate for the channel and ensured good channel estimates for use in the coherent detection and ICIC modules. This reduced the data transfer rate of the system to four fifths of the original system if the original transmission bandwidth is retained.

For the coded system a $2/3$-rate convolutional code with $K = 4$ was used. This resulted in an overall data transmission rate for the coded system equal to $8/15$ times that of a system without PSAM and FEC coding.

Finally, the composite complex TS signal is modulated onto two orthogonal IF carriers. The IF carrier frequencies were chosen at four times the channel symbol rate for simulation purposes. The simulation sampling rate was set at eight times the IF frequency, resulting in 32 samples used per channel symbol.

6.2.3 CHANNEL SPECIFICATION

Rayleigh and Rician fading mobile channels were used in the simulation evaluation of the TS technique. A 3^{rd} order approximation of the theoretical Clarke Doppler spectrum was employed to model the lowpass fading process (see Appendix A). Four different channel fading rates were used in the simulation, namely: $0.5, 1.0, 2.0$ and 4.0 percent of the channel symbol rate respectively. These are consistent with fading rates used in the literature [26, 33, 30], where the performances of communication systems in Rayleigh flat-fading channels were evaluated.

The LOS to fading signal power ratios used for the Rician channel were: $-100, -10, 0$ and 10 dB respectively.

BER results for the different systems were calculated up to $\overline{E}_b/N_0 = 30$ dB or $P_e = 10^{-6}$, which ever came first. This lower bound on the P_e was enforced to prevent simulation runs of excessive duration at lower P_e's.

6.2.4 RECEIVER SPECIFICATION

The TS receiver structure was configured to receive the desired combinations of signals generated by the TS transmitter in Section 6.2.2. In addition to this, the TS receiver was configured with either one

of the following ICIC modules to suppress the ICI in the TS signal:

- The standard estimate, and subtract ICIC (Section 4.5.2).
- The successive ICIC module (Section 4.12).
- The selective AC-ICIC (Section 4.5.4).

Results obtained with the different receiver structures are presented in later sections of this chapter.

6.3 MOBILE CHANNEL VERIFICATION

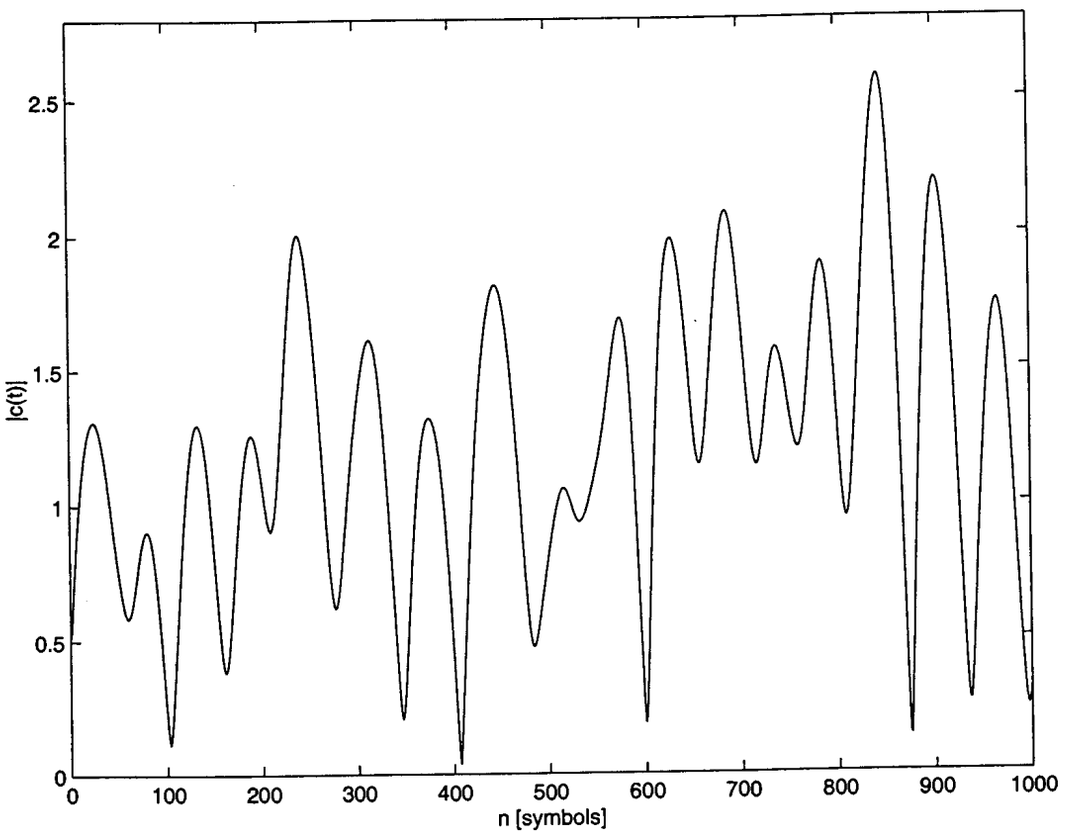

Figure 6.1: Estimated fading envelope for a fading rate of 1% of the channel symbol rate, estimated using 4/5-rate PSAM.

The channel model used for simulation purposes was verified by calculating the envelope PDF, CDF and PSD for the fading process. A portion of the noiseless estimated fading envelope can be seen in Fig. 6.1. The channel fading effects were estimated using the PSAM module with a 19-tap Wiener estimation-interpolation filter and a pilot symbol rate of one in every five channel symbols. The fading envelope PDF calculated for a fading rate of 1% of the channel symbol rate can be seen in Fig. 6.2. Superimposed on the measured PDF in Fig. 6.2 is the theoretical PDF given by (2.11). Note

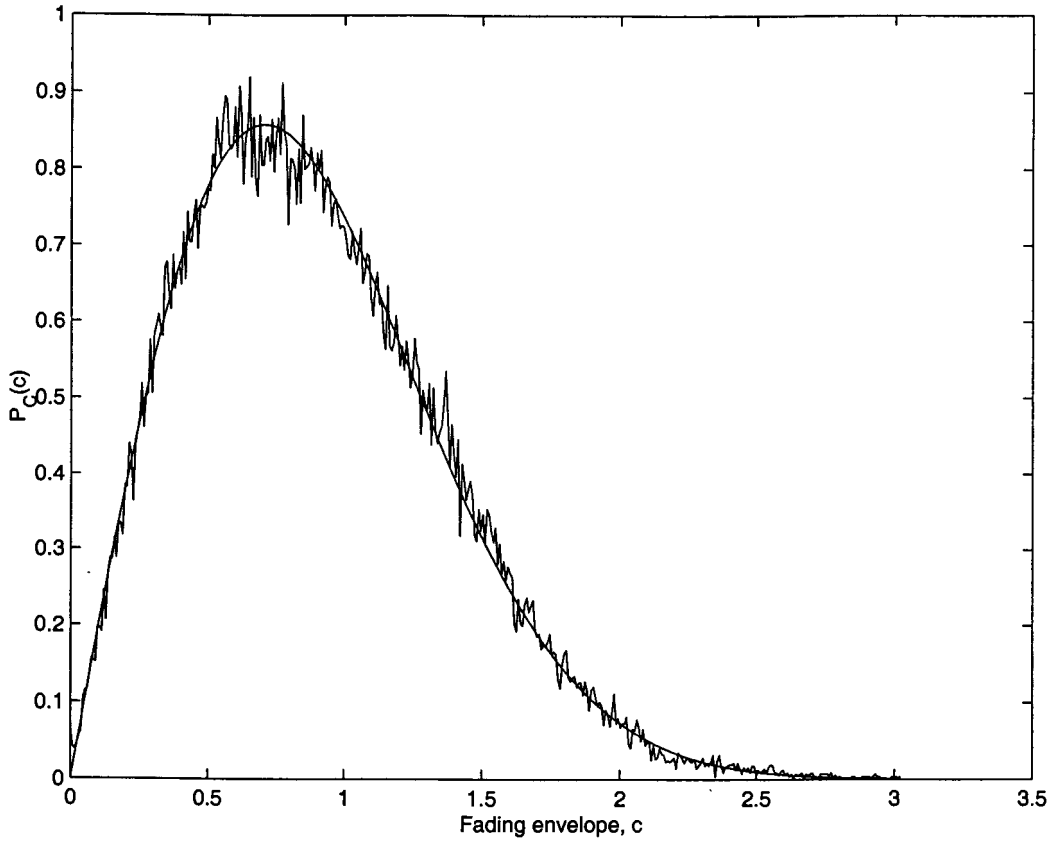

Figure 6.2: The PDF of the estimated and theoretical fading envelopes in the TS receiver with $\sigma_c = 1/\sqrt{2}$.

that the theoretical and simulated PDFs compare favourably. This is confirmed by the superimposed CDFs, shown in Fig. 6.3, for the measured and theoretical fading envelopes respectively.

From Fig. 6.2 and Fig. 6.3 it can be concluded that the fading envelope statistics of the simulated channel correspond closely to the theoretical channel statistics.

Another important statistical parameter regarding a fading channel is its LCR and average duration of a normalized fade below a certain specified level ρ (see Section 2.5.2.3). The average fade duration parameter was verified numerical by means of simulation and is plotted in Fig. 6.4 for different values of ρ. Superimposed on this graph is the theoretical graph calculated according to (2.16). The graphs in Fig. 6.4 are plotted with the amount of symbols as the measurement unit for the y-axis. This illustrates that several symbols are influenced by fading levels below the unity channel gain. Fig. 6.4 illustrates that the average fading durations below a certain threshold does not perfectly match the theoretical values for different values of ρ. The simulated values do however exhibit the correct trend and it is concluded that the higher order statistical requirements of the fading channel is met to a sat-

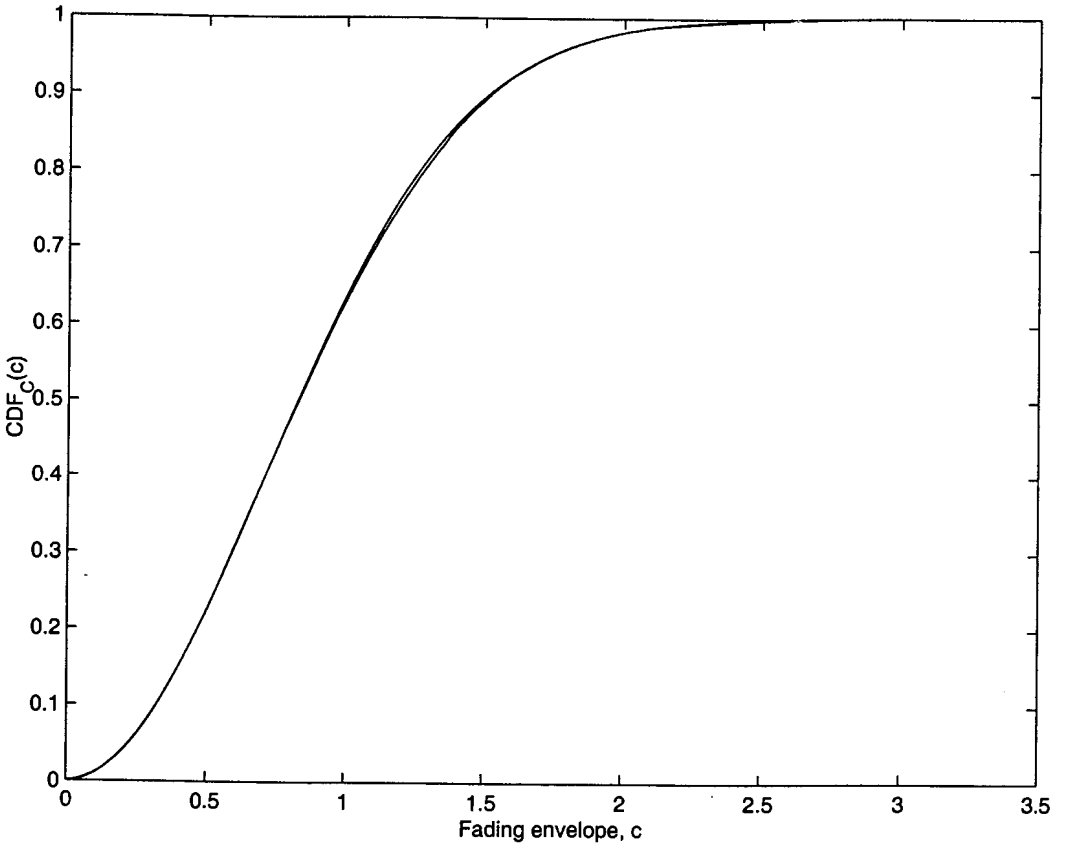

Figure 6.3: The CDF of the estimated and theoretical fading envelopes in the TS receiver with $\sigma_c = 1/\sqrt{2}$.

isfactory level, considering that only a third order approximation was used for the theoretical Clarke Doppler spectrum. The lowpass Doppler filter approximation used in the channel simulation allows fading frequency components above f_m to pass through. These higher fading components cause the average fade durations to be shorter than the theoretical values for the same fading level threshold ρ.

6.4 CHANNEL ESTIMATION AND COHERENT DEMODULATION

Accurate channel estimation techniques are an important requirement for a TS system employing integrated ICIC techniques. A Wiener filter based channel estimation filter with 19 filter taps was used throughout the simulation evaluation of the TS system. Channel sampling was performed at every fifth channel symbol period. The filter coefficients for the estimation-interpolation filter were adapted to take the deviations in the fading spectrum from the theoretical Clarke Doppler spectrum [11] into account. Fading statistics shown in Section 6.3, measured using the channel estimation technique proposed by [30], confirms the credibility of the channel estimation technique.

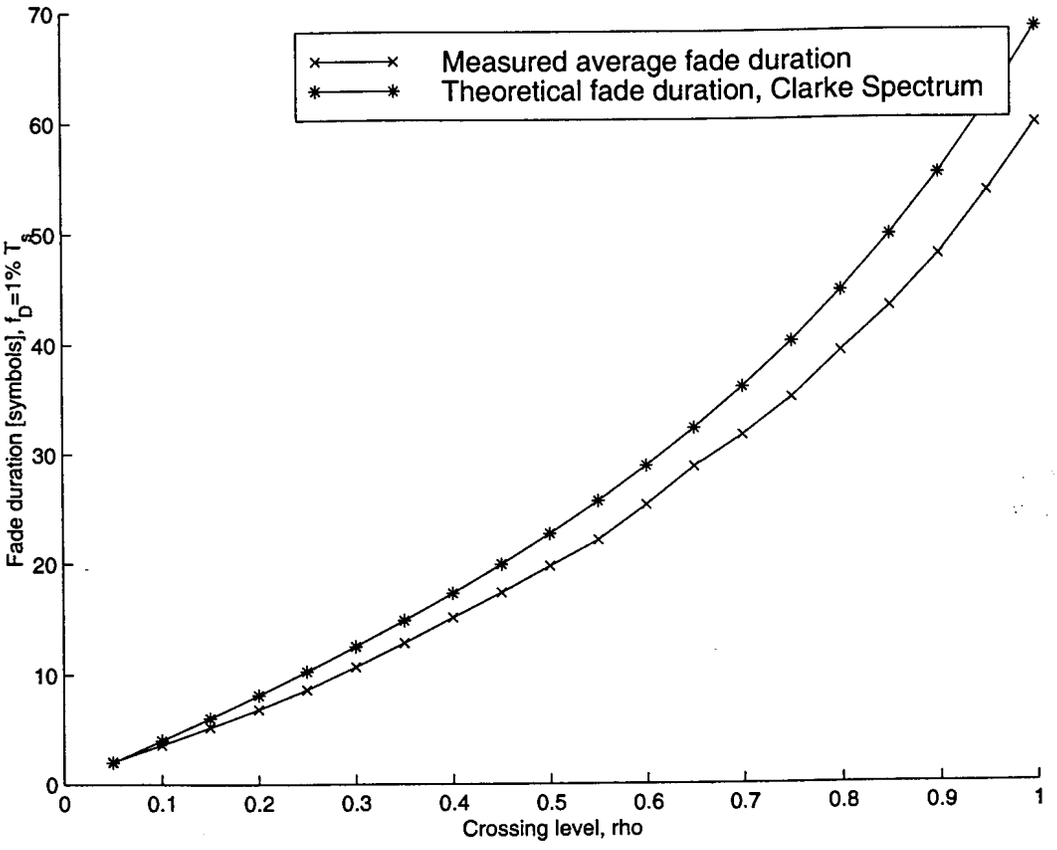

Figure 6.4: Different fading durations calculated for the normalized theoretical Clarke Doppler spectrum and the simulated fading channel as a function of ρ, the fading level threshold.

Benchmark BER results were generated using a BPSK modulation system to evaluate the PSAM technique and to serve as a reference for later results for the TS system. The simulated BER results shown in Fig. 6.5 were compared to results obtained by [30] and agreed to within a fraction of one decibel. The symbols used in this figure are f_D the fading rate in [Hz] and R_s the symbol rate in [bits/sec].

Results illustrating the effect of channel phase estimation and correction for coherent demodulation can be seen in Fig. 6.10. This figure depicts the phase corrected received signal constellation for a TS system using a Dukic-64-y spreading sequence. A more detailed discussion of this result is provided in Section 6.5.2.

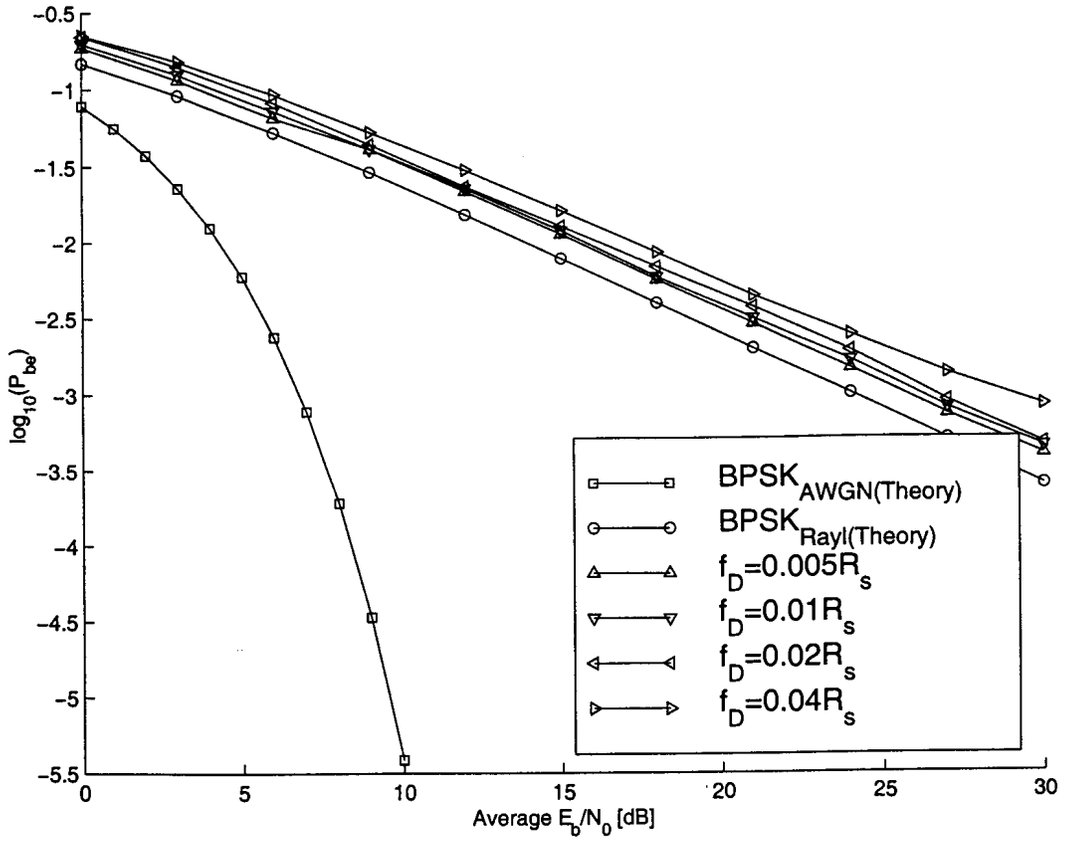

Figure 6.5: Performance of a coherent BPSK system with PSAM in a Rayleigh fading channel with different fading rates, f_D, as a fraction of the symbol rate, R_s.

6.5 CHARACTERISTICS OF TS SIGNALS

This section is concerned with the signals present at different stages in the TS transceiver and their time, spectral and statistical properties.

6.5.1 TRANSMITTER SIGNAL

When bipolar data symbols are spreaded in time by a Dukic-1024 spreading sequence, the resulting in-phase and quadrature-phase time spreaded signals exhibits noise-like amplitude characteristics (see Fig. 6.6).

The noise-like nature of a TS signal is confirmed by the amplitude PDF of the normalized in-phase signal in Fig. 6.6 (see PDF in Fig. 6.7). Note that the envelope of the measured PDF has the shape of a Gaussian PDF. Of further interest is the fact that certain amplitude levels occur with very low probability. This is confirmed by the transmitted signal constellation plotted for 50000 channel symbols, where it can be seen that odd symbol levels occur with a very low probability. Odd symbol levels

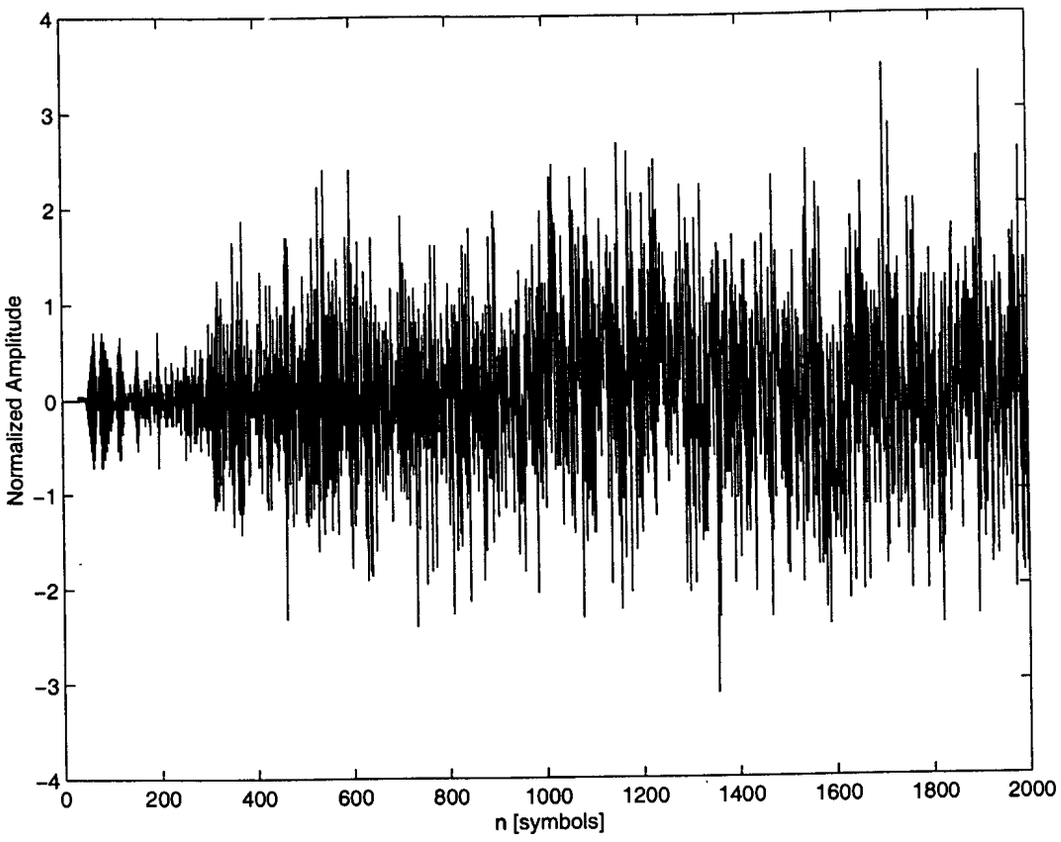

Figure 6.6: An in-phase baseband TS signal employing a Dukic-1024 spreading sequence at the transmitter.

only arise when an odd number of non-zero-level Dukic sequence elements overlap in time and we gather from the TS signal constellation and PDF that this occurs rarely.

Although not clearly visible from Fig. 6.8, the PSD of the transmitted TS signal contains frequency tones at intervals equal to the pilot symbol insertion rate. This is due to the periodicity of the pilot symbols inserted into the data symbol stream. The frequency axis of the PSD graph is normalized to the channel symbol rate and it is clear that the IF frequency modulated by the baseband TS signal is equal to four times the channel symbol rate. Note the narrow band spectrum generated by the TS transmitter, the spectral shape closely resembles that of a non-TS PSK modulation system. Time Spreading does not introduce any spectral shaping and does not increase the bandwidth of a BPSK system, apart from the bandwidth increase caused by the insertion of pilot symbols. The bandwidth expansion factor associated with the PSD of the TS system depicted in Fig. 6.8 is $5/4$ times. Thus, the effective transmitted bit rate for the TS system is only $R_b = 4/5R_s$, when no FEC coding is employed. Fig. 6.8 also illustrates the effect of the $\alpha = 1.0$ roll-off factor square root Nyquist filters used in the transmitter for band limiting and matched filtering purposes.

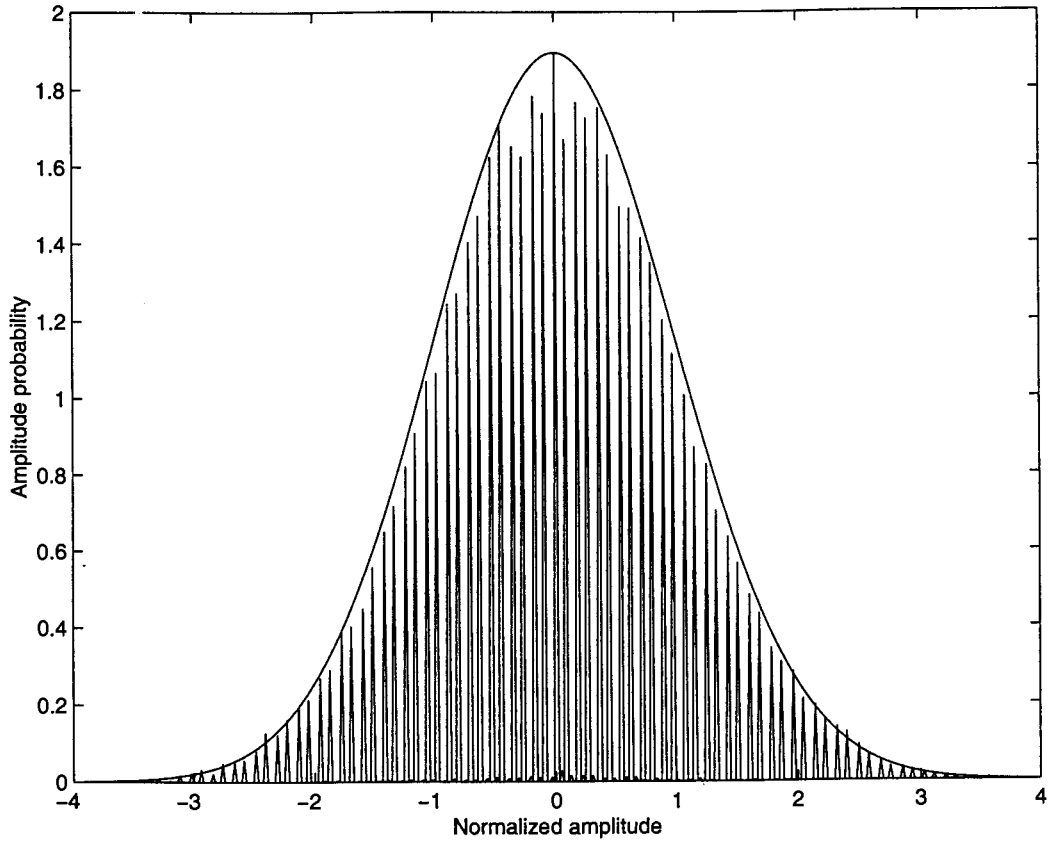

Figure 6.7: The PDF of the in-phase baseband TS signal employing a Dukic-1024 spreading sequence at the transmitter.

The transmitted signal constellation for a TS system using a Dukic-64 spreading sequence can be seen in Fig. 6.9. Note that symbols in the in-phase and quadrature-phase branches with odd numbered symbol levels occur with a very low probability. The complete signal constellation for a length 64 Dukic TS system would contain all the odd and even numbered symbol levels from -64 to 64 in the in-phase and quadrature-phase branches of the constellation. Symbols on the outer parts of the signal constellation do however occur with a low probability and are therefore not visible in the simulated signal constellation, which was created from only 50000 TS symbols. The random nature and the large signal constellation of the transmitted TS signal may provide some form of data security. This may be exploited by cryptographic systems and provide grounds for future research.

6.5.2 RECEIVED SIGNAL

Fig. 6.10 illustrates the phase and selective amplitude corrected signal constellation for a received TS signal after transmission over a Rayleigh fading channel with no AWGN present. The corresponding transmitted signal constellation can be seen in Fig. 6.9. Selective symbol amplitude correction en-

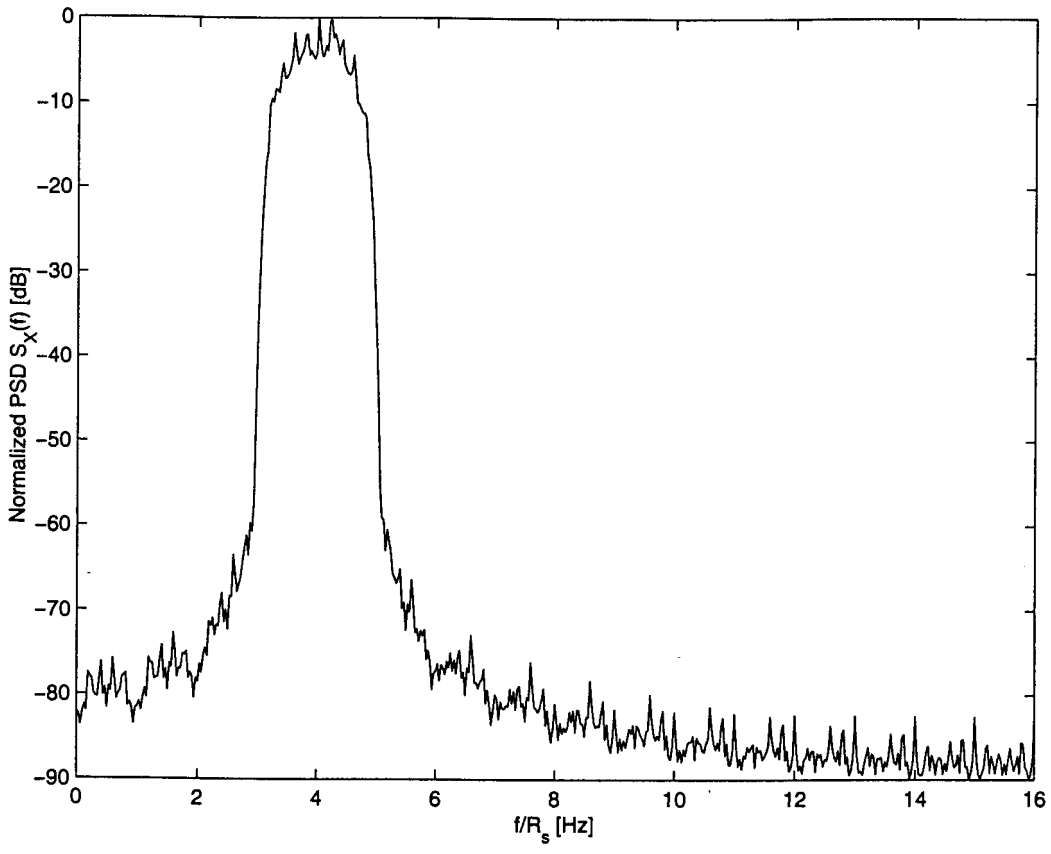

Figure 6.8: The PSD a TS signal employing a Dukic-1024 spreading sequence with 4/5-rate pilot symbol insertion on an IF carrier after frequency and power normalization.

tails the correction of TS symbol levels only when the instantaneous SNR for that symbol is above average. When an attempt is made to correct the amplitude of a TS symbol during a sub-average instantaneous SNR period, the amplitude correction efforts generally induces more noise to the system and is therefore not performed. BER results in Section 6.11 confirm that this fading correction strategy, combined with ICIC, provides very good TS BER performance figures.

6.5.3 THE FUNCTIONING AND PERFORMANCE GAIN OF THE TS TECHNIQUE

The gains obtained from the TS technique is explained in this section, by giving some statistical measurements obtained from different TS systems. This section highlights some important findings made during the completion of this dissertation regarding the behaviour of the TS technique in fading channels. The basic concept of the TS technique is illustrated by Fig. 6.11, where a complete fade with a duration of 174 data symbols was enforced on a baseband TS signal after time spreading. This fade resembles the most severe form of flat-fading possible in a mobile channel, where the transmitted signal is completely attenuated for a period in time. The soft level signal output of the time

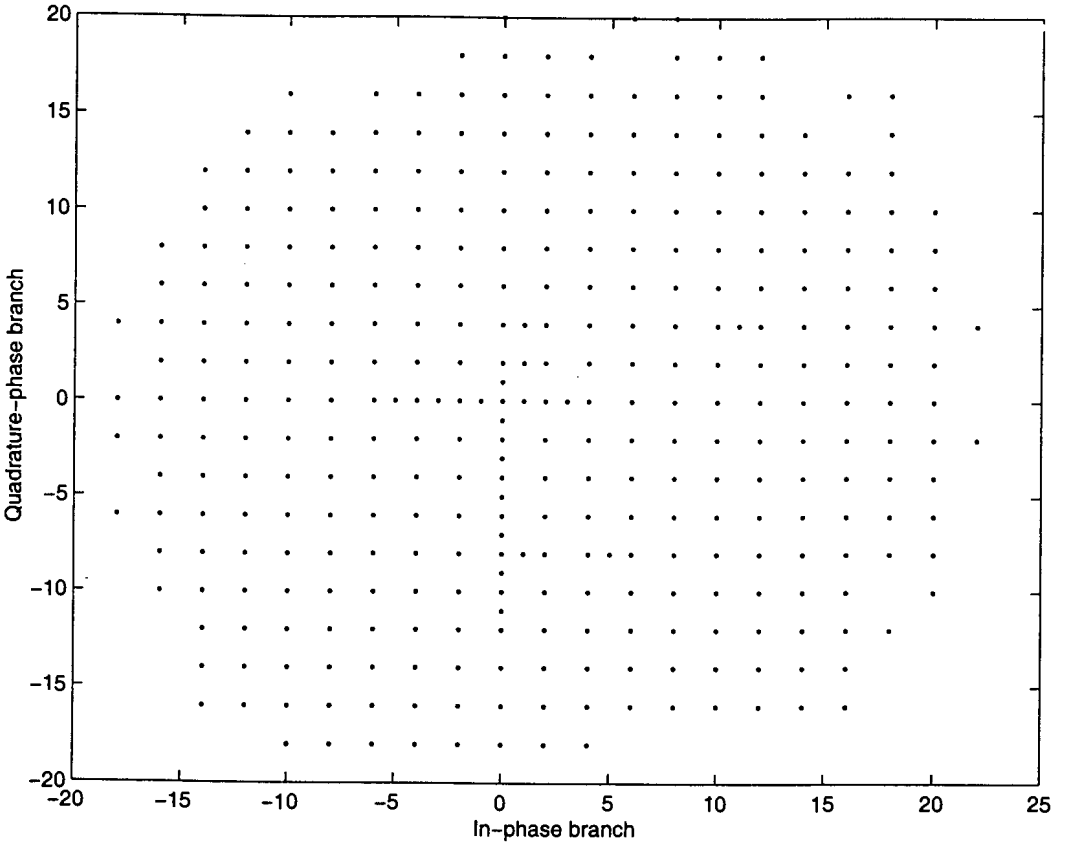

Figure 6.9: The partial transmitted TS signal constellation employing a Dukic-64 spreading sequence.

despreading module in the TS receiver is depicted in Fig. 6.11, together with the output of a PSK system without TS. The tests were conducted in the absence of AWGN and, although the amplitude of the data symbols after time despreading were somewhat distorted, no decision errors were made, compared to the PSK system that made 174 errors.

TS provides a two-fold gain. Firstly it reduces the noise power due to fading at the data symbol decision device with increased ICIC complexity, and secondly it reduces the number of consecutive symbol errors due to slow fading. The first TS gain enables the technique to enhance the performance of an ordinary PSK system in a fading channel without any FEC coding. The reduction of symbol error bursts on the other hand, enhances the performance of FEC codes designed for AWGN channels when used in a fading channel. The next set of figures were generated for different TS receivers operating in a Rayleigh fading channel with an average $\overline{E}_b/N_0 = 10$ dB, using a Dukic-64-16 spreading sequence.

The tendency illustrated in Fig. 6.12 to Fig. 6.15 is clear. An increase in TS receiver efficiency re-

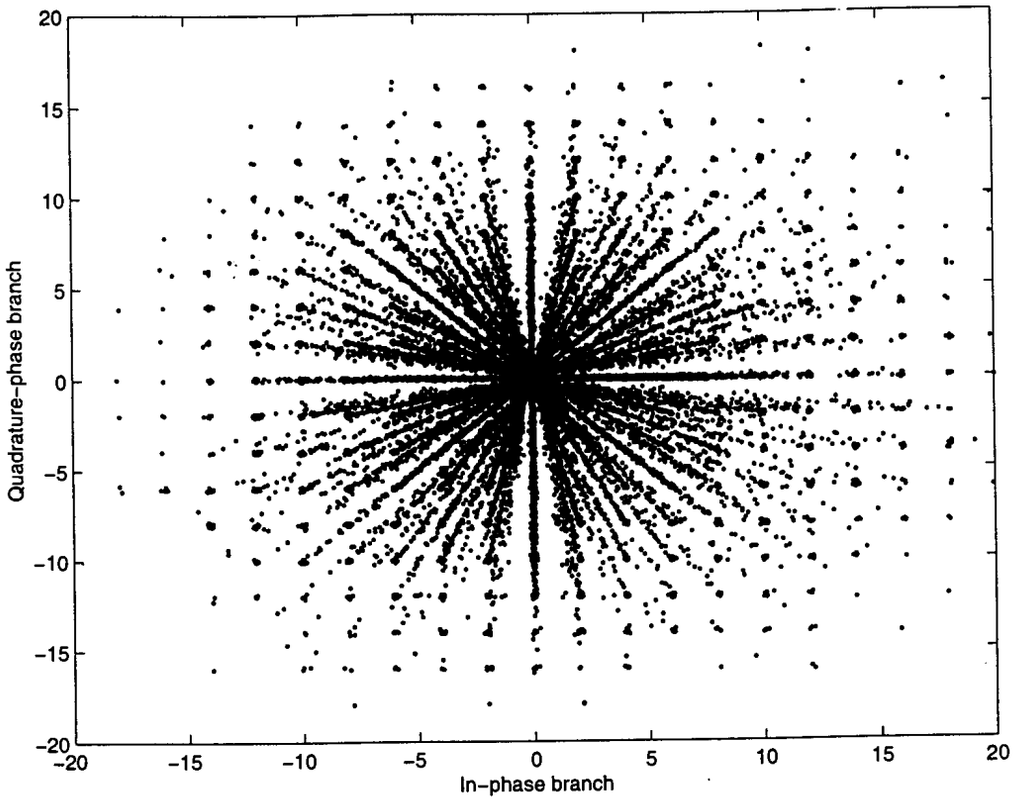

Figure 6.10: The partial received TS signal constellation employing a Dukic-64-y spreading sequence after phase- and selective amplitude correction, transmitted over a fading channel with $f_D = 0.01R_s$.

sults in a decrease in the symbol noise power and a dramatic increase in the average distance between symbol errors. The decrease in symbol noise power explains the gains obtained from time spreading in the absence of FEC measures, while the increase in symbol error distances improves substantially the efficiency of FEC codes designed for AWGN channels. A Gaussian PDF has been fitted to each symbol amplitude error PDF according to the measured standard deviation of each error signal. This theoretical PDF was superimposed on each measured PDF. Note that the PDFs of error signals for the TS systems match the Gaussian PDF very well in all instance where TS is employed. This confirms the ability of the TS technique to Gaussianize a Rayleigh fading channel and supports to the findings in [9], where it is stated that the Gaussianization of fading channels makes it possible to apply code design techniques used in AWGN channels. Note that all the results were measured for a Rayleigh fading channel with a fading rate of 1.0% of the channel symbol rate and a $\overline{E}_b/N_0 = 10$ dB. Results of these measurements are summarized in Table 6.1. BER results for the different systems will be presented in the next sections of this chapter with more elaborate discussions on the different observations.

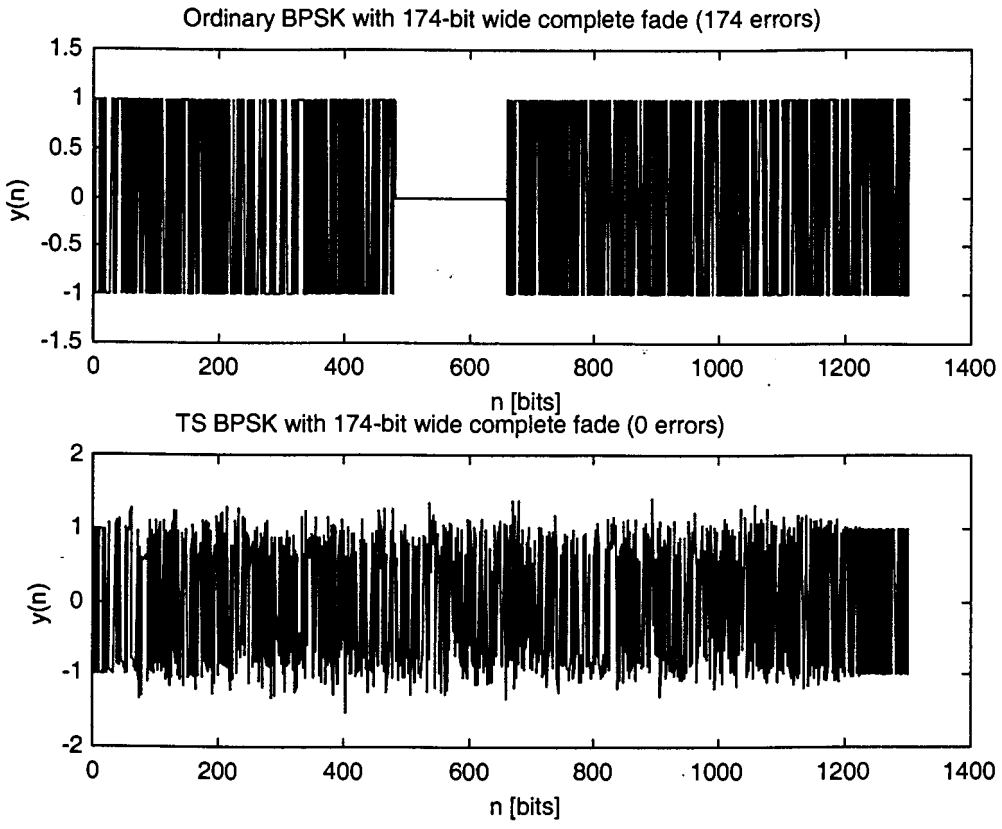

Figure 6.11: The effect of TS on a signal suffering from a complete fade lasting 174 bit intervals. Top: Catastrophic flat fade; Bottom: Reconstructed signal after Time Despreading.

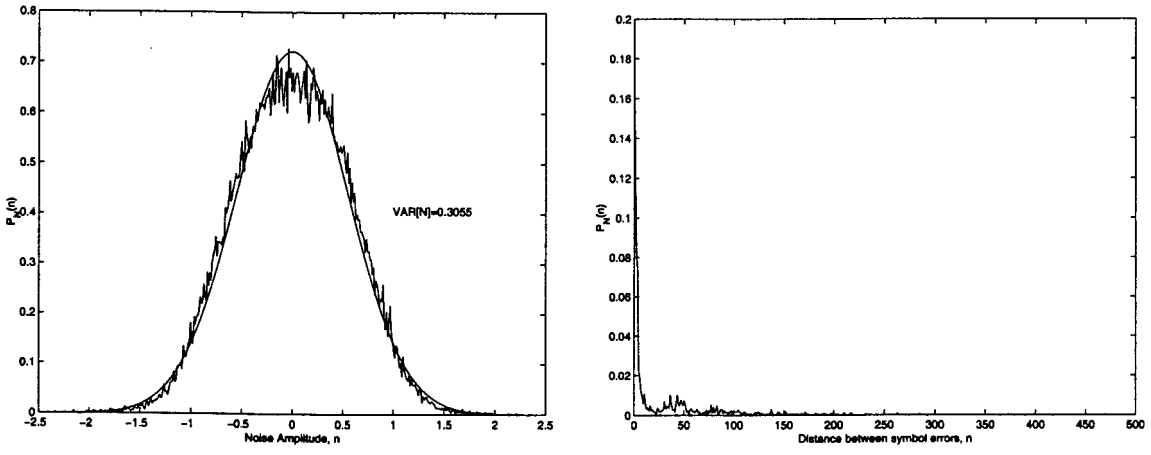

(a) (b)

Figure 6.12: (a) Symbol amplitude error PDF and (b) symbol error distribution for a BPSK system in a Rayleigh fading channel with $\overline{E}_b/N_0 = 10$ dB.

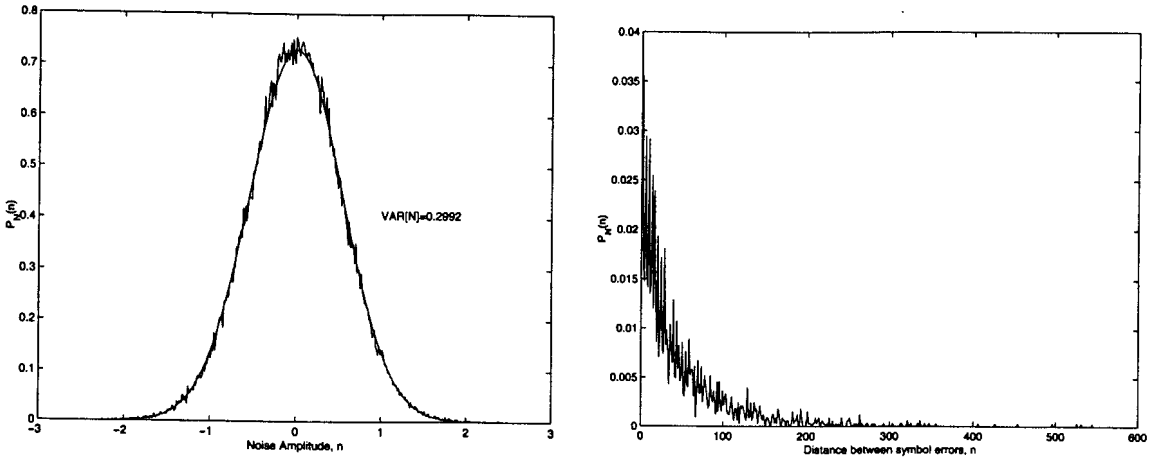

(a) (b)

Figure 6.13: (a) Symbol amplitude error PDF and (b) symbol error distribution for a standard TS system in a Rayleigh fading channel with $\overline{E}_b/N_0 = 10$ dB.

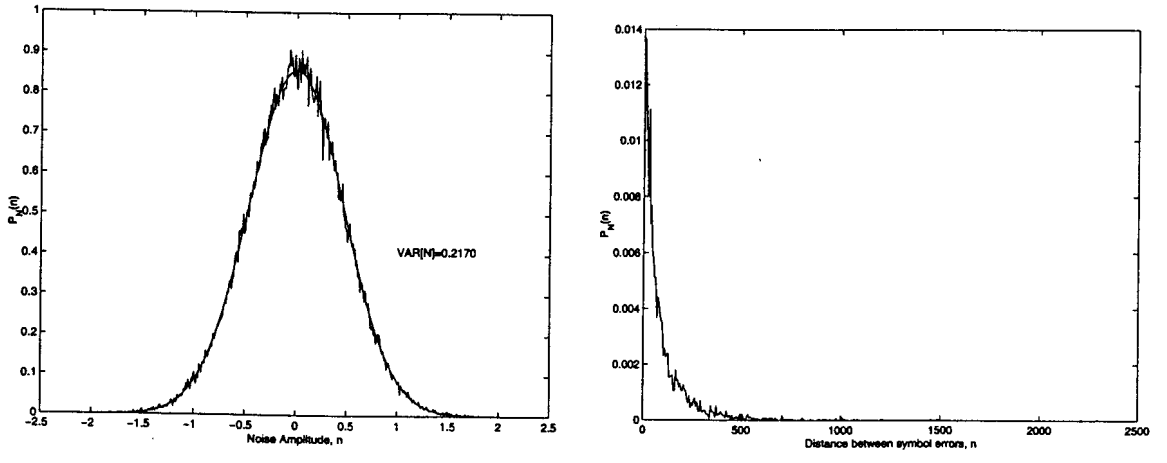

(a) (b)

Figure 6.14: (a) Symbol amplitude error PDF and (b) symbol error distribution for a TS system with standard ICIC in a Rayleigh fading channel with $\overline{E}_b/N_0 = 10$ dB.

6.6 PERFORMANCE OF DIFFERENT TS SEQUENCES

Research towards finding the optimum spreading sequences for use in a TS system has been conducted by [6]. Results were however obtained under perfect coherent demodulation conditions. This section presents BER results obtained with Dukic, FZC and Genetic spreading sequences under more realistic simulation conditions, where the phase references for coherent detection were obtained from channel estimates. The optimum ICIC technique that is discussed in more detail in Section 6.11, was enabled in the TS receiver when the aforementioned sequences were evaluated.

From Fig. 6.16 it is clear that the Dukic spreading sequence performs better than the other sequences

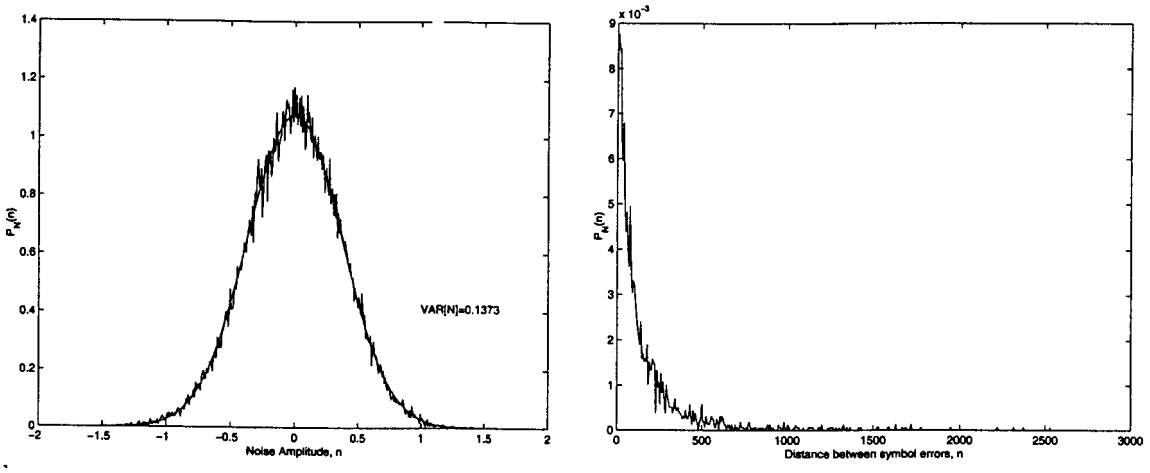

(a) (b)

Figure 6.15: (a) Symbol amplitude error PDF and (b) symbol error distribution for a TS system with AC-ICIC in a Rayleigh fading channel with $\overline{E}_b/N_0 = 10$ dB.

Receiver Type	Symbol σ_N^2	Avg. Error Distance	P_{error}
BPSK	0.3055	<10	0.0282
Std. TS	0.2992	42	0.0200
Std ICIC	0.2170	76	0.0112
AC-ICIC	0.1373	97	0.0063

Table 6.1: Unnormalized symbol noise powers and average error distances for different receivers in a $\overline{E}_b/N_0 = 10$ dB Rayleigh fading channel.

by a substantial margin. It should be noted that the poor performance of the other spreading sequences were not due to inadequate time diversity properties, but rather due to their poor AAC properties, since all sequences were temporally expanded, as explained in Section 3.4, to have comparable time diversity characteristics.

6.7 BER PERFORMANCE IN AWGN

This topic was researched by [6] and it was proved that time spreading provided no gains, nor losses in the BER performance of a standard PSK system operating in an AWGN channel, under the condition that a perfect spreading sequence is used.

When imperfect spreading sequences are used, the performance of a TS system operating in AWGN is worse than the performance of an ideal PSK system. This can be attributed to the occurrence of ICI resulting from imperfect spreading sequence cross correlation properties. Substantial BER performance increases can be obtained if an ICIC module, similar to that used to combat the adverse effects

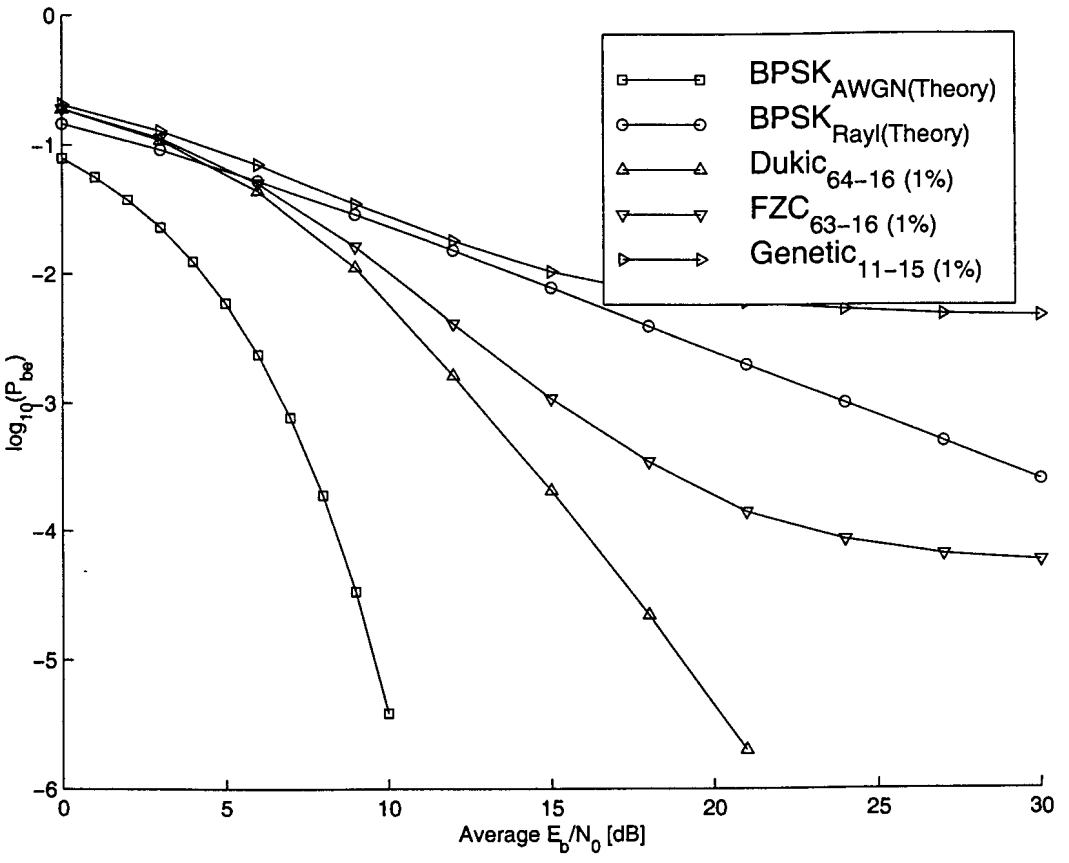

Figure 6.16: Performance of different TS sequences in a 1% ($f_D = 0.01R_s$) fading channel.

of fading, is used for TS systems employing imperfect spreading sequences in AWGN. Fig. 6.17 depicts the BER results obtained for a TS system employing a FZC-63-16 spreading sequence with and without ICIC measures. Note the substantial improvement obtained when using an ICIC module. The performance of an ideal PSK system operating in AWGN could not be met, since channel estimation and correction methods necessary in fading channels were in place when the results were generated. The use of pilot symbols cause an inherent decrease in effective E_b/N_0 levels and channel correction efforts, not needed in AWGN channels, introduce additional noise to the system.

Since the FZC sequence forms part of a spreading sequence family with good CC properties, the use of MU detection receivers with ICIC in a TS system could provide bandwidth efficient MU communication in AWGN channels where different users, separated by a hybrid TS-CDMA scheme, share the same bandwidth, equal to the original data signal bandwidth of a single user.

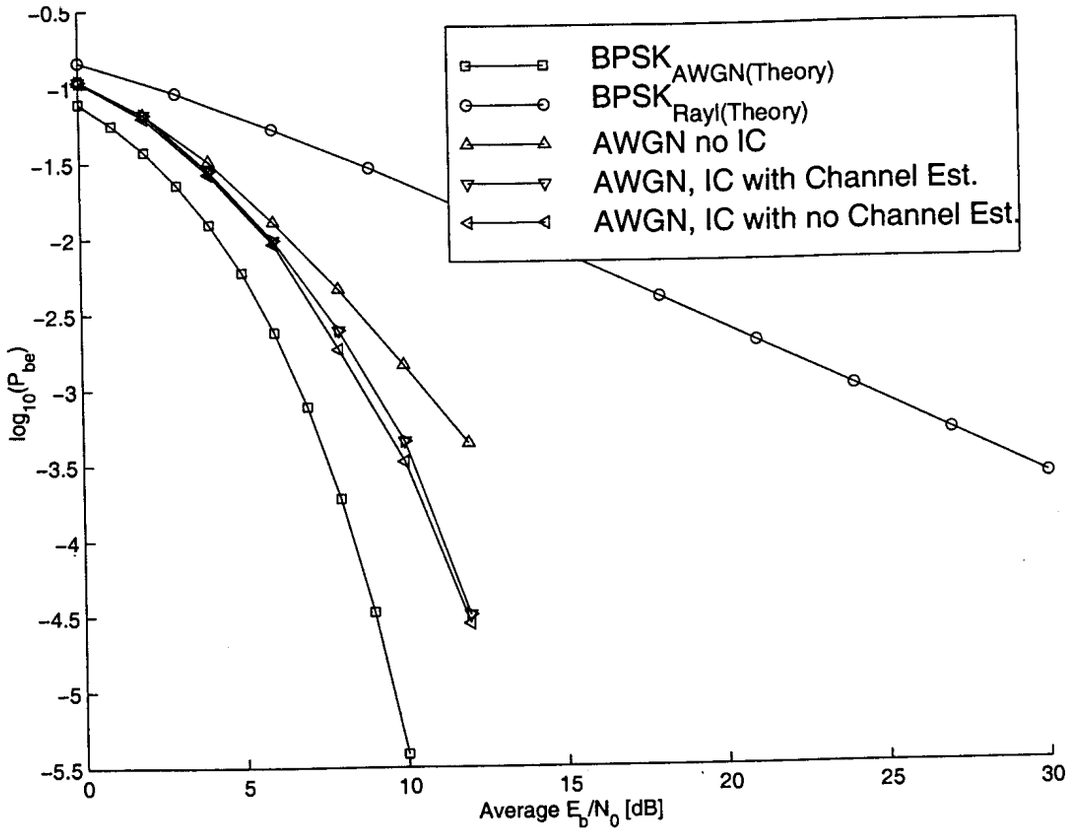

Figure 6.17: Performance of a FZC-63-16 sequence in AWGN with and without ICIC.

6.8 INCREASED TIME DIVERSITY FOR SHORT SPREADING SEQUENCES

The BER results presented in this section correspond to different lengths of Dukic spreading sequences, all temporally expanded to exhibit the same time diversity characteristics of a length 1024 Dukic sequence. All signals were detected using three different types of TS receivers namely:

1. A standard TS receiver (Section 3.6).
2. A TS receiver with standard ICIC measures (Section 4.5.2).
3. A TS receiver employing selective amplitude correction strategies combined with ICIC measures (Section 4.5.4).

A Rayleigh flat-fading channel with a fading rate equal to 1% of the channel symbol rate was used in this evaluation. An interesting result depicted in Fig. 6.18 shows that the shortest fundamental spreading sequence, namely the Dukic-16-64 sequence performs the best, with the sequences derived from longer fundamental sequences performing worse in a descending order as the fundamental sequence length is increased. This can be explained by the fact that, although all the sequences have

similar time diversity characteristics, the TS system employing the shorter fundamental sequences suffer from less ICI since less sequence elements overlap in time. Note that none of the results are substantially better than the theoretical PSK BER in a Rayleigh fading channel and that an error floor is reached at high $\overline{E}_b/N_0$ values that are much worse than the BER performance of a perfect coherent PSK system. Note that a performance loss of approximately 2.5 dB can be attributed to the insertion of pilot symbols and estimation errors. These effects were not taken into account in [6] and may be interpreted as an inaccuracy in the results presented in this reference. However, results depicted in this dissertation are more realistic and physically achievable, since less assumptions were made in the simulation of the different TS systems. The BER cross-over-point for the standard TS systems without ICIC measures ranges from 5 to 6.2 dB; this compares favourably with that of the reference results for non-TS coded systems depicted in Fig. 6.28. Since the BER cross-over-point for the standard TS system is already better than reference results depicted in Fig. 6.28, the TS technique is expected to show substantial gains when used in combination with FEC coding techniques.

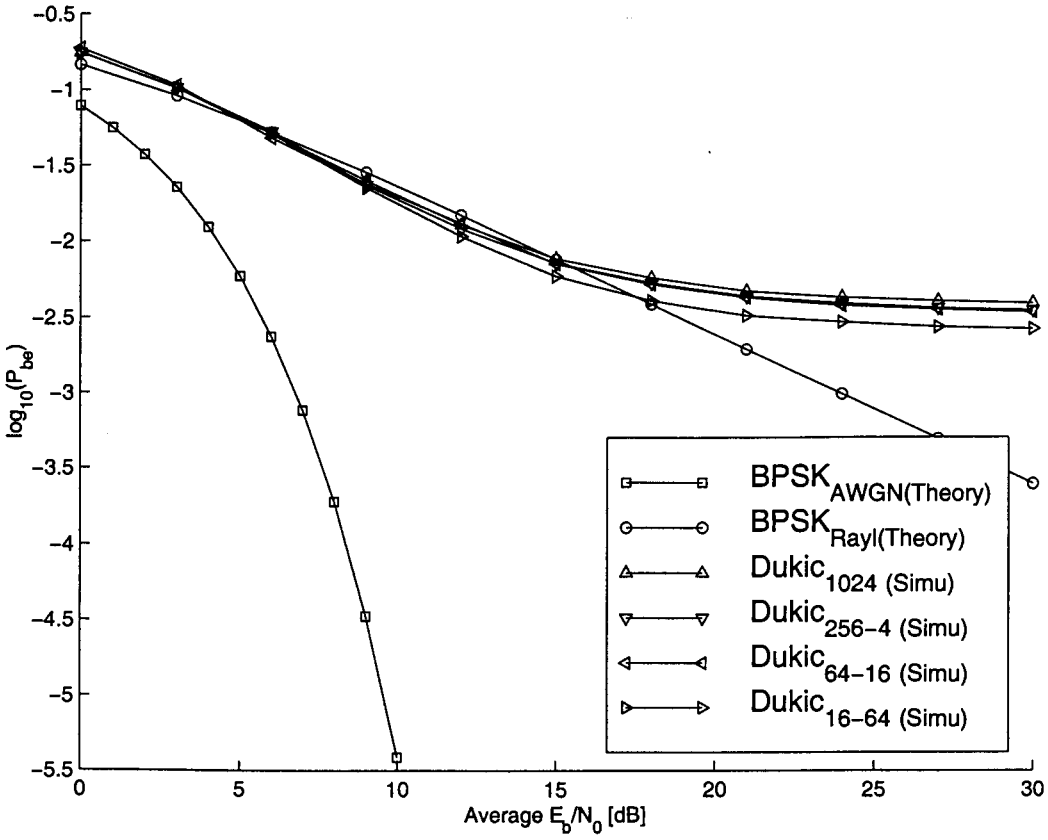

Figure 6.18: Performance of different length Dukic sequences with similar time diversity and an ordinary TS receiver.

The BER results shown in Fig. 6.19 correspond to a TS system with a standard ICIC module that

estimates the current received symbol before subtracting its remainders from the correlation buffer (refer to Sections 4.5.1 and 4.5.2). Note that the Dukic-16-64 sequence does not perform that well with this type of TS receiver when compared to the Dukic-256-4 and Dukic-64-16 sequences. This can be contributed to the fact that the ICIC module has a more dramatic effect on the longer non-interpolated spreading sequences that suffer more severely from ICI, but have stronger correlation properties. When an ICIC module is in place, the Dukic-1024 sequence does not perform much better. This can be explained by the large amount of ICI generated by the long non-interpolated spreading sequence. The Dukic-256-4 and Dukic-64-16 sequences have the same performance and strikes a good balance between non-interpolated sequence length and BER performance. The BER cross-over-point for the TS systems employing standard ICIC measures ranges from 4.2 to 4.5 dB. This compares favourably with that of the reference results for coded systems depicted in Fig. 6.28. Since the BER cross-over-point for the TS system with standard ICIC measures is substantially better than reference results depicted in Fig. 6.28, the TS technique with ICIC measures in place is expected to show significant gains at low SNRs when used in combination with FEC coding techniques.

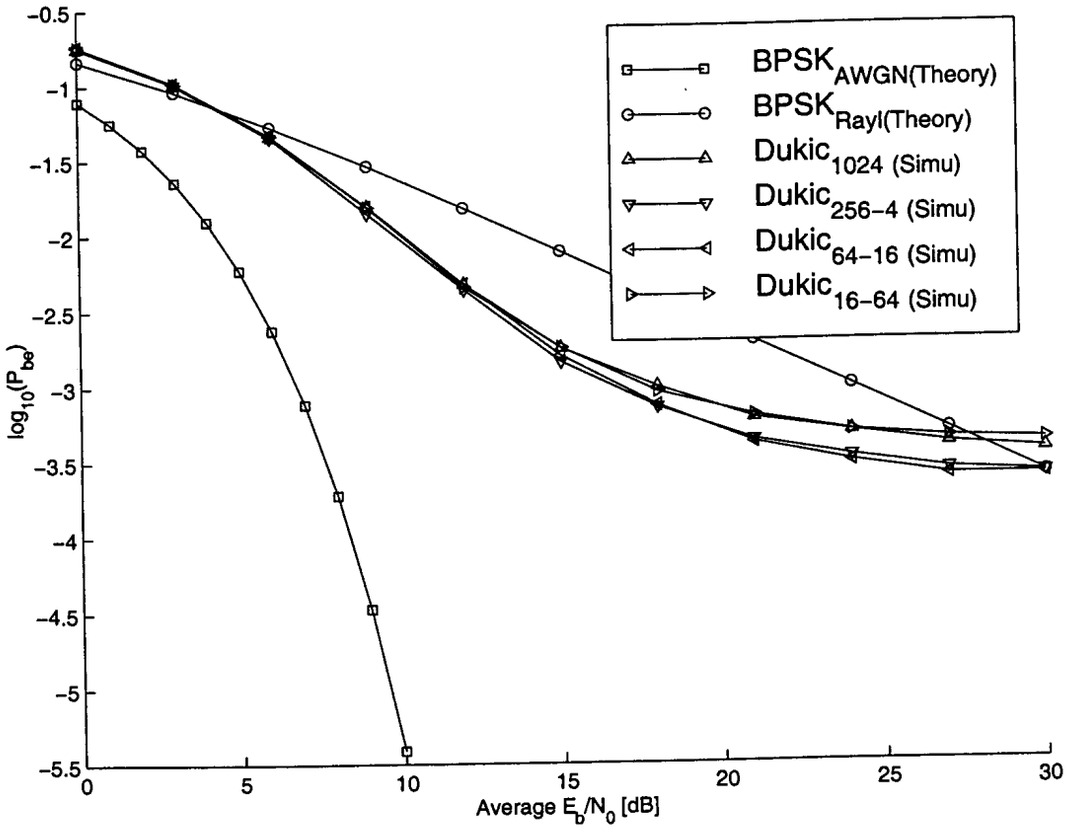

Figure 6.19: Performance of different length Dukic sequences with similar time diversity and a standard ICIC TS receiver.

The BER performance trend illustrated in Fig. 6.19 is continued in Fig. 6.20 where the different sequences are evaluated using the ICIC technique described in Section 4.5.4. This ICIC strategy is very effective and notably suppresses the BER performance floor illustrated in Fig. 6.18 and Fig. 6.19 to levels below $P_e = 10^{-6}$. A significant gain of 15 dB in required average E_b/N_0 over the theoretical PSK performance in a Rayleigh fading channel is obtained at an average bit error probability of $P_e = 10^{-3.5}$. With this ICIC module in place, the TS system performs to within 12 dB from the ideal PSK system in AWGN. Again, the Dukic-256-4 and Dukic-64-16 sequences perform the same, while the other two sequences lag behind by one and two decibels respectively. The BER cross-over-point for the TS systems with selective amplitude correction capabilities ranges between 4.3 and 4.6 dB. This is 0.1 dB worse than the performance of the TS system with standard ICIC measures. The performance loss can be contributed to amplitude correction errors at low average $\overline{E}_b/N_0$ levels. This performance degradation at lower $\overline{E}_b/N_0$ levels is negligible since it is offset by substantial improvements in BER performance at higher $\overline{E}_b/N_0$ levels.

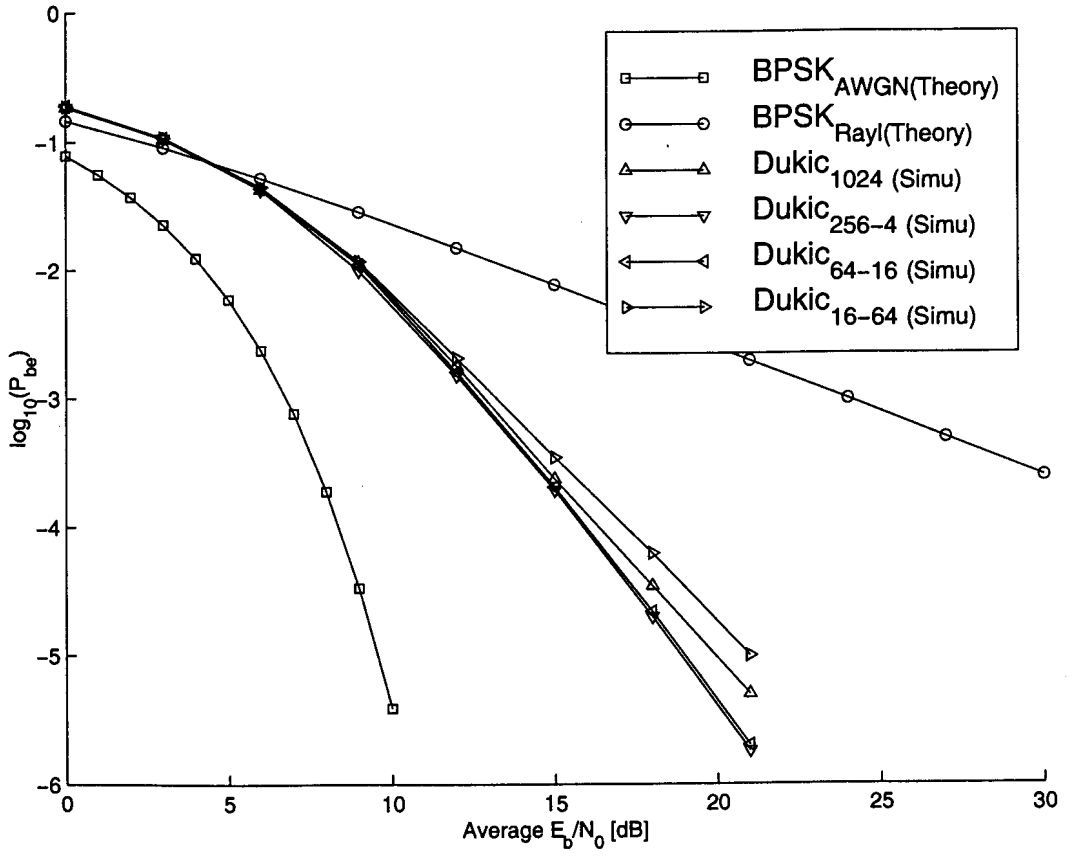

Figure 6.20: Performance of different length Dukic sequences with similar time diversity and a ICIC TS receiver with selective amplitude correction capabilities.

From the results it is concluded that the Dukic-64-16 and Dukic-256-4 sequences show superior

performance in a Rayleigh flat-fading fading channel where $f_D = 0.01R_s$. Furthermore, the use of the temporal sequence expansion technique described in Section 3.4 is effective with regards to the BER performance of the TS system and may be used with good effect to decrease the computational complexity required in the TS receiver, while maintaining good time diversity.

6.9 EFFECT OF DIFFERENT FADING RATES

The BER performance results for two types of transmitted TS signals were evaluated under 1% ($f_D = 0.01R_s$) and 4% ($f_D = 0.04R_s$) fading rate conditions. Two spreading sequences with the same time diversity characteristics were used in the TS systems. The first was configured with a Dukic-1024 sequence, while the second employed a Dukic-64-16 sequence.

Fig. 6.21 depicts the results obtained from the four combinations of spreading sequences and fading rates. Results for the different combinations of fading rates and spreading sequences did not differ much for the standard TS receiver without ICIC. All BER graphs exhibited an error floor of $P_e = 10^{-2.5}$ at high SNRs. The TS systems operating under faster fading conditions did however perform worse under low SNR conditions. The TS system performance under these conditions can be explained by three observations, namely:

1. The signal diversity introduced by TS makes the system more immune to phase estimation errors occurring at higher fading rates with high average SNRs. When estimation errors at high fading rates result in single received elements of a sequence to be in error, these isolated errors are readily corrected by time despreading.

2. When no ICIC strategies are used, the time despreading module itself is not affected by incorrect channel estimations arising from higher channel fading rates.

3. At low SNRs, the Wiener interpolation filter, described in Section 4.2.8, attempts to limit the amount of AWGN entering the channel estimation module by narrowing the filter bandwidth. This decreases the filter's ability to track rapid changes in the channel and results in many channel estimation errors, adversely affecting the performance of the TS receiver under higher fading rate conditions.

The BER cross-over-points for the standard TS systems operating in a 1% ($f_D = 0.01R_s$) fading environment are at 5 and 5.6 dB for the Dukic-64-16 and -1024 sequences respectively. There are no BER cross-over-points for the standard TS systems operating in the 4% fading environments, since the systems never perform better than the ideal coherent PSK systems in the Rayleigh fading channel. The BER results depicted in Fig. 6.22 may seem to contradict the aforementioned results. Careful examination of Fig. 6.21 reveals that the performance of a Dukic-1024 sequence (longer non-interpolated spreading sequence) in a faster fading channel is better than in a slower fading channel

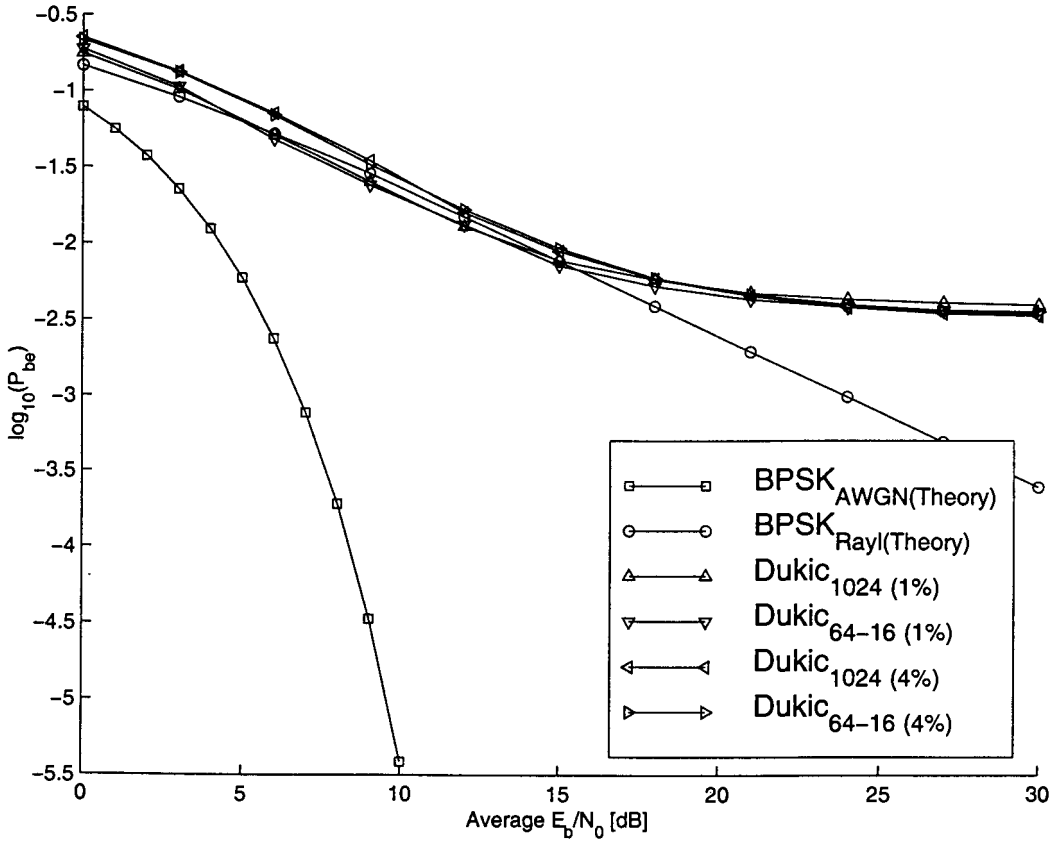

Figure 6.21: Performance with an standard TS receiver.

under high SNR conditions. The Dukic-64-16 systems, however performed similarly under faster and slower fading rates at high SNRs. The good performance of the Dukic-1024 sequence under fast fading conditions with high average SNRs can be explained by the joint effect of ICIC and the occurrence of more regular, shorter fades during each sequence period. This enables the sequence to Gaussianize the fading channel more efficiently, resulting in less data symbol errors. At lower SNRs, the systems perform similar to the TS systems without ICIC. The BER cross-over-points for the TS systems operating in the 4% fading environments employing both the Dukic-64-16 and -1024 sequences, are equal to 8 dB. The cross-over-points for the systems operating in the 1% ($f_D = 0.01R_s$) fading environment are equal to 4.4 dB. This marks a significant performance difference between TS systems with standard ICIC techniques in different fading environment at low average SNRs. It was explained earlier that this performance difference can be attributed to the different Noise Equivalent Bandwidths of the Wiener filters (part of the channel estimation module) optimized for different fading rates.

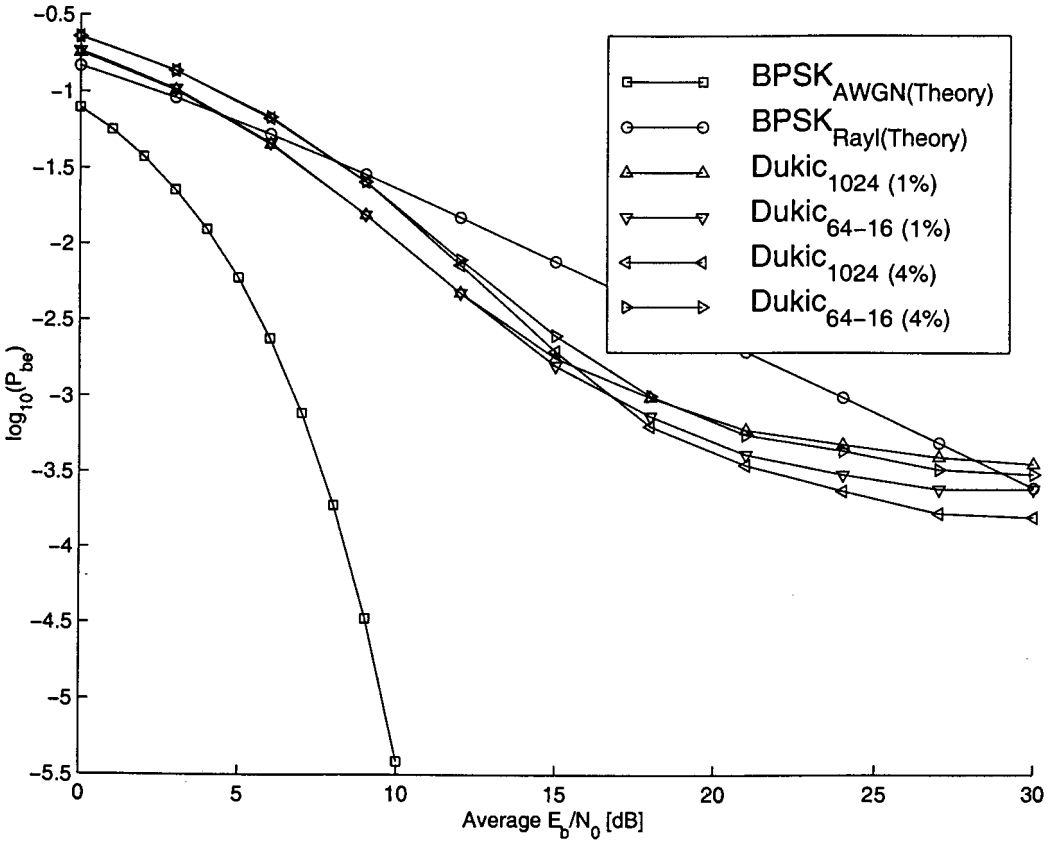

Figure 6.22: Performance with a standard ICIC TS receiver.

Finally, the different combinations of spreading sequences and channel fading rates were evaluated using the most effective ICIC module (refer to Section 4.5.4). Here, the TS receiver and ICIC module rely strongly on good channel estimates for both phase correction and selective amplitude correction methods. The results shown in Fig. 6.23 confirm this observation, where the systems operating under more severe fading conditions perform visibly worse than the systems in 1% ($f_D = 0.01R_s$) fading rate conditions. The performances of the systems employing the Dukic-64-16 sequence for different fading rates become more equal at high $\overline{E}_b/N_0$ conditions, which corresponds well with results depicted in Fig. 6.22. The BER cross-over-points for the systems operating in 1% ($f_D = 0.01R_s$) and 4% ($f_D = 0.04R_s$) fading rate environments were equal to 4.5 and 7.5 dB respectively. This marks a marginal improvement in the BER cross-over-point for the systems operating in the 4% fading rate environment, which can be attributed to the performance improvement introduced by the selective amplitude correction strategy.

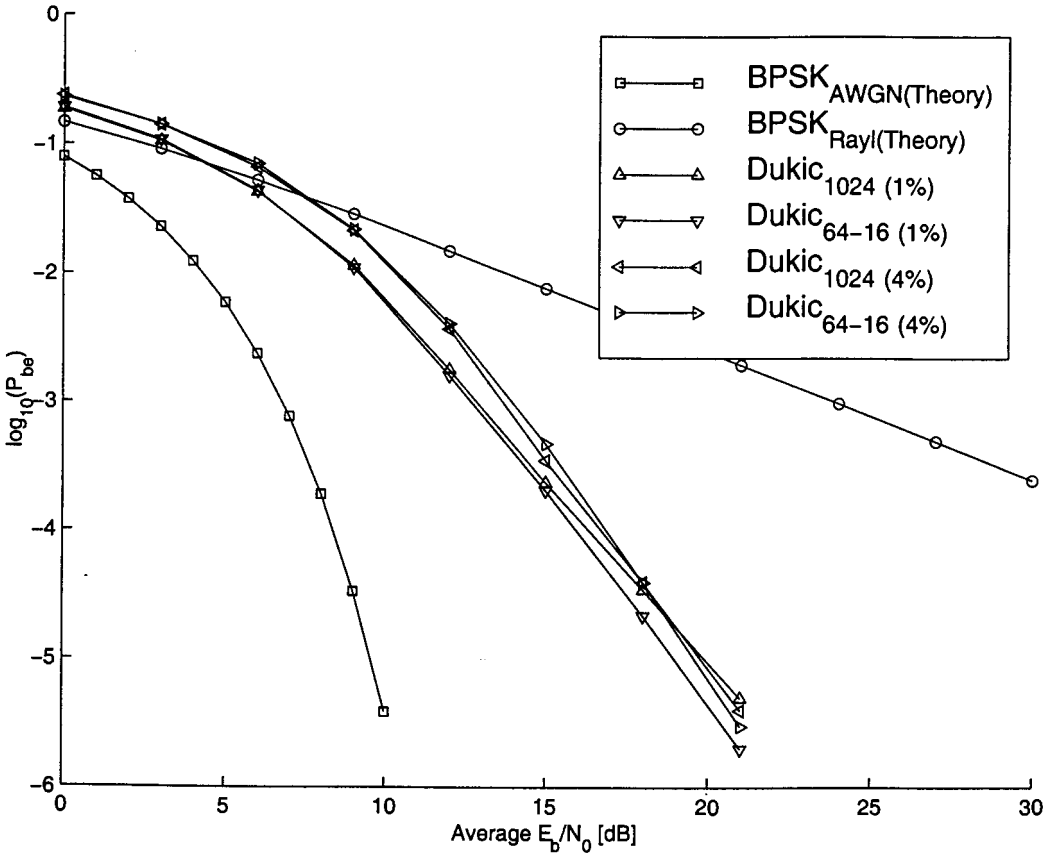

Figure 6.23: Performance with a ICIC TS receiver with selective amplitude correction capabilities.

6.10 TS PERFORMANCE IN A RICIAN FADING CHANNEL

It is mentioned in [9] that diversity techniques provide progressively decreasing gains when a predominantly Rayleigh fading channel is transformed into a AWGN channel. The results of a TS system with ICIC, as described in Section 4.5.4, are therefore presented for different Rician channels for completeness sake only. The fading rate of the channel was set to 1% of the channel symbol rate and the Rician K parameter, defined in (2.14), was chosen as $K = -100, -10, 0, 10$ dB respectively. Fig. 6.24 depicts the BER results obtained with a Dukic-64-16 sequence under the aforementioned channel conditions. Since $K = -100$ and $K = -10$ dB Rician fading channels are very similar to the Rayleigh fading channel, it is therefore not surprising that the TS system performs similarly under these conditions. For higher LOS to scatter path power ratios, the performance of the TS system moves closer to that of a TS system in AWGN as the value of K increases. Here the ability of the TS technique to Gaussianize the fading channel does not play an important role any more since the channel is virtually completely Gaussian when $K = 10$ dB.

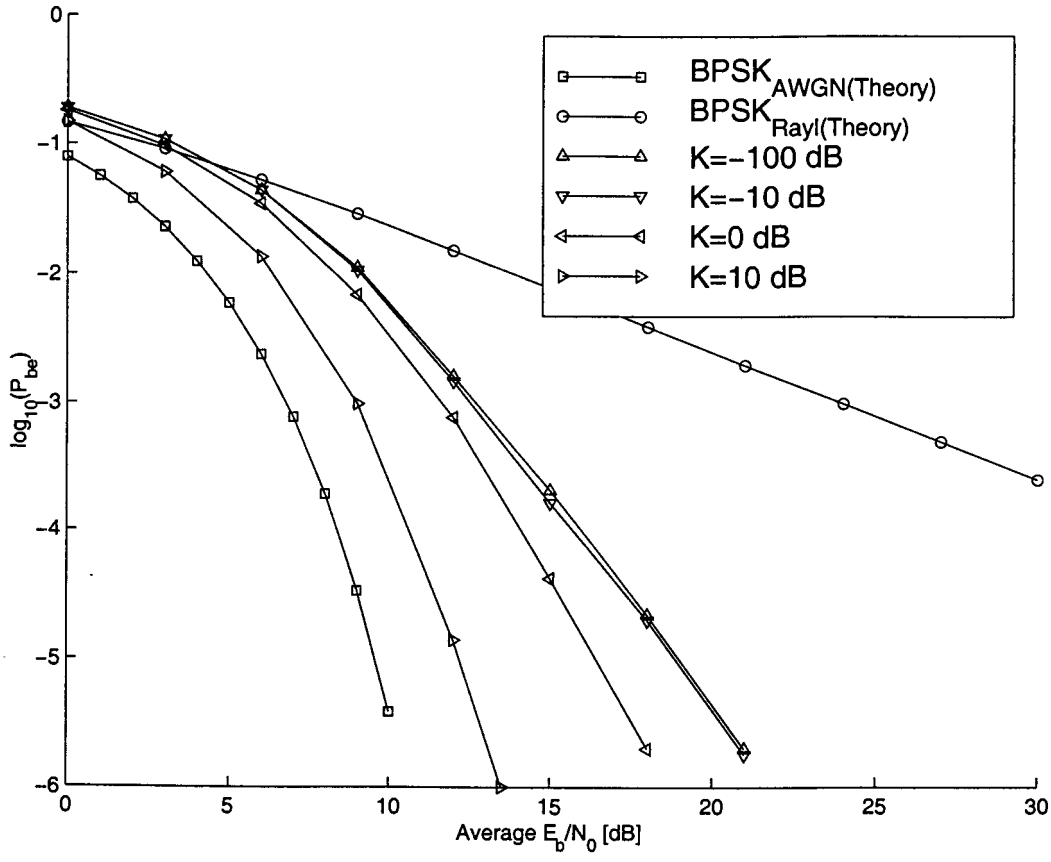

Figure 6.24: Performance of a TS receiver with selective amplitude correction ICIC employing a Dukic-64-16 spreading sequence in different Rician channels.

6.11 TIME SPREAD PERFORMANCE WITH ICIC

Although a number of BER results for TS systems with ICIC have already been presented, this section is aimed at formally discussing the effectiveness of the ICIC techniques proposed in this dissertation.

The evolution of the uncoded TS system performance from the system without any ICIC measures to the best known ICIC technique proposed in this dissertation is illustrated in the BER graphs shown in Fig. 6.26. The BER graphs were all generated with a TS system simulation employing the Dukic-64-16 sequence. This sequence was chosen since it performed very good under all tested channel conditions, while reducing the computational complexity of the TS receiver structures.

This section includes theoretical results obtained for coherent PSK systems with maximal-ratio diversity combination receivers. The results were obtained from [3] and [4] and are depicted in Fig. 6.25 for reference purposes. The number of diversity branches employed by the systems in Fig. 6.25 is indicated by M. These reference results are included in order to compare the inherent diversity gains

offered by the TS-techniques with the theory.

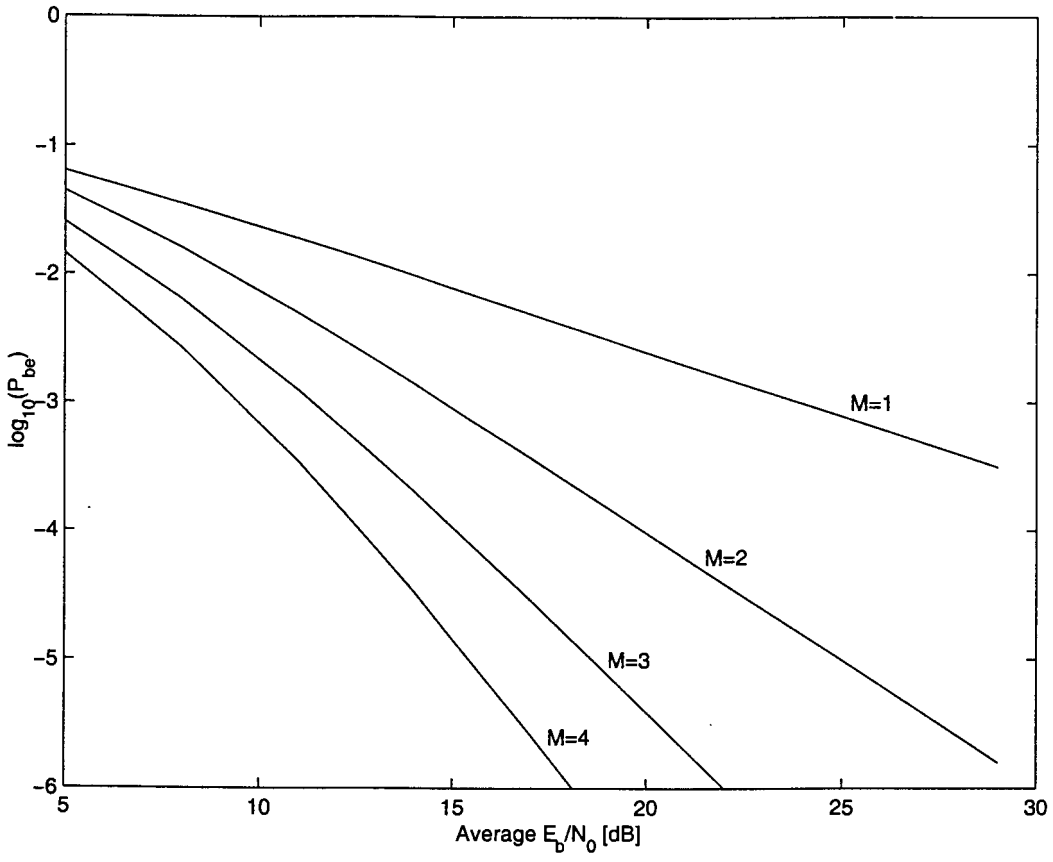

Figure 6.25: Performance of binary PSK signals with maximal-ratio diversity combination. Results taken from [3] and [4] with M denoting the number of independent diversity branches.

The standard ICIC module described in Sections 4.5.1 and 4.5.2 showed an improvement of more than one order in magnitude of the BER performance floor for the standard TS receiver with PSAM. However, the effect of AWGN at low SNRs overshadows the effect of fading and amplitude distortion. All ICIC strategies are solely aimed at eliminating the effects of ICI due to fading and therefore provides no gains at low SNRs.

The use of a selective amplitude correction module without ICIC that only corrects the amplitudes of the faded TS symbols during periods when the instantaneous SNR levels per symbol are above average, also result in an improvement in the BER performance floor of a TS system as can be seen in Fig. 6.26. The lowering in the BER floor using only amplitude correction is as much as one and a half orders of magnitude, which is better than that obtained from the standard ICIC module. It should be noted that this gain would not be attainable for systems that use only phase modulated signals, since

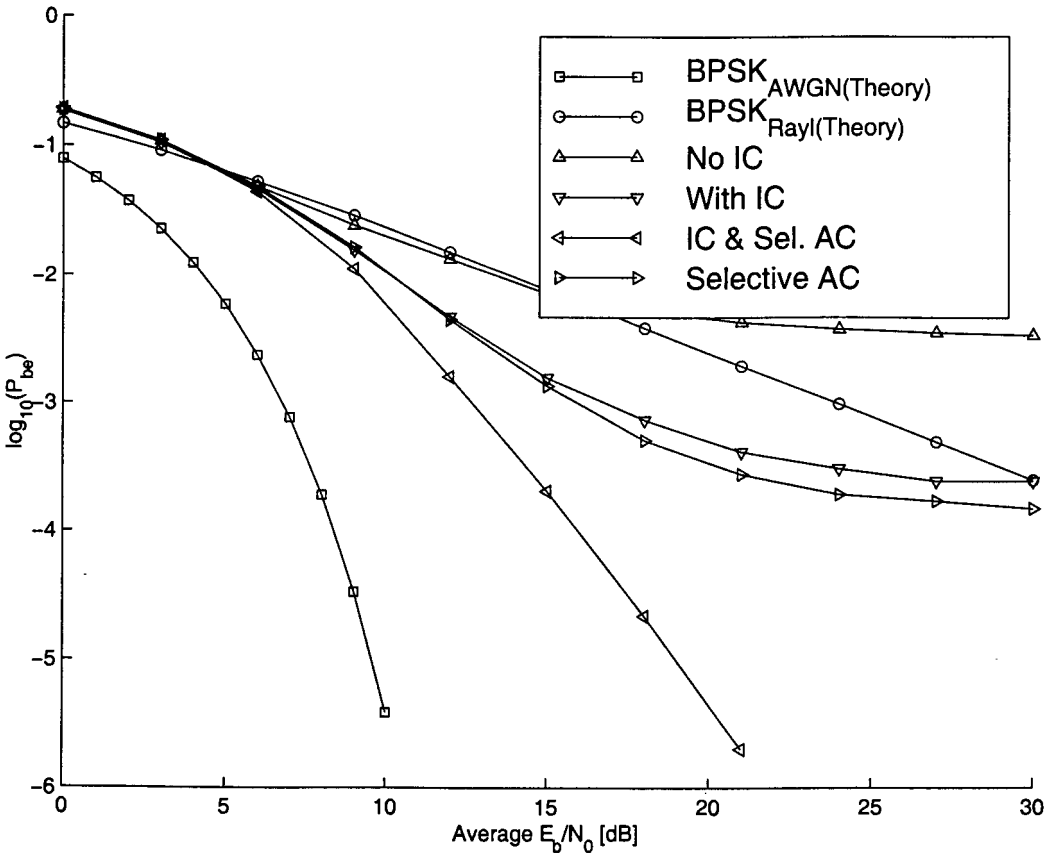

Figure 6.26: Performance of a TS receiver with different ICIC structures employing a Dukic-64-16 spreading sequence in a Rayleigh flat-fading channel with a 1% ($f_D = 0.01R_s$) fading rate.

the symbol information does not reside in the signal amplitude of each channel symbol, but rather in its phase. As illustrated by the signal constellation for a TS system depicted in Fig. 6.9, a TS signal may be regarded as a M-QAM signal of a very high order, hence the dependency on the amplitude levels of each TS symbol.

Combining the effects of selective amplitude correction and ICIC result in very good BER performance figures for the TS system in a Rayleigh fading channel. The BER performance floors, which are visible in both of the aforementioned techniques, are decreased to well below $P_e = 10^{-6}$ using this combined technique. The combined ICIC and selective amplitude correction technique improves the performance of the TS system in a Rayleigh fading channel to within 12 dB of the theoretical PSK AWGN BER curve. TS combined with this ICIC technique provides the same gain as a conventional third order signal diversity system at a bit error probability of $P_e = 10^{-5}$ (see Fig. 6.25). When comparing the results obtained for TS systems in this dissertation to results in the literature, it is important to take into account the performance losses associated with channel estimation and quasi-coherent demodulation techniques, which are usually omitted in the literature. With this in mind, the

TS system compares even more favourably with other diversity systems, since the aforementioned implementation losses are already reflected in the results obtained for the TS systems. Refer to [17], [4] and [3] for more results on conventional diversity techniques.

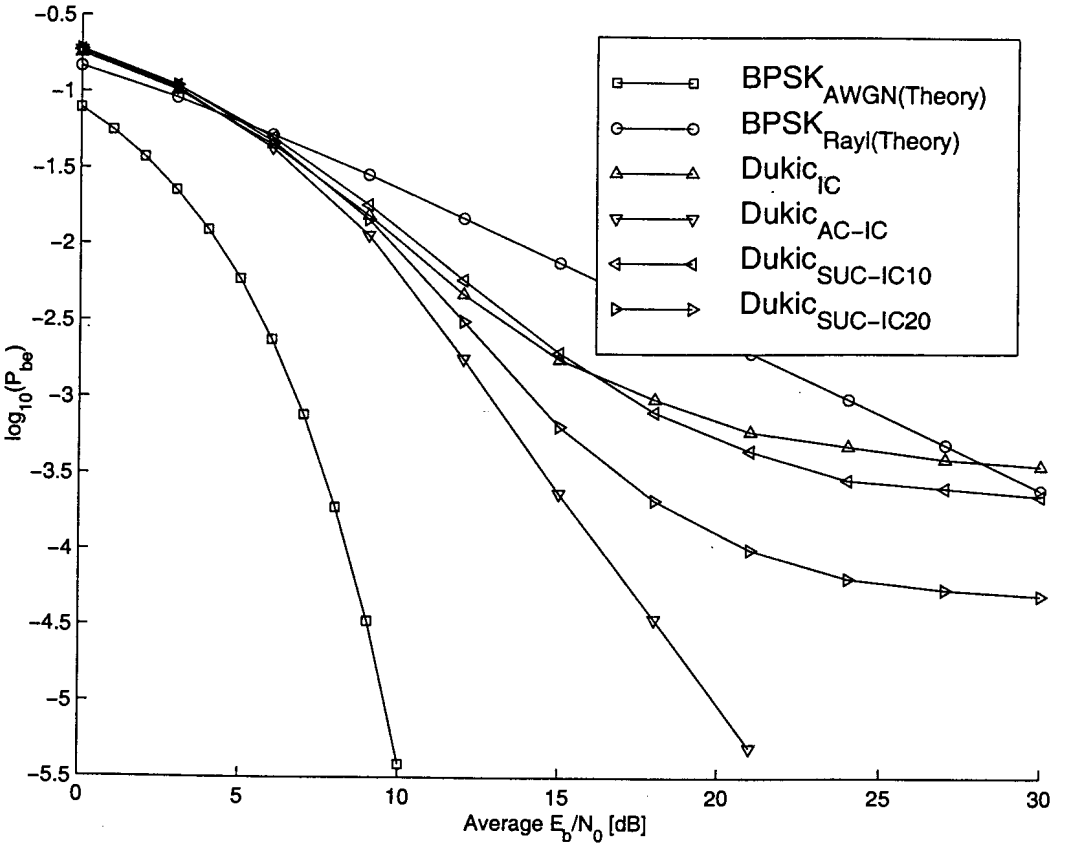

Figure 6.27: Performance of a TS receiver with different ICIC structures employing a Dukic-1024 spreading sequence.

Another ICIC technique was described in Section 4.5.3. This technique involved the preliminary decoding of a number of data symbols that would only be permanently decoded after the current data symbol has been detected. The effects of these preliminary decoded symbols are then cancelled from the correlation buffer before decoding of the current symbol takes place. Selective amplitude correction correction and ICIC methods are then applied. The results for this partial successive ICIC technique are presented in Fig. 6.27. Also shown in this figure is the BER results for the standard ICIC technique with selective amplitude correction discussed earlier in this section. Two sets of BER results are shown for the partial successive ICIC technique. Firstly, the influence of 20 preliminary decoded symbols were cancelled and secondly when only 10 symbols were cancelled. It is clear that this technique performs worse than the AC-ICIC technique. Nevertheless, an increase in the number

of preliminary decoded symbols used for ICIC purposes result in an improvement in the performance of the partial successive ICIC technique. The poor performance of this ICIC technique can be contributed to the occasional inaccurate decoding of preliminary data symbols. It is concluded that the use of partial successive ICIC strategies are not worthwhile since it implies a substantial increase in system complexity and provides less gains than simpler ICIC techniques presented in this document. This technique is consequently omitted from subsequent sections of this dissertation.

6.12 TIME SPREAD PERFORMANCE WITH INTEGRATED CODING

As stated in Chapter 5, no extensive research work was performed towards finding the optimum FEC codes for integration with the TS technique. Instead, a standard $R_c = 2/3$ convolutional code, designed for AWGN channels, was integrated with the different TS systems. Results depicted in this section are therefore solely aimed at illustrating the ability of the TS technique to transform a Rayleigh fading channel into an AWGN-like channel, where well known FEC codes designed for AWGN channels could be used with great efficiency.

Comparative BER results obtained from [5] are documented in this section to place the results obtained with the coded TS technique in proper perspective. These BER results were derived theoretically for $R_c = 2/3$ rate FEC codes and were verified using computer simulations. Results depicted in Fig. 6.28 were obtained for the following types of codes:

- 4-State, $R_c = 2/3$ rate, coded 8-PSK optimized for Rayleigh fading channels
- 4-State, Ungerboeck's $R_c = 2/3$ rate, coded 8-PSK optimized for the AWGN channel
- 8-State, Ungerboeck's $R_c = 2/3$ rate, coded 8-PSK optimized for the AWGN channel.

All the results depicted in Fig. 6.28 were obtained employing coding systems assuming infinite interleaver depths. The codes optimized for the AWGN channel are included in this document to emphasize the gains obtained by integrating relatively simple convolutional codes of the same code rate with the TS technique. Take note of the assumption regarding infinite interleaver depth, since this has a significant effect on the performance of FEC codes in fading channels. The cross-over-point, where the coded system begins to perform better than the perfect coherent PSK system in a Rayleigh fading channel, constitutes an important benchmark for any coding technique. The cross-over-points for the FEC codes taken from [5] are listed in Table 6.2.

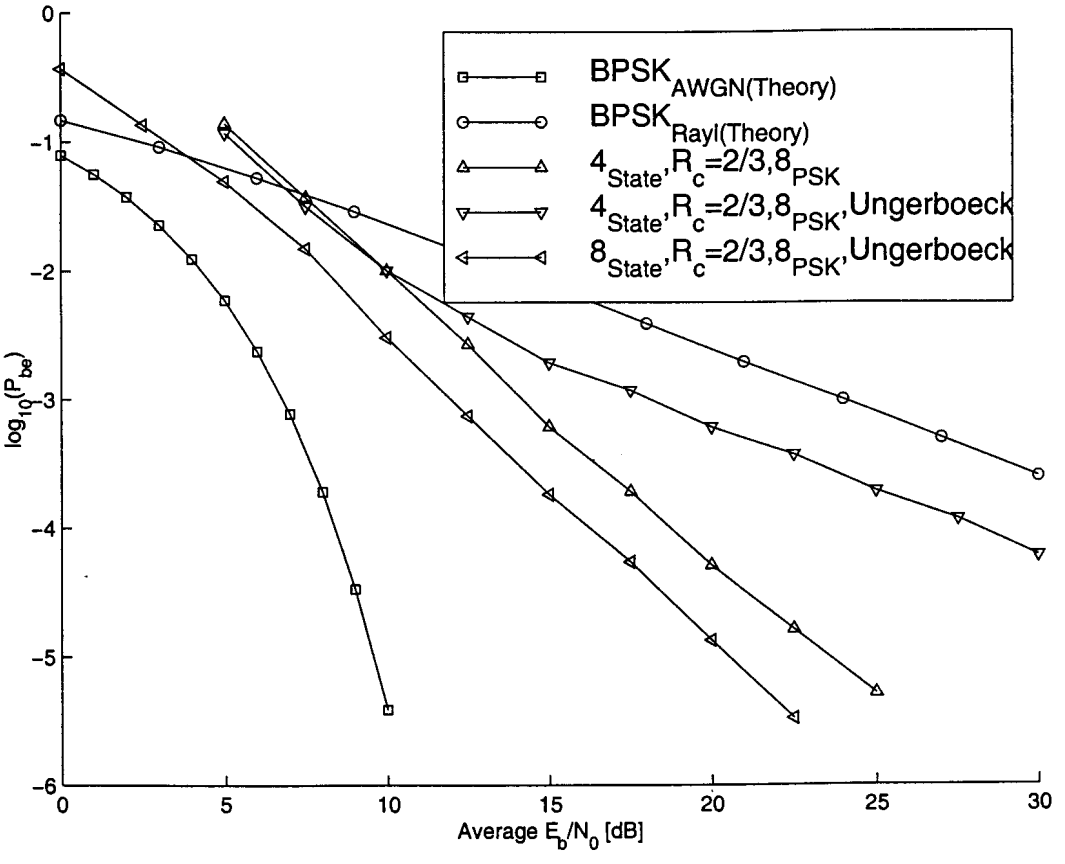

Figure 6.28: Comparative BER performance results for $R_c = 2/3$ rate codes in a Rayleigh fading channel, obtained from [5]. Infinite interleaver depths and perfect coherent reception were assumed for all systems.

Coding Scheme	Cross-Over ($\overline{E}_b/N_0$ dB)
4-State, Ungerboeck $R_c = 2/3$ rate, 8-PSK	6.8
4-State, $R_c = 2/3$ rate for fading channels, 8-PSK	7.4
8-State, Ungerboeck $R_c = 2/3$ rate, 8-PSK	3.9

Table 6.2: BER cross-over-points for codes depicted in Fig. 6.28.

BER results for the aforementioned $R_c = 2/3$ rate convolutional code integrated with different TS systems are depicted in Fig. 6.29. The data was transmitted over a Rayleigh fading channel with a fading rate equal to 1% of the channel symbol rate. A Dukic-64-16 spreading sequence was used for time spreading, and pilot symbols were inserted after every fourth TS symbol. The different types of TS receivers described in Chapter 4 were used in the simulations, except for the partial successive ICIC modules which were proven to be inefficient during trial runs. The coded TS system with AC-ICIC (Smart IC) performs the best while the other receivers perform progressively worse as less effective ICIC strategies are applied. With AC-ICIC enabled, the TS system with integrated coding

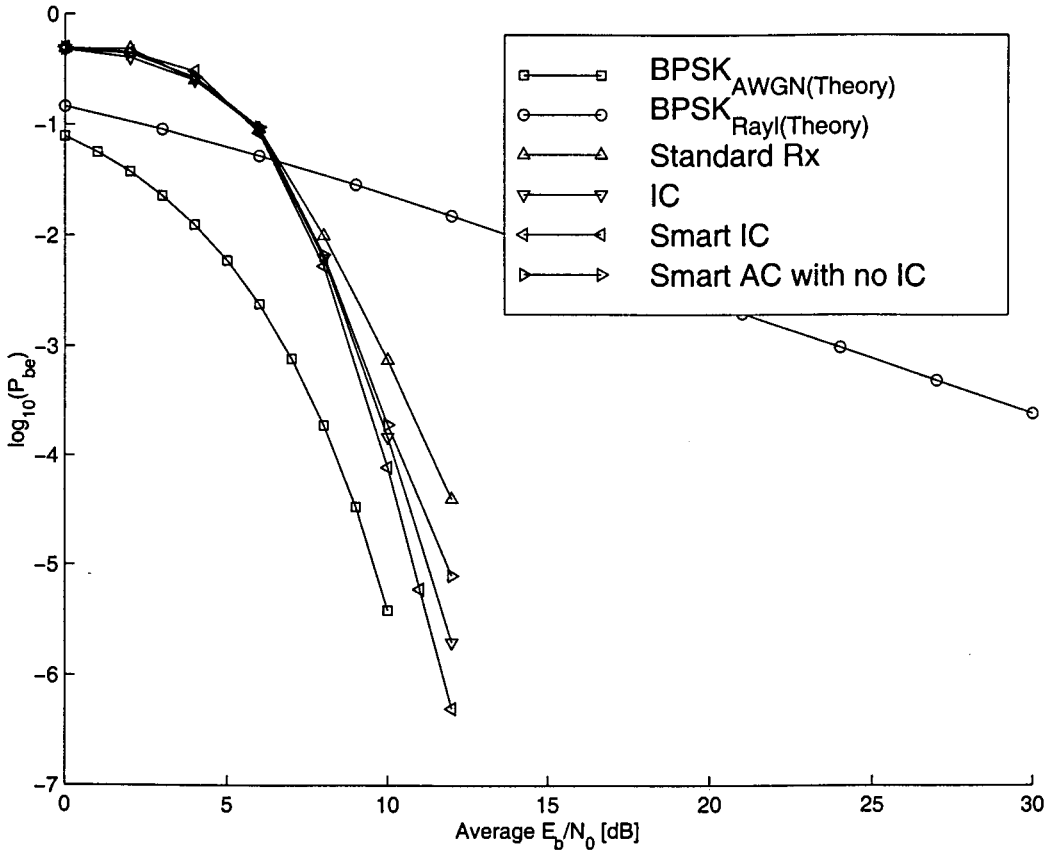

Figure 6.29: Performance of an integrated $R_c = 2/3, K = 4$ convolutional code with different TS receiver structures.

performs to within one decibel of an ideal uncoded PSK system in AWGN. The performances of the different systems correspond well to the trends in average error distance and symbol noise power results presented in Table 6.1. ICIC does not improve the system performance at low $\overline{E}_b/N_0$ values, thus no additional gains were obtained for the coded systems. However, at higher $\overline{E}_b/N_0$ values; as much as two decibels were gained over the standard coded TS system at $P_e = 10^{-5}$, with the AC-ICIC module. Note that the BER for the system using AC-ICIC decreases much faster than that of the other systems at higher $\overline{E}_b/N_0$ levels, i.e. no distinct error floors are visible in this case.

The BER cross-over-point for the coded TS systems ranges from 6.4 to 6.6 dB and compares favourably with that of the codes documented in [5]. The results depicted in Fig. 6.28 must be interpreted with the implementation losses with regards to perfect coherent demodulation in mind. These losses amount to approximately 2.5 dB in average $\overline{E}_b/N_0$ requirements for the TS system at hand. Thus, if a similar assumption was made with regards to the coded TS technique, the BER cross-over-points would be situated between 3.9 and 4.1 dB, which is substantially better than that of the codes documented in [5]. Note that the gradients of the BER graphs for the coded TS system in Fig. 6.29 are much steeper

than those depicted in Fig. 6.28. Considering that only a standard convolutional code designed for the AWGN channel was used with the TS technique, the advantages of employing the TS technique are obvious.

6.13 SUMMARY

The results obtained from the simulation study of different TS systems evaluated under a number of channel conditions were documented in this chapter. The different transceiver and channel configurations that were used were described in the introductory sections. Next, some results from tests conducted to verify the credibility of the simulated channel were presented. The fading envelope was shown to have the correct amplitude PDF. The graph of the average fading duration versus the fading level threshold differed slightly from the theoretical graph. It was concluded that this difference was due to the third order approximation of the Doppler spectrum used in the mobile channel simulation.

The next set of figures depicted some of the typical TS signals in the time, frequency and signal constellation domains. A BER graph, illustrating the performance of the PSAM channel estimation module was given. The noise-like nature of a typical baseband TS signal was illustrated by a PDF of the in-phase TS signal at baseband frequency. The ability of the TS technique to Gaussianize a fading channel and to reduce the correlation between symbol errors were illustrated for different types of TS receivers and were compared to results obtained for a BPSK system under similar channel conditions.

Various aspects of time spreading were then analyzed through BER performance results. These included the effects of different fading rates, different spreading sequences, temporal expansion of sequences, and different ICIC techniques. Finally, some BER results of a TS system with integrated coding were presented. It was shown that high gains could be obtained from simple standard convolutional codes when used in conjunction with TS and efficient ICIC measures.

CHAPTER SEVEN

CONCLUSION

This dissertation was concerned with the extended analysis and enhancement of an existing TS technique, aimed at reducing the adverse effects of a Rayleigh flat-fading channel on communication systems. Previous work on the TS technique was conducted from the perspective that time spreading provided a method to reconstruct the missing portion of a signal, due to an signal envelope fade, using the signal energy not affected by the fade. In this dissertation, the TS technique was regarded as a transmitter time diversity technique and various ICIC and FEC coding strategies were proposed and analyzed from this perspective.

The mobile communication channel was briefly discussed in Chapter 2, with the emphasis on channel parameters that are important to the performance of the TS technique. The accurate implementation of a channel model for system evaluation constitutes an integral part of any simulation study of a communication system. An important part of the fading channel model is the lowpass filter that simulates the multiplicative fading process. No clear cut method exists to implement this process and it was approximated by a third order lowpass filter. Results in Chapter 6 provided concluding results which showed that even the higher order statistics of the simulated Rayleigh fading channel matched that of the theory to a satisfactory extent. Thus, this channel model implementation was regarded sufficiently accurate for simulation purposes.

The criteria for providing optimal TS performance has been identified by [6]. Intuitively, the spreading sequences used in the TS system should have perfect AAC properties. A set of polyphase root of unity spreading sequences designed by Dukic was found to be optimal for use in TS systems. These sequences do not support asynchronous multiuser applications and therefore only single user systems were considered in this dissertation. The need for long spreading sequences to span extensive fades has been identified in [6]. Such long sequences are not readily available and increase the computational complexity required in the TS system. A technique was developed to elongate a fundamental

spreading sequence which increased the time diversity obtained from relatively short spreading sequences. This technique also reduces the computational complexity required in the time spreading and despreading modules and was discussed in Chapter 3 as one of the primary contributions made by this dissertation. Important to note at this stage, is that the inherent diversity obtained from a TS-sequence can not be increased indefinitely. The average fade duration and coherence time of the communication channel plays an important role in determining the inherent diversity of a TS-sequence. If the duration of a spreading sequence becomes comparable to the aforementioned parameters, no additional diversity gains can be obtained by increasing the TS-sequence length.

Good channel estimation techniques are of the utmost importance for coherent demodulation and *Interference Cancellation* (IC) schemes. A PSAM technique proposed by [30] was adapted and integrated with the TS technique to enable quasi-coherent detection of the faded TS symbols while providing fading estimates employed in the ICIC modules. The technique relies on channel estimates obtained from the periodic detection of known inserted pilot symbols and the interpolation thereof. A coherent BPSK system using this PSAM technique was shown to perform to within 1.8 dB of the ideal theoretical BER curve. This loss due to estimation errors and pilot symbol power consumption is present in all physical systems and is often neglected or omitted in theoretical and simulation evaluation results found in the literature. It should however be taken into account when comparing the results in this document with other theoretical results. Results have shown that the use of noiseless channel estimates provide only a 0.2 order improvement in the BER performance of TS systems at low $\overline{E}_b/N_0$ values. It is therefore concluded that this technique is suitable for use with ICIC strategies in the TS system since it is very effective in limiting the effect of AWGN on the accuracy of channel estimates.

Various ICIC techniques have been proposed and evaluated. These included simple techniques that only cancelled the effects of the last detected data symbol in the TS receiver to more complex successive ICIC techniques that cancelled the effects of blocks of data symbols. The effect of ICI is overshadowed by that of AWGN at low $\overline{E}_b/N_0$ values, thus none of the ICIC structures provided any additional gains over the original TS systems under these conditions. It was concluded from simulation results that a hybrid ICIC technique which made optimal use of the available instantaneous E_b/N_0 levels provided the best BER performance results. The canceller used in this technique only cancels the effects of previously detected data symbols and completely eliminates the BER performance floor visible for other TS systems. The diversity gains obtained from this technique at $\overline{E}_b/N_0$ values above 10 dB are comparable to gains obtained from ideal coherent third order spatial diversity techniques. These results bring us to the conclusion that TS with effective ICIC provides a viable alternative to other more complex diversity techniques at $\overline{E}_b/N_0$ values above 10 dB. The effect of AWGN does however limit the effectiveness of the system under very noisy channel conditions, but

it can be argued that the same applies to other diversity techniques under non-ideal conditions.

Simulation results showed that a simple $R_c = 2/3$ rate convolutional code combined with the TS technique can provide substantial BER performance improvements for systems operating in Rayleigh flat-fading channels. It was shown that the ability of the TS technique to Gaussianize a fading channel makes FEC codes designed for AWGN channels very effective in fading channels. The transparency of the TS technique with regards to its inclusion in existing systems is highlighted by the ease with which the soft decision Viterbi decoder is used to decode the convolutionally encode symbols at the output of the time despreading module. TS time diversity can be obtained from existing systems without any alteration to the physical system other than modifications to the transmitter and receiver *Digital Signal Processing* (DSP) software. Fig. 7.1 depicts the BER results obtained for the new TS system compared to those of existing systems. A few important results depicted in this figure can be singled out. At a BER of $P_e = 10^{-6}$, the new uncoded TS system, in a Rayleigh flat-fading channel, performs only 11.5 dB worse than a coherent PSK system in an AWGN channel. This result becomes significant when compared to the original TS system which suffered from a BER performance floor occurring at $P_e = 10^{-2.5}$. The performance of the new TS system used in combination with a $R_c = 2/3$ rate convolutional code reaches to within 1 dB from that of an uncoded PSK system in AWGN at a BER of $P_e = 10^{-6}$. At a BER of $P_e = 10^{-3}$, the new uncoded and coded TS systems require 12 and 16 dB less transmitted signal power to perform at the same level as a standard coherent PSK modem in a Rayleigh flat-fading channel. The new uncoded TS system is also shown to perform similar to an uncoded 3^{rd} order diversity system using coherent PSK in a Rayleigh flat-fading channel. Comparative results from [3] and [4] were used as performance reference. When compared to coded PSK systems with infinite interleaver depth in a Rayleigh flat-fading channel. The $R_c = 2/3$ rate coded TS system requires 14 dB less transmitted signal power to ensure a BER of $P_e = 10^{-6}$. Comparative results for a 8-state $R_c = 2/3$ rate 8-PSK Ungerboeck coded system, taken from [9], was used as performance reference.

A technique to combine TC schemes with the proposed TS system has been proposed. This technique relies strongly on the transparency and Gaussianizing ability of the TS system. It has been pointed out that TC schemes are very sensitive to inaccurate CSI values. By using the TS technique, however, determination of the average SNR of the Gaussianized faded TS symbols through CSI is significantly improved. This again reduces the complexity of existing TC schemes and makes them more robust.

Although the ICIC structures proposed in this dissertation were shown to be very effective, they are still reliant on accurate channel estimates. Valuable future work may seek more robust adaptive ICIC strategies which are less dependent on channel estimates. Furthermore, the current TS systems

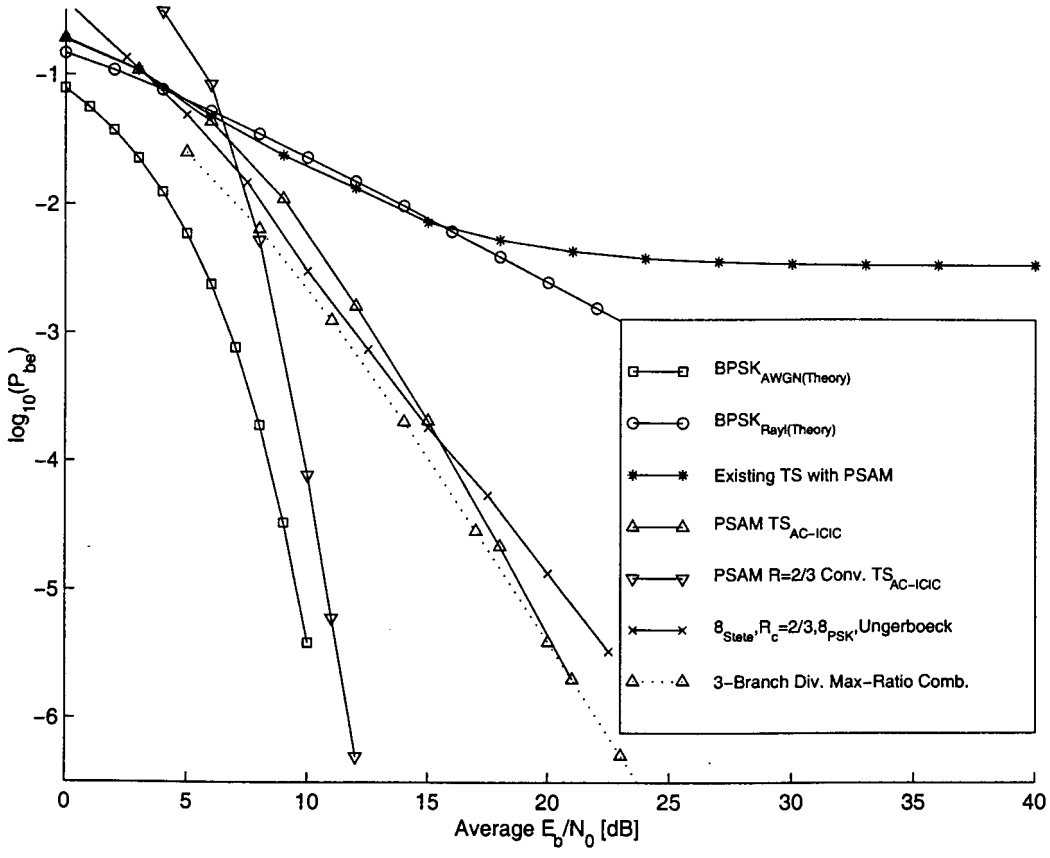

Figure 7.1: BER results summarizing the contributions made in this dissertation towards improving the BER performance of systems operating in Rayleigh fading channels vs. existing techniques.

were only designed for, and tested in frequency non-selective channels. These flat-fading channels, although commonly used to evaluate PSAM and different diversity and coding techniques, do not include discrete multipath effects that so often occur in mobile communication channels. Future research efforts may seek techniques to integrate equalizer or RAKE receiver structures within the existing TS technique to allow operation in frequency selective fading channels. Due to the transparency of the TS technique, it may be possible to combine TS with conventional lower-order spatial diversity techniques, thereby obtaining substantial signal diversity gains.

Application of the TS technique to systems outside the wireless communications arena may also be investigated. Possible applications include use in storage devices and Voice over IP applications suffering from burst-like signal losses. Here the TS technique may be employed to reconstruct information lost as a result of lost data packets.

It has been shown that efficient ICIC strategies can significantly improve the BER performance of a TS system employing imperfect spreading sequences. This is especially true for systems operating in AWGN. These imperfect spreading sequences belong to families of spreading sequences with good periodic CC properties and are used in spread spectrum CDMA systems for user separation purposes. Future research may investigate the possibility to accommodate multiple users in the same bandwidth of a single narrowband user using a combined TS-CDMA technique. This system would rely on efficient MUI cancellation as well as ICIC techniques for optimal performance.

This dissertation was aimed at developing efficient ICIC techniques to combat the BER performance floor occurring in TS systems at high $\overline{E}_b/N_0$ levels due to ICI. An efficient strategy to integrate FEC coding with the existing TS technique had to be found as well. The first objective was met with unexpected success and the BER performance floor was eliminated completely. Gains in average SNR requirements similar to third order spatial diversity schemes were obtained using a single transmitter-receiver antenna pair with only a minute increase in the transmission bandwidth. Due to the transparency with which TS can be inserted into existing systems, a very efficient FEC scheme could be integrated with the TS technique without significant changes to the system. A simple "off-the-shelf" convolutional coding scheme was integrated with the TS system with great ease and success and BER performance levels close to that of uncoded PSK systems in AWGN were recorded for the coded TS system operating in a Rayleigh flat-fading channel.

REFERENCES

[1] L. P. Linde, "Time Spread (TS) Technique to Combat Deep Fades in Mobile Communications," tech. rep., Laboratory for Advanced Engineering Pty. (Ltd.), 1994.

[2] P. Patel and J. Holtzman, "Analysis of a simple successive interference cancellation scheme in a DS/CDMA system," *IEEE JSAC*, vol. 12, pp. 796–807, June 1994.

[3] S. Benedetto and E. Biglieri, *Principals of Digital Transmission with Wireless Applications*. Plenum Press, to be published.

[4] J. Proakis, *Digital Communications*. Electrical Engineering, Singapore: McGraw-Hill, third ed., 1995.

[5] J. Ventura-Traveset, G. Caire, E. Biglieri, and G. Taricco, "Impact of diversity reception on fading channels with coded modulation - Part II: Differential block detection," *IEEE Trans. on Commun.*, vol. 45, pp. 676–686, June 1997.

[6] E. T. J. Davies, "Investigation of a time spread technique to combat flat fades in mobile digital communication," Master's thesis, Faculty of Engineering, University of Pretoria, Nov. 1997.

[7] E. T. J. Davies, "A novel technique to combat flat fading," *in Proceedings of IEEE COMSIG '97*, pp. 59–63, Sept. 1997.

[8] G. W. Wornell, "Spread-response precoding for communication over fading channels," *IEEE Trans. on Inform. Theory*, vol. 42, pp. 488–501, March 1996.

[9] E. Biglieri, G. Caire, and G. Taricco, "Coding for the fading channel: A survey," *in Proc. of the 1998 NATO-ASI, Il Ciocco, Italy*, July 1998.

[10] C. K. Pauw, "Coding vs. diversity on fading channels," Tech. Rep. LGI 89/103, Laboratory for Advanced Engineering Pty. (Ltd), Nov. 1989.

[11] T. S. Rappaport, *Wireless Communications, Principals and Practice*. Upper Saddle River, New Jersey 07485: Prentice Hall, 1996.

[12] K. Feher, *Wireless Digital Communications, Modulation and Spread Spectrum Applications.* Digital and Wireless Communication, Upper Saddle River, New Jersey 07458: Prentice Hall, 1995.

[13] B. Sklar, "Rayleigh fading channels in mobile digital communication systems - Part I: Characterization," *IEEE Communications magazine*, pp. 136–155, Sept. 1997.

[14] J. S. Swarts, "Aspects of multipath channel characterization," Master's thesis, Dept. of Electrical Engineering, Engineering Faculty, Rand Afrikaans University, Nov. 1998.

[15] A. P. R. Opperman, "BHF/UHF channel characterization and modelling for mobile digital communication," Master's thesis, Faculty of Engineering, University of Pretoria, Feb. 1995.

[16] J. Ventura-Traveset, G. Caire, E. Biglieri, and G. Taricco, "Impact of diversity reception on fading channels with coded modulation - Part I: Coherent detection," *IEEE Trans. on Commun.*, vol. 45, pp. 563–572, May 1997.

[17] A. Klein, B. Steiner, and A. Steil, "Known and novel diversity approaches as a powerful means to enhance the performance of cellular mobile radio systems," *IEEE JSAC*, vol. 14, pp. 1784–1795, Des. 1996.

[18] S. Haykin, *Communication systems.* John Wiley and Sons, Inc., third ed., 1994.

[19] J. Ventura-Traveset, G. Caire, E. Biglieri, and G. Taricco, "Impact of Diversity Reception on Fading Channels with Coded Modulation - Part III: Co-channel Interference," *IEEE Trans. on Commun.*, vol. 45, pp. 809–818, July 1997.

[20] M. L. Dukic and Z. S. Dobrosavljevic, "A method of a spread-spectrum radar polyphase code design," *IEEE JSAC*, vol. 8, pp. 743–749, June 1990.

[21] R. L. Frank and S. A. Zadoff, "Phase shift pulse codes with good correlation properties," *IRE Trans. on IT*, pp. 254–257, Oct. 1961.

[22] D. Chu, "Poly phase codes with good correlation properties," *IEEE Trans. on IT*, vol. 18, pp. 531–532, July 1972.

[23] Popovic, "Generalised chirp-like polyphase sequences with optimum correlation properties.," *IEEE Trans. on IT*, vol. IT-38, pp. 1406–1409, July 1992.

[24] B. H. Waldeck, S. A. Swanepoel, and L. P. Linde, "TFO Q^2PSK: A multidimensional spectrally efficient modulation scheme.," *COMSIG '98, University of Cape Town*, pp. 39–42, Sept. 1998.

[25] A. J. Bateman *et al.*, "Speech and data communications over 942 MHz TAB and TTIB single sideband mobile radio systems incorporating feed-forward signal regeneration," *IEEE Trans. Veh. Technol.*, vol. 34, pp. 13–21, Feb. 1985.

[26] J. K. Cavers, "The performance of phase locked transparent tone-in-band with symmetric phase detection," *IEEE Trans. on Commun.*, vol. 39, pp. 1389–1399, Sept. 1991.

[27] F. Davarian, "Mobile digital communications via tone calibration," *IEEE Trans. on Veh. Technol.*, vol. 36, pp. 55–62, May 1987.

[28] J. P. McGeehan and A. Bateman, "Phase locked transparent tone in band (TTIB): A new spectrum configuration particularly suited to the transmission of data over SSB mobile radio networks," *IEEE Trans. on Commun.*, vol. 32, pp. 81–87, Jan. 1984.

[29] F. G. Stremler, *Introduction to Communication Systems*. Addison Wesley, third ed., 1990.

[30] J. K. Cavers, "An analysis of pilot symbol assisted modulation for Rayleigh fading channels," *IEEE Trans. on Veh. Technol.*, vol. 40, pp. 686–693, Nov. 1991.

[31] S. Sampei and T. Sunaga, "Rayleigh fading compensation for QAM in land mobile radio communications," *IEEE Trans. on Veh. Technol.*, vol. 42, pp. 137–146, May 1993.

[32] M. Moher and J. Lodge, "TCMP - a modulation and coding strategy for Rician fading channels," *IEEE JSAC*, vol. 7, pp. 1347–1355, Dec. 1989.

[33] J. K. Cavers, "Cochannel interference and pilot symbol assisted modulation," *IEEE Trans. on Veh. Technol.*, vol. 42, pp. 407–413, Nov. 1993.

[34] J. K. Cavers, "Pilot symbol assisted modulation and differential detection in fading and delay spread," *IEEE Trans. on Commun.*, vol. 43, pp. 2206–2212, Jul. 1995.

[35] W. Kuo and M. P. Fitz, "Frequency offset compensation of pilot symbol assisted modulation in frequency flat fading," *IEEE Trans. on Commun.*, vol. 45, pp. 1412–1416, Nov. 1997.

[36] P. Schramm and R. Müller, "Pilot symbol assisted BPSK on Rayleigh fading channels with diversity: Performance analysis and parameter optimazation," *IEEE Trans. on Commun.*, vol. 46, pp. 1560–1563, Dec. 1998.

[37] A. N. D'Andrea, A. Diglio, and U. Mengali, "Symbol-aided channel estimation with nonselective Rayleigh fading channels," *IEEE Trans. on Veh. Technol.*, vol. 44, pp. 41–48, Feb. 1995.

[38] Rhode and Schwartz, Muhldorfstrasse 15, D-81671 Munchen, P.O. Box 801469, D-81614 Munchen, *Going Global with W-CDMA, Mobile radio of the third generation and measurements.*

[39] P. K. Ho, J. Cavers, and J. L. Varaldi, "The effects of constellation density on trellis-coded modulation in fading channels," *IEEE Trans. on Vech. Technol.*, vol. 42, pp. 318–325, Aug. 1993.

[40] J. A. Gansman, M. P. Fitz, and J. V. Krogmeier, "Optimum and suboptimum frame synchronization for pilot symbol assisted modulation," *IEEE Trans. on Commun.*, vol. 45, pp. 1327–1337, Oct. 1997.

[41] J. A. Gansman, M. P. Fitz, and J. V. Krogmeier, "Frame synchronization for PSAM on Rayleigh fading channels," *in Proc. of the 29th Asilomar Conference on Signals, Systems, and Computers, Pacific Grove, CA*, pp. 260–264, Nov. 1995.

[42] S. M. Bozic, *Digital and Kalman filtering*. London, Melbourne, Auckland: Edward Arnold: A division of Hodder and Stoughton, 1979.

[43] Y. Sanada and M. Nakagawa, "A multiuser interference cancellation technique utilizing convolutional codes and orthogonal multicarrier modulation for wireless indoor communications," *IEEE JSAC*, vol. 14, pp. 1500–1509, Oct. 1996.

[44] R. Singh and L. B. Milstein, "Interference suppression for DS/CDMA," *IEEE Trans. on Commun.*, vol. 47, pp. 446–453, March 1999.

[45] A. Soong and W. A. Krzymien, "A novel CDMA multiuser interference cancellation receiver with reference symbol aided estimation of channel parameters," *IEEE JSAC*, vol. 14, pp. 1536–1547, Oct. 1996.

[46] T. F. Wong, T. M. Lok, and J. S. Lehnert, "Asynchronous multiple-access interference suppression and chip waveform selection with aperiodic random sequences," *IEEE Trans. on Commun.*, vol. 47, pp. 103–114, Jan. 1999.

[47] S. Glisic and B. Vucetic, *Spread Spectrum CDMA systems for wireless communications*. Artech House, Inc., 1997.

[48] A. Klein, *Multi-user detection of CDMA signals - algorithms and their application to cellular mobile radio*. Fortschr.-Ber. VDI Rheide 10 Nr. 423, Düsseldorf: VDIVerlag, 1996.

[49] A. Johansson and L. K. Rasmussen, "Linear group-wise successive interference cancellation in CDMA," *in Proc. of the ISSSTA '98, Sun City, South Africa*, vol. 1, pp. 121–126, Sept. 1998.

[50] C. Boulanger, L. Ouvry, and M. Bouvier des Noës, "Multistage linear DS-CDMA receivers," *in Proc. of the ISSSTA '98, Sun City, South Africa*, vol. 2, pp. 663–667, Sept. 1998.

[51] E. Biglieri, J. Proakis, and S. Shamai, "Fading channels: Information-theoretic and communications aspects," *IEEE Trans. on Inform. Theory*, vol. 44, pp. 2619–2693, Oct. 1998.

[52] D. J. Rhee, S. Rajpal, and S. Lin, "Some block- and trellis coded modulations for the Rayleigh fading channel," *IEEE Trans. on Commun.*, vol. 44, pp. 34–42, Jan. 1996.

[53] G. D. Forney, JR., "The Viterbi algorithm," *in Proc. of the IEEE*, vol. 61, pp. 268–277, March 1973.

[54] C. Berrou, A. Clavieux, and P. Thitimasjshima, "Near Shannon limit error-correcting coding and decoding," *in ICC'93: International Conference on Communications, Geneva, Switserland*, pp. 1064–1070, May 1993.

APPENDIX A

CHANNEL MODEL IMPLEMENTATION

A.1 OVERVIEW

This appendix is concerned with the implementation of the Rician/Rayleigh flat-fading channel used in the evaluation of the TS technique. The method for calculating the poles and zeros for the baseband Doppler filters used in the simulation model, Fig. 2.4, is discussed and the equations relating the Doppler filters' gains and the LOS parameter to the Rician parameter, K, are given.

A.2 DOPPLER FILTER

This approximation for the Doppler fading spectrum is taken from [14]. The equations for calculating the IIR filter coefficients for a third order approximation of the Doppler fading spectrum are given for a maximum Doppler frequency of ω_c [rad/s] and a sampling frequency of f_s [Hz], resulting in a sampling period of $T_s = 1/f_s$.

Three constants are defined:

$$\begin{aligned} A &= 1.55 \\ B &= 1.090625 \\ C &= 0.9953125 \end{aligned} \quad . \tag{A.1}$$

The difference equation coefficients for the IIR filter are then given by

$$\begin{aligned} b(1), b(4) &= \omega_c^3 \\ b(2), b(3) &= 3\omega_c^3 \end{aligned} \tag{A.2}$$

and

$$\begin{aligned} a(1) &= 8 + 4A\omega_c T_s + 2B((\omega_c T_s)^2) + C((\omega_c T_s)^3) \\ a(2) &= -24 - 4A\omega_c T_s + 2B((\omega_c T_s)^2) + 3C((\omega_c T_s)^3) \\ a(3) &= 24 - 4A\omega_c T_s - 2B((\omega_c T_s)^2) + 3C((\omega_c T_s)^3) \\ a(4) &= -8 + 4A\omega_c T_s - 2B((\omega_c T_s)^2) + C((\omega_c T_s)^3) \end{aligned}, \tag{A.3}$$

where the difference equation for the IIR filter is defined as follows:

$$\begin{aligned} a(1)y(n) =& b(1)x(n) + b(2)x(n-1) + b(3)x(n-2) + b(4)x(n-3) \\ & - a(2)y(n-1) - a(3)y(n-2) - a(4)y(n-3) \end{aligned}. \tag{A.4}$$

The complexity of the fading channel simulator is reduced when the coefficients of the Doppler filters are scaled such that a 1 [Watt] noise input results in a 1 [Watt] lowpass noise output.

A.3 CHANNEL NORMALIZATION

Assuming the lowpass noise processes to have a variance of one, the equations relating the in-phase and quadrature-phase noise processes to the LOS parameter and the Rician K factor is as follows.

$$k_{LOS} = 10^{K/20} \tag{A.5}$$

and

$$y(t) = \frac{x_i(t)(f_i(t) + k_{LOS}) + x_q(t)f_q(t)}{\sqrt{1 + k_{LOS}^2}}, \tag{A.6}$$

where $x_i(t)$ and $x_q(t)$ are the in-phase and quadrature phase versions respectively of the transmitted signal and $y(t)$ is the fading channel output without AWGN. Variables $f_i(t)$ and $f_q(t)$ are the unity variance lowpass noise processes used to simulate the effect of Rayleigh fading.

A.4 SNR VERSUS E_B/N_0

E_b/N_0 is a very important parameter when comparing different communication systems. In practice, it is not always possible to measure this value directly and the received signal correct power in-band noise power is measured in stead. However, these values are bandwidth dependent and are not suitable to compare systems operating at different bandwidths.

By specifying the required E_b/N_0 ratio, the correct scale factor is calculated by which each noise sample must be weighed to produce the correct in-band noise variance σ_r. With W, the noise equivalent bandwidth of a system in [Hz] and $N_0/2$ the two-sided noise PSD function in [W/Hz], the in-band noise power for a system is given by:

$$\sigma_r^2 = W.N_0 \qquad [\text{W}]$$

In a simulated system, the channel noise power is given by:

$$\sigma_n^2 = f_s.N_0/2 \qquad [\text{W}]$$

where f_s is the simulation sampling frequency. Then SNR at that point in the system is given by:

$$SNR = \frac{\sigma_s^2}{\sigma_r^2} = \frac{E_b.R_b}{N_0.W}$$

where E_b is the average energy per bit and R_b is the rate at which bits are transferred. Thus,

$$\sigma_n = \sqrt{\frac{\sigma_s^2.f_s}{2.R_b 10^{\frac{1}{10}\frac{E_b}{N_0}}}}$$

Using (A.4), the amount of noise (AWGN) that must be added in the channel to obtain a desired E_b/N_0 dB ratio, can be calculated for a particular simulation.